Terminal Project Report

of the project titled

"Green synthesis of copper and silver nanoparticles mediated by extracts of medicinal plant species of Ethiopia for potential antimicrobial applications"

(ANSD/04/0453/11-2018)

Submitted By

Dr. Tegene Desalegn Zeleke (PI)

Dr. H C Ananda Murthy (PI-Expatriate)

Applied Chemistry Department

School of Applied Natural Science

Adama Science and Technology University

Adama, Ethiopia

April, 2021

Green synthesis of copper and silver nanoparticles mediated by extracts of medicinal plant species of Ethiopia for potential antimicrobial applications.

ABSTRACT

The research on the fabrication of plant mediated copper and silver NPs for multifunctional applications has gained prominence in the recent years. However, the toxicity of Ag and Cu NPs is found to depend on numerous morphological and physicochemical properties of the NPs. These consist of the nano features of the nanoparticles as well as the coating of Ag and Cu NPs by phytoconstituents which may decrease the risk of cytotoxicity. Hence it is a great challenge for researchers to synthesize green Cu and Ag NPs which are environment friendly with suitable size and shape. Thus we present the eco-friendly green synthesis of copper and silver nanoparticles using medicinal plant leaf extract at low temperature to investigate synergistic influence of phytochemicals present around the copper and silver nanoparticles on bacterial strains.

Ethiopian medicinal plants, Vernonia amygdalina del., Hagenia abyssinica (Brace) JF. Gmel., Artemisia absinthium L., Carum copticum L., Echinops sp. and Syzygium guineense (Willd.) DC mediated green Ag NPs and Cu/CuO NPs were successfully synthesized for the first time. The surface amalgamation of biomolecules of plant leaf extract around Ag and Cu NPs has also been approved by the most advanced techniques which were employed to characterize the NPs. The presence of absorbance maxima in UV-Vis (Ultra Violet-visible) spectra confirms the formation of Ag and Cu NPs. The DRS (Diffused Reflectance spectra) studies revealed the band gap varying in the range from 1.95 eV to 2.23 eV and 1.95 eV to 2.17 eV for Ag and Cu/CuO NPs respectively. The role of biomolecules as capping agents for NPs was authenticated by FT-IR (Fourier Transform-Infra Red) spectra. The presence of sharp peaks in the XRD (X-Ray Diffraction) pattern of NPs confirmed the highly crystalline nature of Ag, Cu and CuO NPs. The Cu NPs synthesised by using Echinops sp. plant root extract only yielded partially amorphous NPs which is believed to be due to the ineffective nucleation and capping of Cu NPs by the phytoconstituents. The TGA-DTA (Thermogravimetric analysis) and Differential thermal analysis) studies revealed that Ag and Cu/CuO NPs were thermally stable above 570 oC and 480 oC, respectively. The superficial morphology and purity of the NPs were corroborated by SEM-EDS (Scanning Electron Microscopy and Energy Dispersive Spectroscopy) analysis. The average particle sizes of Ag NPs and Cu NPs were deduced to vary between 18.72 nm to 36.88 and 27.1 to 34.76 nm, respectively. In addition, TEM micrographs revealed the presence of varieties of nano-sized shapes for Ag, Cu and CuO NPs. TEM-HRTEM-SAED (Transmission Electron Microscopy-High Resolution TEM- Selective Area Electron Diffraction) analysis of Ag and Cu NPs corroborated the existence of crystalline nature in biogenic silver and copper NPs. The interplanar d-spacing values varied from 0.126 nm to 0.262 nm for various planes of Ag and Cu NPs. The synergistic influence of surface amalgamated bioactive compounds and biogenic Ag and Cu NPs proved to exhibit highly effective antibacterial mechanism against pathogens, S. aureus, E. coli, P. aeruginosa, and E. aerogenes with 18 mm as a highest zone of inhibition. The antibacterial activity of all the Ag NPs was found to be superior when compared with that of Cu NPs. Thus it can be concluded that the cumulative effect of Ag and Cu NPs coupled with phytochemicals of plant extract proved to be detrimental for bacteria. The medicinal plants proved to have served as the better source of bioactive compounds for the synthesis of Ag and Cu NPs.

Keywords: *Medicinal plants; Green synthesis; Ag NPs; Cu NPs; Phytochemicals; Antibacterial activity.*

ACKNOWLEDGEMENTS

The authors are very much grateful to Adama Science and Technology University (ASTU) for supporting this project through ASTU‟s 13th cycle research grant. The authors express gratitude to Research and Publication Office of ASTU for cooperating and facilitating research project related issues timely. The authors extend their thanks to department of applied chemistry and department of materials science and engineering at Adama Science and Technology University for providing facilities such as thermal Analyzer, XRD. The authors are thankful to Addis Ababa university, Debre Tabor University, East west institute of technology, India and PSG IAS, India for their support towards plant authentication, FTIR, UV-Vis-DRS and SEM-EDAX-TEM-HRTEM-SAED characterization of Ag and Cu nanoparticles respectively and Oromia Regional Laboratory for antimicrobial assay.

We would also like to extend our heartfelt thanks to Mr. Buzuayehu Abebe, Ms. Emebet, Mr. Mebratu, Mr. Guta Amanu, Mr. Eticha Abdisa, Mr. Yeshaneh Adimasu, and Mr. Demeke for their assistance during our work and sample characterization. Moreover, we would also like to extend my gratitude to my family for their unreserved moral support. Last but not least, my heartfelt gratitude goes to our colleagues and friends for their generous support and contributions.

TABLE CONTENTS

List of Tables

List of Figures

LIST OF ABBREVIATIONS

Abbreviation	Full name
NPs	Nanoparticles
TGA	Thermo gravimetric analysis
SEM	Scanning electron microscopy
UV-vis-DRS	UV–visible diffuse reflectance
HRTEM	High-resolution transmission electron microscopy
PE1	*Vernonia amygdalina* Del.
PE2	Hagenia abyssinica (Brace) JF. Gmel.
PE3	*Artemisia absinthium* L.
PE4	*Carum copticum L.*
PE5	Echinops sp.
PE6	*Syzygium guineense* (Willd.) DC
A1	Ag NPs from PE1
A2	Ag NPs from PE2
A3	Ag NPs from PE3
A4	Ag NPs from PE4
A5	Ag NPs from PE5
A6	Ag NPs from PE6
C1	CuO NPs from PE1
C2	Cu NPs from PE2
C3	Cu NPs from PE3
C4	Cu NPs from PE4
C5	Cu NPs from PE5

C6	CuO NPs from PE6
S. aureus	*Staphylococcus aureus*
E. coli	*Escherichia coli*
TEM	Transmission electron microscopy
HRTEM	High Resolution TEM
DTA	Differential thermal analysis
SAED	Selected area electron diffraction
XRD	X-ray powder diffraction
SEM-EDAX	Scanning electron microscopy- Energy-dispersive analysis of X-ray
MHA	Mueller-Hinton Agar
CFU/mL	Colony Forming Unit / mL
FTIR	Fourier Transform Infrared
XRD	X-ray diffractometer
λmax	Absorbance maximum
DMSO	Dimethyl Sulphoxide
TSB	Tryptic Soy Broth
E_g	Energy gap
eV	Electron Volt
IPS	Interplanar spacing
nm	Nanometer
mm	Millimeter
ZoI	Zone of inhibition
IFFT	Inverse Fast Fourier Transition
ICSD	Inorganic Crystal Structure Database
cm^{-1}	Unit of wavenumber

ATCC	American Type Culture Collection
RNA	Ribonucleic acid
P. aeruginosa	*Pseudomonas aeruginosa*
E. aerogenes	*Enterobacter aerogenes*
DNA	Deoxyribose Nucleic acid
SPV	Surface Plasmon Vibration
Fcc (FCC)	Face centred cubic
DTG	Derivative Thermogravimetric
DSC	Differential Scanning Calorimeter
ROS	Reactive Oxygen Species

1. INTRODUCTION

Nanotechnology is the understanding and control of matter at dimensions between approximately 1 and 100 nanometers (nm), where unique phenomena enable novel applications. Nanoscale material is currently being used in electronic, magnetic and optoelectronic, biomedical, pharmaceutical, cosmetic, energy, catalytic and materials applications. The research on synthesized nanomaterials and their characterization is an emerging field of nanotechnology due to their huge applications in the fields of physics, chemistry, biology and medicine. Encompassing nanoscale science, engineering, and technology, nanotechnology involves imaging, measuring, modeling, and manipulating matter at this length scale. Metallic nanoparticles (NPs) are multifunctional in nature. Metal nanoparticles have been extensively used in a variety of sectors of industries and medicine including drug delivery, cancer treatment, wastewater treatment, DNA (Deoxyribose nucleic acid) analysis, as antibacterial agents and biosensors and in solar power generation and catalysis (Mittal et al. 2013). The green synthesis of metallic NPs has been proposed as a cost-effective and environmentally friendly alternative to chemical and physical methods. The plant mediated synthesis of nanoparticles is a green chemistry approach that connects nanotechnology with plants (Sorbiun et al. 2018a).

Materials scientists have been trying to develop the novel metal NPs with superior properties, better functionality and lower cost than the existing ones. The synthesis of metal NPs is the dynamic area of scientific research and more significantly application research in nanomaterials world. Several physical, chemical, mechanical and biological methods have been developed to enhance the performance of nanomaterials displaying improved properties with the aim to have a better control over the particle size, distribution. This biogenic reduction of metal ion to base metal is quite rapid, readily conducted at room temperature and pressure, and easily scaled up. Synthesis mediated by plant extracts is environmentally benign. Water is always considered an ideal and suitable solvent system for synthesis processes.

Nanoparticle formation involves the nucleation process in the beginning to yield nanoclusters and later slow growth of small crystals results in the formation of bigger particles. The synthesis of Cu NPs has been schematically represented as shown in Figure 1. The nucleation step basically controls the morphological features of the nanoparticles including the size and shape patterns. The tuning of the size of the nano metal oxides can be achieved by controlling nucleation and growth rates. The slow nucleation always yields

small nanoparticles whereas bigger particles formation is because of enhanced nucleation process.

Both gold and silver nanoparticles have been commonly found to have broad spectrum antimicrobial activity against human and animal pathogens (Annu et al. 2018). Silver NPs are already widely used as antimicrobial agents in commercial medical and consumer products (Asghar et al. 2018). In recent years, copper nano particles have attracted much attention of researchers due to their applications in industries and medicine. However, other NPs, such as platinum, gold, iron oxide, silicon oxides and nickel have not shown bactericidal effects in studies with *Escherichia coli* (Williams et al. 2006). The study on antibacterial effects of silver and copper nanoparticles using *E. coli* and *Bacillus subtilis*, revealed the fact that the copper NPs exhibited superior antibacterial activity compared to the silver NPs. Copper NPs have wide applications as heat transfer systems, antimicrobial materials, sensors and catalysts (Yoon et al. 2007).

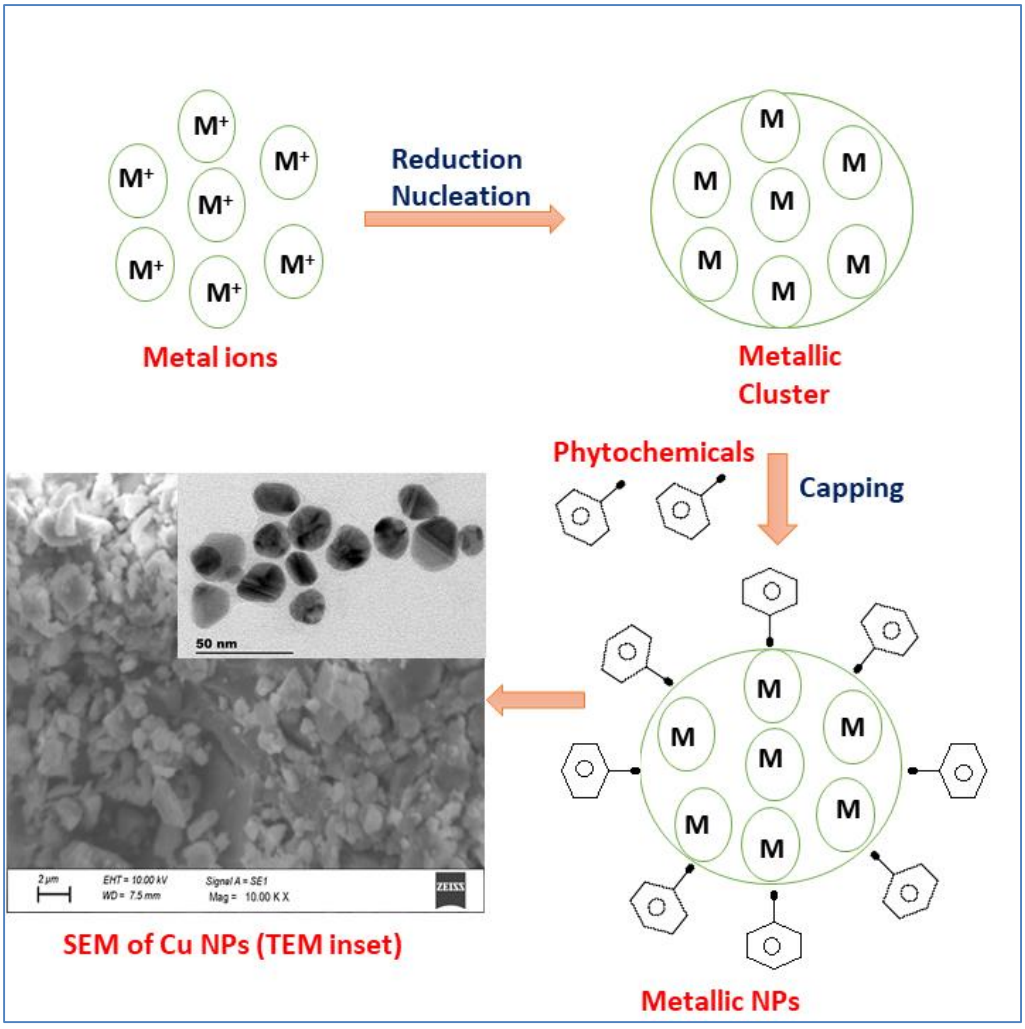

Figure 1. A simple mechanism of formation of Cu nanoparticles.

Copper, silver and gold NPs have been synthesized by using extracts of various plants found all over the globe (Ahmed et al. 2016a). But no research has been conducted as far as green synthesis of copper and silver nanoparticles is concerned using extracts of medicinal plants of Ethiopia.

The utilization of various medicinal plant parts as traditional medicine for varieties of ailments of man has been very common among many nations of the world since centuries. The vast majority of the rural people in the world completely rely on locally available plants with medicinal values. Africa has been one of the center of bio diversities in the world. Traditional medicine performs a tremendous role in most parts of Africa and rest of the world, in which massive majority of the population lives in rural regions with little access to health offerings (Tesfahuneygn and Gebreegziabher 2019). Ethiopia has very rich biodiversity in the world with 6, 500 species of higher plants. Most of the rural population of Ethiopia is dependent on traditional medicine who have little access to health services. In recent years, numerous medicinal plants have been validated in a scientific empirical framework through phytochemical analysis and subsequent bioassays. It is understood that 25% of the modern medicine enter the market utilizing either directly or indirectly traditional medicinal plant parts. But in the manufacture of pharmaceuticals, as high as 60% of these local plants were used (Abera 2014). The medicinal plants species are used to treat number of diseases (Judžentiene 2016).

The research on the fabrication of plant mediated copper and silver NPs for multifunctional applications has gained significance in the recent years. The green copper and silver NPs have been used for photocatalytic, electrocatalytic, industrial dye degradation, nano medicinal, environmental and catalytic applications since many decades (Murthy et al. 2020). These Cu and Ag nanostructures such as nanoparticles, nanocrystals, nanorods, nanotubes, nanosheets exhibit versatile properties and hence found to exhibit inhibitory activity against many microorganisms and bacterial strains (Hemmati et al. 2018). The safety of Cu and Ag NPs on human health rises a great concern among researchers. However, the toxicity of Cu and Ag NPs is found to depend on numerous morphological and physicochemical properties of the nanoparticles. These consist of the nano features of the nanoparticles as well as the coating of Cu and Ag NPs by phytoconstituents which may decrease the risk of cytotoxicity. Hence it is a great challenge for researchers to synthesize green Cu and Ag NPs which are environment friendly with suitable size and shape.

A very few medicinal plants such as *Azadirachta indica* (Ahmed et al. 2016b), *Dioscorea bulbifera* (Ghosh et al. 2015), *Barleria prionitis* (Bhagwat et al. 2018), *Hagenia abyssinica*

(Wolde et al. 2016), *Mentha longifolia* (Javed et al. 2020)and *Jatropha curcas* (Ghosh et al. 2020) have been applied to synthesize silver gold, copper and their oxides in the recent past for multifunctional applications.

In the recent days, not much work has been executed especially with the utility of medicinal plant extracts to reduce and cap copper and silver ions towards the synthesis of copper and silver nanoparticles for biomedical, photocatalytic, electrochemical sensor and antibacterial applications. In order to explore the influence of biomolecules of medicinal plant on the eco-friendly synthesis of cu and Ag NPs, few selected medicinal plants of Ethiopia have been chosen for our work. Thus we present the eco-friendly green synthesis of copper and silver NPs using medicinal plant leaf extract at low temperature to investigate synergistic influence of phytochemicals present around the copper and silver NPs on bacterial strains.

Therefore, the present research work is proposed to explore the green synthesis of copper and silver NPs using extracts of medicinal plants of Ethiopia. More than 95% of traditional medical preparations in Ethiopia are of plant origin. A few medicinal plant species of Ethiopia identified for the biogenic synthesis of Cu and Ag nanoparticles in aqueous media includes *Vernonia amygdalina, Hagenia abyssinica, Artemisia afra, Carum copticum, Echinops kebericho Mesfin* and *Syzygium guineense* plants.

The first stage of the proposed research work includes the green synthesis of copper and silver NPs mediated by medicinal plant species of Ethiopia. The integration of bioactive compounds of these medicinal plants with Cu and Ag nanoparticles is believed to be extremely beneficial for varieties of ailments.

The biogenically synthesized copper and silver nanoparticles have been characterized in the second stage of research, using UV-Visible spectroscopy, UV-DRS, FTIR, XRD, EDAX, TGA and DTA, SEM, TEM, HRTEM and SAED techniques. The third stage of the research includes bioassay analysis involving the evaluation of antimicrobial properties of biogenic copper and silver nanoparticles using few selected bacterial and fungal strains.

The research project is expected to provide various green synthetic routes for copper and silver NPs and their characterization results. In addition, more significantly, the project gives comprehensive report on antibacterial activity of biogenic copper and silver NPs which in turn will have significant impact on medical applications.

1.1. Statement of the Problem

Environmental antibiotic resistance developed by the bacterial and fungal strains are a global concern due to their capability causing community-acquired infection (Ortiz et al. 2014). So, searching safe and effective antimicrobial agents for therapeutic and non-therapeutic purposes has been continuously encouraged. Such problems have led to the resurgence in the use of nanomaterial-based antiseptics linked to broad-spectrum activity and far lower tendency for induce microbial resistance. The chemical method of synthesizing nano particles is extremely expensive and also involves the use of toxic, hazardous chemicals, which pose potential environmental and biological risks. The method for biosynthesis process is used of plants for the fabrication of nanoparticles is a rapid, low cost, ecofriendly. The advancement of green syntheses over chemical and physical methods is: environment friendly, cost effective and easily scaled up for large scale syntheses of nanoparticles, furthermore there is no need to use high temperature, pressure, energy and toxic chemicals. The plant mediated nanoparticles synthesis is preferred as it is cost effective, environmental friendly and safe for human therapeutic use. Ethiopia is endowed with diverse biological resources due to significant geographical diversity, which favored the formation of different habitat and vegetation zones. Plants contain abundant natural compounds such as alkaloids, flavonoids, saponins, steroids, tannins and other nutritional compounds. The above mentioned plants have proven record for their antihelmintic, antitumor, antimutagenic, antibacterial and fungicidal properties. Thus the synthesis of copper and silver nanoparticles capped with bioactive phytochemicals will be the safe and effective antimicrobial agents for therapeutic and non-therapeutic purposes.

1.2 Objectives

1.2.1 General objective

- To synthesize and characterize the copper and silver nanoparticles via green synthetic routes using extracts of medicinal plants of Ethiopia for potential antimicrobial applications.

1.2.2 Specific objectives

- To extract the leaves / seeds /roots of six selected medicinal plants of Ethiopia in aqueous medium. The plant species includes *Vernonia amygdalina, Hagenia*

abyssinica, *Artemisia afra*, *Carum copticum*, *Echinops kebericho Mesfin* and *Syzygium guineense* plants.

- To evaluate natural plant extracts for phyto-constituents.
- To synthesize copper and silver nanoparticles (Cu/CuO and Ag NPs) biogenically using medicinal plant extracts in aqueous media.
- To characterize the biogenic Cu/CuO and Ag NPs by UV-Visible spectroscopy, XRD, EDAX, TGA-DTA, SEM, TEM, HRTEM, SAED and FTIR for their size, shape, surface area, crystallinity, morphology and dispersity.
- To investigate in vitro antimicrobial activities of biogenic Cu/CuO and Ag NPs and compare with reference drugs.

1.3 Significance of the study

The infectious diseases are one of the leading causes of death of children, adolescents and olds. The development of alarming resistance of microbes towards antimicrobial agents is a major global public health problem. Thus, we need to have effective alternate antimicrobials to combat such resistant bugs. There has been an alarming increase in the side-effects caused by synthetic drugs encouraging switch over to herbal drugs. This study explored the green synthetic route to synthesize copper and silver NPs at moderately low temperature in a simple, ecofriendly and non-toxic mode without the imposition of many laboratory constraints. The role of phytoconstituents of few selected medicinal plant extracts of Ethiopia, has been established with the evidence for the formation of crystalline Ag and Cu/CuO NPs. The integration of bioactive compounds of medicinal plants with Cu/CuO and Ag NPs is believed to be extremely beneficial for varieties of ailments of man. The study corroborated the effective surface amalgamation of biomolecules around the Ag, Cu and CuO NPs to deteriorate the cell wall of bacteria and hence higher zone of inhibitions were recorded for all the NPs. This study provides detailed information on the synthesis, characterization and antibacterial activities of green Ag, Cu and CuO NPs.

1.4 Scope of the study

The present study reveals the importance of phytochemicals of aqueous extracts of medicinal plants of Ethiopia towards the synthesis of Ag and Cu/CuO NPs. The surface amalgamation of biomolecules with Ag and Cu NPs approves the synergistic

influence towards efficient antibacterial action on gram-positive and gram-negative bacterial strains. So medicinal plants mediated green metallic NPs can be synthesised for futuristic biomedical applications such as, antimalarial, anticancer and cytotoxic applications. The application of these Ag and Cu NPs is not just limited to antibacterial activity, instead, green Ag and Cu NPs can also be used as herbal drug or nanomedicine for human ailments. In addition, these green Ag and Cu NPs can also be used as catalysts, photocatalysts and electrochemical sensor materials.

2. LITERATURE REVIEW

2.1. Nanotechnology, Nanomaterials and Nanoparticles

Nanotechnology is a rapidly growing field in science and technology, due to the possibility of manufacturing new materials on the nanoscale level. Nanotechnology ("Nanotech") is a manipulation of matter on an atomic, molecular, and supramolecular scale. The earliest, widespread description of nanotechnology referred to the particular technological goal of precisely manipulating atoms and molecules for fabrication of macro scale products, also now referred to as molecular nanotechnology (Kalińska et al. 2019). Nanotechnology involves all of the following:

1. Research and technology development at the atomic, molecular or macromolecular levels, in the length scale of approximately 1 - 100 nanometer range.
2. Creating and using structures, devices and systems that have novel properties and functions because of their small and/or intermediate size.
3. Ability to control or manipulate on the atomic scale.

Nanotechnology is the science and technology of small things–in particular, things that are less than 100 nm in size. Scientists have discovered that materials at small dimensions' small particles, thin films, etc. can have significantly unique properties than the same materials at larger scale. The nanostructured objects are not new and they were not first created by man. There are many examples of nanostructures in nature in the way that plants and animals have evolved. Similarly, there are many natural nano scale materials, such as catalysts, porous materials, certain minerals, soot particles, etc., that have unique properties particularly because of the nano-scale features. In the past decade, innovations in our understanding of nanoscience and nanotechnology have enabled us to understand and control these structures and properties in order to make new functional materials and devices (Mittal et al. 2013).

Nanomaterials plays a very important role in modern research due to their potentiality in many fields, such as pharmacy, electronics, health, food, biomedical sciences, pharmaceuticals, chemistry and chemical industry, energy sciences, cosmetics, environmental health, mechanics and space industry. Among these wide applications, using metal nanoparticles have found considerable results in several applications including nanochemistry. In the last years, there were a wide interest between scientists in utilizing

the principles of green chemistry to synthesize metal nanoparticles for several applications (Rabiee et al. 2020).

A varieties of nanomaterials in various morphological forms such as nano particles, nano flowers, nano rods, nano wires, nano flakes, nano tubes, nanocubes, etc., have been synthesised and applied for diverse applications. In addition, various nanomaterials have also been decorated/supported on number of solid support materials such as, graphene, reduced graphene, polymers and carbon nanotubes.

A good number of synthetic methods have been explored to synthesise high performance nanomaterials with enhanced properties as a consequence to change in their particle sizes. The more fundamental methods of nanomaterials include Top down and Bottom up processes. Top-down method basically begins with bulk materials as starting materials. Many physical and mechanical methods such as grinding, milling, laser abrasion, etc., are employed to bring down the size of these materials to nanolevels. Top-down approaches have serious drawbacks such as formation of irregularly shaped particles, difficulty in tuning the surface morphology and hence inefficient surface properties. The conventional top-down technique also accompanies severe structural distortion of the NMs resulting in the loss of their desirable properties.

Bottom–up routes involves building-up of a nanomaterial or nanostructure from the atomic level. That means to build structure from the fundamental unit of matter i.e., atom. This method aims to prepare nanoparticles with uniform size and shape.

Nanoparticles (NPs) are particles in the nano size range between 1 nm and 100 nm with surrounding interfacial layer. They are very small particles with improved thermal conductivity, catalytic reactivity, nonlinear optical performance, and chemical stability due to their larger surface area – to- volume ratio. NPs are the great scientific interest as they are, in effect a bridge between bulk material and atomic or molecular structures. A bulk material should have constant physical properties regardless of its size, but at Nano scale size dependent properties are often observed (Jawaad et al. 2014).

2.2. Cu and Ag nanoparticles

Among the several noble metal nanoparticles, silver nanoparticles have attracted special attention due to their distinct proper- ties, which include favorable electrical conductivity, chemical stability, and catalytic and antibacterial activity. Silver at the nanoscale also has different properties from bulk silver. Synthesis of Ag NPs is an emerging area and is much sought after (Priya, Banerjee. et al. 2014). The green synthesis of Ag NPs has been

accomplished using plants, microorganisms, and other biopolymers. Wet chemical synthesis can be robustly scaled for the large-scale synthesis of Ag NPs of tunable shape and size through optimization of synthesis conditions. However, wet chemical methods use toxic chemicals, which are hazardous for the environment and usually result in the adsorption of toxic chemicals on to the surface of synthesized Ag NPs, making them unsuitable for biomedical applications (Lee and Jun 2019). In contrast, physical methods are expensive and cumbersome for the large- scale production of nanoparticles.

Copper is considered to be a vital element for the growth and health of plants, it is basic nutrient, active redox metal essential for humans. Oxidative stress has a significant role and a major source of diabetic problems. Cu NPs are capable of slowing down the lipid formation from peroxidation activity and stops the ROS production. Copper nanoparticles (Cu-NPs) is one among the highly consumed NPs and used in various products such as catalysis, filtration, aqueous solutions to conduct heat, solar panels, electronics, gas sensors, batteries, ceramics, textiles, glass and superconducting materials (Thiruvengadam et al. 2019). Therefore, the development of environmentally conscious, energy-efficient, facile, and rapid green synthesis methods that avoid toxic and hazardous chemicals has attracted significant interest (Chung et al. 2016).

2.3.Green synthesis of Metallic Cu and Ag nanoparticles

Green synthesis of metallic nanoparticles (NPs) for varieties of applications in catalysis, photocatalysis, biomedical, electrochemical and antibacterial sectors, has gained utmost significance due to its simplicity and eco-friendly nature. Metallic nanoparticles are multifunctional in nature and hence finds huge number of applications in various sectors for environmental, biomedical and antimicrobial, solar power generation and catalytic causes. Application of plant extracts to synthesize copper and its oxide nanoparticles is a green chemistry methodology which establishes strong relationship between natural plant material and nanosynthesis. It has been reported in the past study that copper, gold and silver NPs exhibited excellent antimicrobial activity against various disease causing pathogens. Plants consists of large number of biologically active compounds and hence, most of the plants have proven record for their anthelmintic, antitumor, antimutagenic, antibacterial and fungicidal properties.

The synthesis of metallic NPs involves simple mixing of metal solution with extract of plant. Nanoparticles are produced in the medium due to reduction of metal ions. In producing nanoparticles using plant extracts, the extract is simply mixed with a solution of the metal

salt at room temperature. The reaction is complete within minutes. Nanoparticles of silver, gold and many other metals have been produced this way (Ahmed et al. 2016a). The nature of the plant extract, its concentration, the concentration of the metal salt, the pH, temperature and contact time are known to affect the rate of production of the nanoparticles, their quantity and other characteristics (Li et al. 2011). Synthesis of silver nanoparticles using a leaf extract of *Polyalthia longifolia* was reported. An average particle size of about 58 nm was obtained. Silver and gold ions could be reduced to nanoparticles using a leaf extract of *Cinnamomum camphora* (Manandhar et al. 2019). The reduction was ascribed to the phenolics, terpenoids, polysaccharides and flavones compounds present in the extract. These nanoparticles were found to have a peak bactericidal activity at a concentration of 45 μg/mL (Zhang et al. 2011). They were most active against the yeast *Candida albicans*. An aqueous extract of *Ficus benghalensis* leaves (Ravindra et al. 2010) were used to produce silver nanoparticles that had an average diameter of 16 nm.

A tuber extract of *Dioscorea bulbifera* was used to produce gold and silver nanoparticles of various shapes (Ghosh et al. 2015). These nanoparticles in combination with antibiotics were found to have a synergistic antibacterial activity against test microorganisms, particularly against *Pseudomonas aeruginosa*, *Escherichia coli* and *Acinetobacter baumannii* (Lediga et al. 2018). Use of antibiotics in combination with silver nanoparticles has been reported also for effective control of otherwise antibiotic-resistant microorganisms. The Ag NPs had a uniform spherical shape and ranged in size from about 18 to 41 nm. These nanoparticles were found to have a significant cytotoxic effect on HEp-2 cancer cells (Rehana et al. 2017). Banerjee used an extract of *Syzygium cumini* (jambul) seeds to produce silver nanoparticles. Extract of banana (*Musa paradisiaca*) peels has been used to produce silver nanoparticles (Priya, Banerjee. et al. 2014). These nanoparticles displayed antifungal activity against the yeasts *Candida albicans and Candida lipolytica,* and antibacterial activity against *E. coli, Shigella sp., Klebsiella sp.* and *Enterobacter aerogenes*.

Valodkar et al., synthesized nanoparticles (5–10 nm) of silver and copper using latex of *Euphorbiaceae*. These nanoparticles exhibited excellent bactericidal activity towards both Gram-negative and Gram-positive bacteria. The detailed literature survey about silver nanoparticles revealed that they are already widely used as antimicrobial agents in commercial medical and consumer products.

Green Synthesis of copper nanoparticles is of great interest because of many advantages. Copper is highly conductive and also cheaper than silver and gold. In recent years, Cu nanoparticles have attracted much attention of researchers due to its application in wound

dressings and biocidal properties, potential industrial use such as gas sensors, catalytic process, high temperature superconductors and solar cells.

Green synthesis and characterization of copper nanoparticles has been reported (Nasrollahzadeh et al. 2017)

Although the biosynthesis of Cu NPs by plants such as *Euphorbia nivulia* (Maham et al. 2017), *plantago asiatica* (Siddiqi and Husen 2020), *Syzygium aromaticum* Cloves (Rajesh et al. 2018) has previously been reported, the potential of plants as biological materials for the synthesis of nanoparticles is yet to be fully explored, especially with medicinal plants indigenous to Ethiopia.

Formation of greenly synthesized copper nano particles capped with *T. cordifolia* (Cu NPs@Tc) was also reported (Udayabhanu et al. 2015). Synthesis of Cu nanoparticles has been successful with extracts of various parts of plant species that include, *Citrus medica Linn.* (Idilimbu) juice (Shende et al. 2015), *Ziziphus spina-christi* (L.) Willd (Khani et al. 2018), *Asparagus adscendens Roxb*. Root and Leaf (Thakur et al. 2018), *Eclipta prostrata* leaves (Chung et al. 2017), *Ginkgo biloba Linn* (Nasrollahzadeh and Mohammad Sajadi 2015), *Plantago asiatica* leaf (Nasrollahzadeh et al. 2017), *Thymus vulgaris* L (Issaabadi et al. 2017), *black tea* leaves (Asghar et al. 2018) and *Terminalia catappa* leaf (Muthulakshmi et al. 2017) and many more presented in Table 1.

Table 1. Various plants extracts used in the synthesis of Cu and CuO NPs and their applications.

Plant	Image	Precursor	Size, morphology, surface plasmon vibration (SPV)	Applications	Ref
Syzygium aromaticum bud		Cupric acetate (monohydrate) ($(CH_3COO)_2Cu{\cdot}H_2O$)	~12 nm, spherical, SPV@ ~580 nm	Antimicrobial properties	(Rajesh et al. 2018)
Stachys lavandulifolia		Copper chloride di-hydrate ($CuCl_2.\ 2H_2O$)	80 ± 8 nm, near-spherical, SPV@ ~ 590 nm	antibacterial activity	(Khatami et al. 2017)
black bean		Copper sulfate pentahydrate ($CuSO_4.5H_2O$)	~26.6 nm, spherical, hexagonal and uneven shapes,	anticancer activity	(Nagajyothi et al. 2017)

Azadirachta indica leaves		Cupric chloride di-hydrate ($CuCl_2.2H_2O$)	48nm, cubical, SPV@ ~ 506 nm	-	(Rehana et al. 2017)
Tinospora cordifolia		Copper chloride ($CuCl_2$(II))	50–130 nm, spherical, SPV@ ~ 250 nm	Catalytic Degradation	(Udayabhanu et al. 2015)
Citrus medica Linn. (Idilimbu) juice		Copper sulphate ($CuSO_4$)	33 nm, SPV@ ~ 631 nm nm	antimicrobial activity	(Shende et al. 2015)
Ziziphus spina-christi (L.) Willd		Copper sulphate ($CuSO_4$)	8–15 nm, spherical, SPV@ ~ 551 nm	triphenylmethane dye and antibacterial assay	(MEMON et al. 2020)
Asparagus adscendens Roxb. Root and Leaf		Copper sulphate ($CuSO_4$)	10– 15 nm, Spherical, SPV@ ~ 500 to 700 nm	Antimicrobial Activities	(Thakur et al. 2018)
Eclipta prostrata leaves		Copper acetate ($Cu(OAc)_2$)	31±1.2 nm, spherical, hexagonal and cubical, SPV@ ~ 565 nm	antioxidant and cytotoxic activities	(Chung et al. 2017)
Ginkgo biloba Linn		Copper chloride ($CuCl_2$)	15-20 nm, spherical, SPV@ ~ 560 to 580 nm	catalytic activity	(Nasrollahzadeh and Mohammad Sajadi 2015)
Plantago asiatica leaf		Cupric chloride di-hydrate, ($CuCl_2{\cdot}2H_2O$)	7–35 nm, spherical, SPV@ ~ 565 nm	catalytic activity	(Nasrollahzadeh et al. 2017)
Thymus vulgaris L.		Copper sulphate ($CuSO_4$)	various sizes, sheeted, SPV@ ~ 520 nm	catalytic activity (MB)	(Issaabadi et al. 2017)
black tea leaves		Copper sulphate ($CuSO_4$)	26–40nm, Spherical,	antibacterial, antifungal and aflatoxin B1 adsorption activity	(Asghar et al. 2018)

Terminalia catappa leaf		Copper sulphate pentahydrate ($CuSO_4.5H_2O$)	21–30 nm, Spherical,	Antibacterial test	(Muthulakshmi et al. 2017)
Aloe vera extract		$CuSO_4$	15 and 30 nm, dispersed, versatile and spherical, SPV@ ~ 265 and 285 nm	-	(Gunalan et al. 2012)
Oak Fruit Hull (Jaft)		Copper acetate ($Cu(CH_3COO)_2$)	34nm, quasi-spherical, SPV@ ~ 590 nm	Photocatalytic Degradation (Violet 3)	(Sorbiun et al. 2018b)
Ixoro coccinea leaf		Copper sulphate ($CuSO_4$)	80–110 nm, Spherical, SPV@ ~ 191 nm	-	(Vishveshvar et al. 2018)
Syzygium alternifolium (Wt.) Walp.		Copper sulfate pentahydrate ($CuSO_4.5H_2O$)	17.5 nm, spherical, SPV@ ~ 285 nm	Antiviral Activity	(Yugandhar et al. 2018)
Ferulago angulata (schlecht) boiss		Copper acetate ($Cu(CH_3COO)_2$)	~ 44 nm SPV@ ~ 554 nm	photocatalytic degradation of Rhodamine B (RhB)	(Shayegan Mehr et al. 2018)
Rosa canina fruit		Cupric acetate $Cu(OAc)_2$	Spherical, 15-25 SPV@ ~ 262 nm	C-N Ullmann coupling reactions	(Hemmati et al. 2018)
Azadirachta indica		Copper nitrate trihydrate ($Cu(NO_3)_2.3H=O$)	28-35 nm, spherical, SPV@ ~ 262 nm	antibacterial activity(*E. coli*)	(Nagar and Devra 2018)
Olea europaea leaf		Copper sulphate ($CuSO_4$)	20–50 nm, Spherical, SPV@ ~ 289 nm	their toxicity activities	(Sulaiman et al.)
Malus Domestica leaf		Copper sulphate ($CuSO_4$)	18 - 20 nm, spherical and crystalline, SPV@ ~ 335 nm	antibacterial, antioxidant, DNA	(Jadhav et al. 2018)

				cleavage activities	
Bauhinia tomentosa leaf		$CuSO_4$	22-40nm, Clustered & spherical, SPV@ ~ 384 nm	antibacterial	(Sharmila et al. 2018)
E. camaldulensis		copper nitrate $Cu(NO_3)_2$	89.24 nm	Biofilm Formation	(Zainab J. Shanan 2018)
Moringa oleifera Leaves		Copper sulfate pentahydrate ($CuSO_4.5H_2O$)	6 and 61 nm	Nitrates Removal	(Galan et al. 2018)
Abutilon indicum leaf		Copper (II) nitrate trihydrate ($Cu(NO_3)_2.3H_2O$)	nanometer range (not homogenous) agglomerated, hexagonal wurtzite, SPV@ ~ 725 nm	Antimicrobial, antioxidant and photocatalytic dye degradation activities	(Ijaz et al. 2017)
Calotropis procera		Copper sulfate pentahydrate ($CuSO_4.5H_2O$)	15–20 nm, quasi-spherical, SPV@ ~ 565 nm	adsorptive of Cr(VI)	(Dubey and Sharma 2017)
Euphorbia Chamaesyce leaf		Copper chloride ($CuCl_2$)	~36–40 nm, Spherical, face-centered cubic (fcc), SPV@ ~ 325 nm	catalytic activity(4-nitrophenol)	(Maham et al. 2017)
Rheum palmatum L.		Copper chloride ($CuCl_2$)	10–20 nm, Spherical, SPV@ ~ 250–300 nm	catalytic activity	(Bordbar et al. 2017)
Leucaena leucocephala L.		Copper acetate monohydrate ($Cu(CH_3COO)_2.H_2O$)	10-25 nm, Spherical, -	upshot against	(Aher et al. 2017)

				human pathogens	
Drypetes sepiaria		Cupper nitrate tri-hydrate ($Cu(NO_3)_2.3H_2O$)	spherical, 25 nm, SPV@ ~ 298 nm	catalytic activity	(Narasaiah et al. 2017)
Banana peel		Copper nitrate trihydrate ($Cu(NO_3)_2.3H_2O$)	50-85nm, spherical, SPV@ ~ 495 nm	photocatalytic activities	(Aminuzzaman et al. 2017)
Gloriosa superba L.		Copper nitrate ($Cu(NO_3)_2$)	5-10nm, Spherical, SPV@ ~ 380 nm	antibacterial activity	(Naika et al. 2015)
Coffee Powder		Copper nitrate nonahydrate ($Cu(NO_3)_3.9H_2O$)	20-60 nm, monoclinic, SPV@ ~ 262 nm	-	(Taghavi Fardood and Ramazani 2016)
Thymbra spicata		Cupric acetate $Cu(OAc)_2$	10–20 nm, spherical	catalyst	(Veisi et al. 2018)
Aglaia elaeagnoidea		Copper nitrate nonahydrate ($Cu(NO_3)_3.9H_2O$)	20–45 nm, spherical, SPV@ ~ 250–350 nm	Catalyst	(Manjari et al. 2017)
Caloropis procera leaf		Cupric acetate $Cu(OAc)_2$	40 nm, monoclinic structure (cylindrical), SPV@ ~ 291 and 355 nm	-	(Reddy 2017)
Carica papaya		Copper sulfate pentahydrate ($CuSO_4.5H_2O$)	140 nm, rod, SPV@ ~ 250–300 nm	photo catalysis (dye degradation)	(Sankar et al. 2014)
Anthemis nobilis flower		Copper chloride ($CuCl_2$)	18-60nm, face-centered cubic (fcc), SPV@ ~ 250 nm	catalytic activity(A^3 coupling reaction)	(Nasrollahzadeh et al. 2015)

Saraca indica Leaves		Copper chloride monotahydrate ($CuCl_2.H_2O$)	13–15 nm, spherical, SPV@ ~ 213 and 339 nm	Photolumine scence Studies	(Prasad et al. 2017)
Henna leaves		Copper sulfate Pentahydrate ($CuSO_4.5H_2O$)	as-synthesized (27 nm) and calcined (45 nm), agglomerated spherical, SPV@ ~ 570 nm	Electrical conductivity	(Cheirmad urai et al. 2014)
Punica granatum		copper sulfate ($CuSO_4$)	15 to 20 nm, spherical, SPV@ ~ 585 nm	antimicrobia l activity (opportunisti c pathogens)	(Kaur et al. 2016)
Zingiber Officinale stem		copper sulfate ($CuSO_4.2H_2O$)	3nm, Spherical, SPV@ ~ 208nm	-	(Delma and Jaya Rajan 2016)
Tabernaemonta na divaricate leaf		copper sulfate ($CuSO_4.2H_2O$)	48 ± 4 nm, spherical, SPV@ ~ 220–225 nm	antibacterial activity (urinary tract)	(Sivaraj et al. 2014)
P. granatum seeds		Copper chloride ($CuCl_2$)	40–80 nm, semi spherical, SPV@ ~ 553 nm	photo-catalytic activity	(Nazar et al. 2018)

To date, several plant parts including the seeds, stem, fruits, root and leaf have been employed for synthesizing different sizes and shapes of Ag NPs such as *Iresine herbstii* leaf (Bar et al. 2009), oak fruit hull (Sorbiun et al. 2018b), *Cocus nucifera* leaf and root (Uddin et al. 2020), *Eriobotrya japonica* leaf (Rajivgandhi et al. 2019), *Coffea arabica* seed (Dhand et al. 2016) and so on. Otherwise, researchers also utilized the berry extract of Sea Buckthorn to obtain the Ag NPs with superior antioxidation and anticancer activity. A few more researchers have reported the synthesis of Ag NPs (Table 2) using the medicinal plants across the globe for multifunctional applications.

Table 2. Various plants extracts used in the synthesis of Ag NPs and their morphological features.

Plants	**Size of NPs (nm)**	**Plant's part**	**Shape of NPs**	**Reference**
Pistacia atlantica	10–50	Seeds	Spherical	(Veisi et al. 2019)
Eclipta prostrate	35-60	Leaves	Triangles, pentagons, hexagons	(Chung et al. 2017)
Ipomoea asarifolia (Convolvulaceae)	20-60	Leaves	Spherical	(Khaled et al. 2017)
Hagenia abyssinica (Brace) JF. Gmel.	8-42	Leaves	cylindrical, prismatic, hexagonal, triangular	(Murthy et al. 2020)
Cornus Officinal	50-60	Fruit	Spherical, Polygonal	(Wang et al. 2020)
Catharanthus roseus	5-20	Flower	Spherical	(Ponarulselvam et al. 2012)
Clinacanthus nutans	10-300 10-180	Leaves Stem	Spherical	(Mat Yusuf et al. 2020)
Mentha longifolia	13-50	Branches	Nearly Spherical	(Javed et al. 2020)
Ferulago macrocarpa	14-25	Flowers	Spherical	(Azarbani and Shiravand 2020)
Ligustrum lucidum	10-25	Leaves	Nearly Spherical	(Huang et al. 2020)
Terminalia arjuna	15-30	Leaves	Spherical	(Dudhane et al. 2019)

2.4. Characterization and Antimicrobial applications of Cu and Ag NPs

The characterization of biogenically synthesized Cu and CuO nanoparticles has been carried out by using analytical tools namely, UV-Visible spectroscopy, XRD, EDAX, SEM, TEM, FTIR, HRTEM, particle analyzer, Surface Plasmon resonance etc. The UV–Vis absorption spectroscopy was applied to detect color change in Cu nanoparticle synthesised by using *Ziziphus spina-christi* leaves which is possibly due to the surface plasmon vibrations. The surface plasmon vibration bands for Cu-NPs synthesised by many plant extracts was found to be between 191 nm and 721 nm as given in Table 1.

XRD patterns obtained for the Cu NPs synthesized using citron juice and Aloe vera extract showed intense peak confirming crystalline copper (Shende et al. 2015)and crystalline CuO NPs (Gunalan et al. 2012) respectively.

The analysis of FT IR spectra provides information about functional groups of biomolecules present in plant extracts. IR peaks were observed at 3,333 cm^{-1} for the hydroxyl group (H-bonded OH stretch); 2,917 cm^{-1} for methylene C-H asym. / sym. stretch; 1,615 cm^{-1} for aromatic ring stretch (Chung et al. 2017). The peaks at about 3400, 1650, 1595, 1400 and 1100 cm^{-1} corresponds to -OH, C=O, C=C, C-OH and C-H vibrations (Nasrollahzadeh et al. 2015). The common IR bands (Muthulakshmi et al. 2017) for cellulose were usually found at 3304 cm^{-1}, 2891 cm^{-1}, 1664 cm^{-1}, 1011 cm^{-1} corresponds to vibrations of -OH, CH_2, H_2O, and C-OH groups. Peaks at 610, 499 and 415 cm^{-1} confirmed Cu–O bond vibrations that support the presence of monoclinic phases of CuO synthesised by *Aloe barbadensis Miller* extract (Gunalan et al. 2012). The IR band recorded at about 800 cm^{-1} corresponds to C–H out of plane bending vibrations due to adsorbed phenolic compound on to the CuO NPs (Sorbiun et al. 2018a).

Electron microscopy is used for morphological characterization and internal composition of biogenic copper and silver nanoparticles. EDAX will reveal the elemental composition of the particles.

Homogeneous and spherical morphology of biogenic Cu NPs were revealed by FESEM images. The average particle size varied from 20 nm to 500 nm. TEM micrographs also revealed spherical nature for NPs with least tendency towards agglomeration. DLS studies reveal particle size distribution of Cu NPs. The average particle size of NPs synthesised by using *Azadirachta indica* leaves was found to be around 50 nm.

The spherical morphology and narrow diameter distributions of Cu NPs were also confirmed by TEM images. The biomolecules present in *Aloe vera* extract believed to act as stabilizing

and capping agent for copper caused a raise in the size of NP up to 30 nm but without change in shape.

FESEM images of CuO NPs too confirmed their spherical nature (20 nm to 300 nm). CuO NPs synthesised by Oak fruit extract exhibited average diameter of 34 nm (Sorbiun et al. 2018b). CuO NPs were found to exhibit agglomeration tendency thus enhancing average particle size to as high as 300 nm. HRTEM studies involving in-depth analysis of CuO NPs synthesised by using fruit extract of *Syzygium alternifolium* (Yugandhar et al. 2018) recorded particle size of 2 nm.

CuO NPs with relatively good monodispersed and virtually spherical structures were obtained with size range of 15 to 25 nm without *agglomeration* (Hemmati et al. 2018). TEM analysis of CuO NPs synthesized using *B. tomentosa* leaf extract (Sharmila et al. 2018)also showed spherical morphology (size of 22 to 40 nm).

Cu NPs demonstrated good antimicrobial influence on *Bacillus spp.* and prominent fungicidal influence on Penicillium spp. Microorganisms (Rajesh et al. 2018). Cu NPs exhibited greater inhibition on *Escherichia coli* in comparison with *Klebsiella pneumoniae*, *Pseudomonas aeruginosa*, *Propionibacterium acnes* and *Salmonella typhi*. *Fusarium culmorum* was found to establish more sensitive *plant pathogenic fungi*. Cu NPs were also used for antioxidant and cytotoxic activities (Noor et al. 2020).

Similarly, Ag NPs too exhibited various morphological features as presented in Table 2. Silver nanoparticles synthesised using medicinal *Catharanthus roseus Linn*. G. Don plant leaves extract (Ponarulselvam et al. 2012) were found to possess spherical morphology with crystalline nature and an average size ranging between 35 nm and 55 nm. These Ag NPs showed good antiplasmodial activity against *P. falciparum*. In another work, Ag NPs were synthesised by using fever-reducing plants of South African origin, namely Eucomis autumnalis and Gunnera perpensa. These researchers were successful in combining the biomolecules of medicinal plant extracts with Ag NPs. The efficiency in the antibacterial activity of green Ag NPs was found to increase by 50-fold compared with that of plant extracts (Lediga et al. 2018). Ipomoea asarifolia has many medicinal uses throughout Africa and Asia. The Ag NPs synthesised by using *I. asarifolia* leaf extract exhibited superior antibacterial activity against human pathogenic bacterial strains with highest zone of inhibition of 9.33 mm for *S. aureus* bacterial strain (Khaled et al. 2017). The biomolecules covered Ag NPs were obtained by the application of aqueous leaf extracts of three *Congolese* plant species, namely *Brillantaisia patula*, *Crossopteryx febrifuga* and *Senna siamea*. The successful formation of colloidal particles from silver ions in the presence of

aqueous leaf extracts of the *Congolese* plants was reported where the particles were almost spherical with average size of 45 nm (Kambale et al. 2020). The reported minimum inhibitory concentration of 300 μg/mL for Ag NPs confirmed the role of biomolecules present around the Ag NPs as shell in antibacterial action. Biosynthesis of Ag NPs using plant extract of *S. spinose* grown in vitro was reported (Pirtarighat et al. 2019). It has been proved that carboxylic acid present in carnosic acid and flavonoids supported the bio reduction and the stabilization during the formation of Ag NPs.

Not much metallic nanoparticles synthesis research has been done using medicinal plants of Ethiopia. About 85% of world population uses herbal medicines for prevention and treatment of diseases, and the demand is increasing in developed and developing countries. It has been observed that people of Ethiopia uses lot of plants for medicinal applications. Based on the available literature on traditional medicinal plants of Ethiopia (Tesfahuneygn and Gebreegziabher 2019), the following plants were selected for our studies: *Vernonia amygdalina, Hagenia abyssinica, Artemisia afra, Carum copticum, Echinops kebericho Mesfin* and *Syzygium guineense*.

Vernonia amygdalina Del., one of the top 10 ranked medicinal vegetation in Ethiopia, is being used for the remedy of stomach pain, worms, and malaria (Widyaningtyas et al. 2019). The leaves of Vernonia amygdalina Del. tastes bitter and hence cooked leaves are served in soups and stews of distinct cultures of Africa. Hagenia abyssinica (Brace) JF. Gmel, a member of the Rosaceae family, is a species of flowering plant native to the high-elevation Afromontane regions of central and eastern Africa from Sudan and Ethiopia. It is known in English as African redwood and East African rosewood and in Amharic language as kosso. Hagenia abyssinica is a slender tree up to 20m tall, with a short trunk and thick branches. The roots are cooked with meat and the soup drunk for general illness and malaria, while the dried and pounded female inflorescence is used as an anthelmintic (especially for tapeworm).

Artemisia absinthium L., one of the top ranked medicinal vegetation in Ethiopia, has been reported to have antipyretic, antimicrobial and antioxidant activities. Ajowan (Carum copticum) is an annual herbaceous plant. Carum copticum essential oil exhibit antioxidant and antimicrobial activities. The seeds of Carum copticum have a therapeutic effect on some cutaneous, neural, and urinary tract disorders. Echinops Sp., is valued primarily for its root parts and its medicinal uses are documented in the ancient medico-religious pharmacopoeia. The roots of Echinops Sp., have been used in the preparation of medicines against migraine, mental illness, heart pain, leprosy, kidney disease, malaria and syphilis (Judžentienė 2016).

Syzygium guineense (Willd.) DC is a medium-sized or tall evergreen tree, 15-30 m high. Its Amharic name is dokma, whereas, in English it is called by several names such as water pear, water boom and water berry. The ripe fruits are edible for humans, birds, and some wild animals. It is considered a famine food, eaten by subsistence farmers when their crops fail. In southern Ethiopia, S. guineense is a much-appreciated shade tree for both the homestead and the home garden. Many herbalists and native doctors in Africa proposes their aqueous extracts for their patients as treatment for forms of illnesses (Abera 2014).

The present work was proposed to explore the green synthetic routes for both silver and copper nanoparticles using extracts of medicinal plants indigenous to Ethiopia in aqueous medium. The biogenically synthesized copper and silver nanoparticles were characterized using UV-Visible spectroscopy, XRD, EDAX, TGA-DTA, SEM, TEM, HRTEM, SAED and FTIR techniques. The characterization is followed by evaluation of antimicrobial properties of biogenic copper and silver nanoparticles.

3. MATERIAL AND METHODS

3.1. Chemicals and Reagents

All the chemicals, $AgNO_3$, $(Cu(NO_3)_2 \cdot 3H_2O$, ethanol, Dimethyl sulfoxide (DMSO) and MH agar solution used in the experiments were of analytical grade (purchased from Merck chemical Industrial company) and used without any further purification.

3.2. Collection and authentication of plant materials

The following 4 medicinal plant species were collected from the Ethiopian Agricultural research centre, Wendoganet;

Vernonia amygdalina Del. (Grawa in Amharic), *Hagenia abyssinica* (Brace) JF. Gmel. (Kosso in Amharic), *Artemisia absinthium L.* (Ariti in Amharic) and *Echinops sp.* (Qebericho in Amharic). The coordinates of the research center are N 7°5 31.509 ″E 38° 37 54.7284″and N 7°5 35.5128″ E 38 ° 37′59.0304″.

Figure 2. A selected few medicinal plants of Ethiopia.

The 5th plant, *Syzygium guineense* (Willd.) DC plant leaves were collected from the Arsi zone, Ethiopia. The identification of the plants was performed at the National Herbarium, Department of Biology, Addis Ababa University, Addis Ababa, Ethiopia. The last plant *Carum copticum L.* seeds (Netch-azmud in Amharic) were purchased from the market at Adama. The images of all the plants are depicted in Figure 2. The details of plant species along with their codes used throughout the document are presented in the table 3.

Table 3. The botanical names and family names with various parts of the selected six medicinal plants along with code names.

Sl. No.	**Botanical name of the plant**	**Family**	**Plant part/ Code**	**Plant extract code**	**Plant powder code**
1	*Vernonia amygdalina* Del.	*Asteraceae*	Leaves / P1	PE1	PP1
2	Hagenia abyssinica (Brace) JF. Gmel.	*Rosaceae*	Leaves / P2	PE2	PP2
3	*Artemisia absinthium* L.	*Asteraceae*	Leaves, Flowers/P3	PE3	PP3
4	*Carum copticum L.*	*Apiaceae*	Seeds / P4	PE4	PP4
5	Echinops sp.	*Asteraceae*	Roots / P5	PE5	PP5
6	*Syzygium guineense* (Willd.) DC	*Myrtaceae*	Leaves / P6	PE6	PP6

3.3. Preparation of plant powders and aqueous extracts

The leaves, flowers, roots and seeds of the selected medicinal plants (Table 3) were surface cleaned and washed repeatedly with tap water followed by distilled water to remove dust particles and then allowed to dry under shadow for 15 days to cast off moisture contents. The dried leaves, roots and seeds were ground using a grinding machine to get powders (as shown in Figure 3) followed by packing in separate brown bottles. The extraction was carried out by taking 20 g of the powdered leaves, roots and seeds separately in different 500 ml of conical flasks containing 400 ml of deionized water. These flasks were later covered with aluminum foil, to prevent the effect of light. After that, the mixtures were

shaken using a mechanical shaker for 90 minutes and allowed to warm at 50 °C for 1 hr on a magnetic stirrer; then these mixtures were allowed to cool down to room temperature overnight. The prepared solutions were filtered through Whatman No.1 filter paper to get clear solutions. The prepared extracts were stored at 4 °C for future experiments.

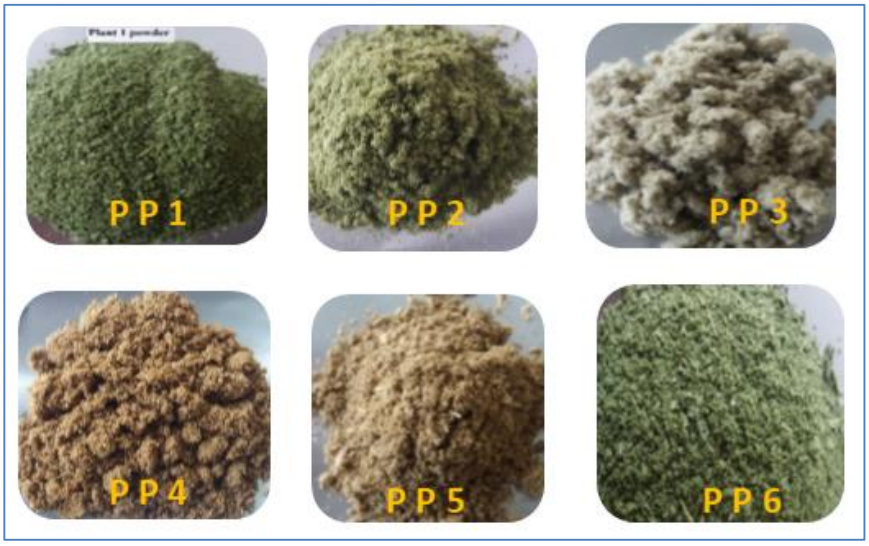

Figure 3. The powder form of all the selected medicinal plants of Ethiopia.

3.4. Phytochemical Qualitative Analysis

The plant extracts and methanolic and ethanolic aqueous solutions were assessed for the existence of the phytochemical analysis by using the following standard methods (Gul et al. 2017).

3.4.1. Test for Anthraquinones

10 ml of benzene was added in 6 g of the Ephedra powder sample in a conical flask and soaked for 10 minutes and then filtered. Further 10 ml of 10% ammonia solution was added to the filtrate and shaken vigorously for 30 seconds and pink, violet, or red color indicated the presence of anthraquinones in the ammonia phase.

3.4.2. Test for Tannins

10 ml of bromine water was added to the 0.5 g aqueous extract. Decoloration of bromine water showed the presence of tannins.

3.4.3. Test for Saponins

5.0 ml of distilled water was mixed with aqueous crude plant extract in a test tube and it was mixed vigorously. The frothing was mixed with few drops of olive oil and mixed vigorously and the foam appearance showed the presence of saponins.

3.4.4. Tests for Flavonoids

Shinoda Test: Pieces of magnesium ribbon and HCl concentrated were mixed with aqueous crude plant extract after few minutes and pink color showed the presence of flavonoid.

Alkaline Reagent Test: 2 ml of 2.0% NaOH mixture was mixed with aqueous plant crude extract; concentrated yellow color was produced, which became colorless when we added 2 drops of diluted acid to mixture. This result showed the presence of flavonoids.

3.4.5. Tests for Glycosides

Liebermann's Test: We added 2.0 ml of acetic acid and 2 ml of chloroform with whole aqueous plant crude extract. The mixture was then cooled and we added H_2SO_4 concentrated. Green color showed the entity of aglycone, steroidal part of glycosides.

Keller-Kiliani Test: A solution of glacial acetic acid (4.0 ml) with 1 drop of 2.0% $FeCl_3$ mixture was mixed with the 10 ml aqueous plant extract and 1 ml H_2SO_4 concentrated. A brown ring formed between the layers which showed the entity of cardiac steroidal glycosides.

Salkowski's Test. We added 2 ml H_2SO_4 concentrated to the whole aqueous plant crude extract. A reddish brown color formed which indicated the presence of steroidal aglycone part of the glycoside.

3.4.6. Test for Terpenoids

2.0 ml of chloroform was added with the 5 ml aqueous plant extract and evaporated on the water path and then boiled with 3 ml of H_2SO_4 concentrated. A grey color formed which showed the entity of terpenoids.

3.4.7. Test for Steroids

2 ml of chloroform and concentrated H_2SO_4 were added with the 5 ml aqueous plant crude extract. In the lower chloroform layer red color appeared that indicated the presence of steroids.

3.4.8. Test for Alkaloids

To about 3 ml of sample solution, a few drops of Wagner's reagent are added. Formation of the brownish precipitate, confirms the presence of alkaloids.

3.5. Green synthesis of Cu/CuO and Ag NPs

To investigate the optimum ratio for the synthesis of NPs, the plant extract and precursor solutions were mixed at different ratios (1:1, 1:2, 1;4 and 1:9). The color of the solution was observed to change slowly from blue to light brownish indicating the formation of Cu/CuO NPs, which is believed to be due to the excitation of surface plasmon vibrations in the inoculated NPs. To examine the formation of NPs, a small amount of all the mixtures was diluted separately with the deionized water (1:1, 1:1, 1:2, 1;4 and 1:9) and monitored by measuring absorbance at different time intervals. The maximum absorbance was found with the mixture containing 1:4 ratio of planet extracts and precursor salt solutions. Thus Cu/CuO and Ag NPs were prepared using the same ratio. On the similar lines the optimized concentration for the precursor salt solution was determined to be 0.2M among the used concentrations of 0.05 M, 0.1 M, 0.2 M and 0.3 M.

A 0.2 M aqueous Cu $(NO_3)_2 \cdot 3H_2O$ solution was prepared and stored in brown bottles. 100 ml of each plant extract was mixed with 400 ml of 0.2M Cu $(NO_3)_2 \cdot 3H_2O$ solution (1:4) slowly dropwise with constant stirring. The mixture has been incubated at room temperature for 24 hrs. The color change was checked periodically (After 30 min and 60 min) (Nagar and Devra 2018).

The change in color from blue to light brownish visually indicates the formation of Cu NPs and then the solution was centrifuged for 15 min at 10000 rpm. The obtained Cu NPs (Figure 4) were washed by deionized water and ethanol to remove any impurities. Thereafter, the NPs were allowed to dry and ground so as to be used for further analysis. The similar procedure was followed to synthesize the Ag NPs (Figure 4) using all the plant extracts (Kasithevar et al. 2017).

All the copper and silver NPs synthesised using the six medicinal plant extracts have been assigned a specific code for convenient discussion throughout the document as mentioned in table 4. The corresponding packed samples are presented in Figure 5.

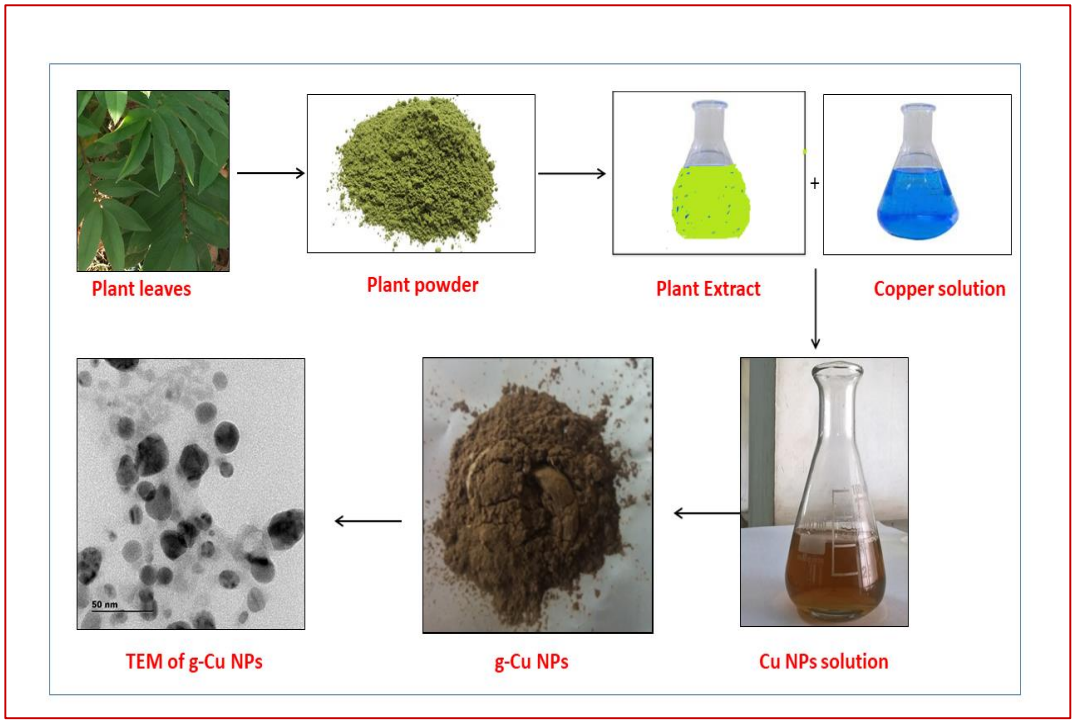

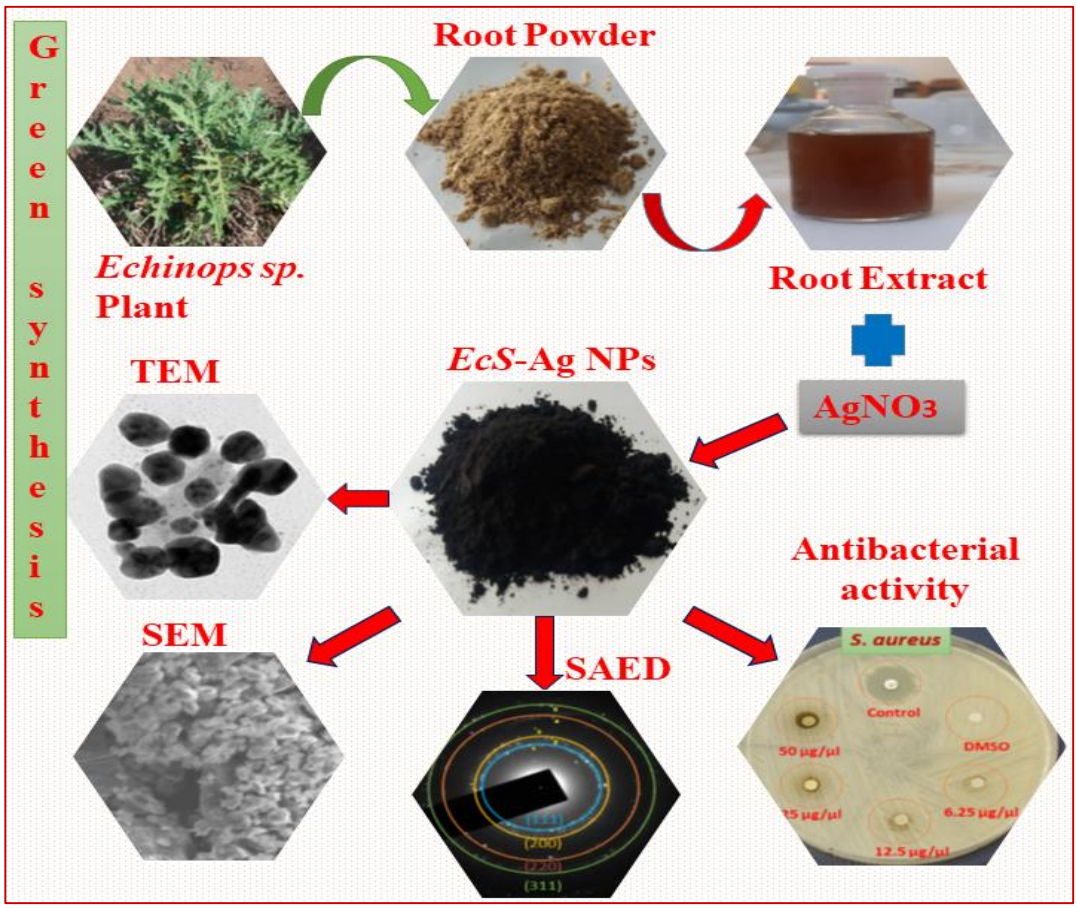

Figure 4. The scheme of green synthesis of green copper (g-Cu) and green silver (g-Cu) NPs.

Table 4. The sample codes of six Ag NPs and six Cu/CuO NPs synthesised using the six medicinal plants mentioned in table 3, respectively.

Sl. No.	Sample code	Sample details
1	A1	Ag NPs from PE1 (V-Ag NPs)
2	A2	Ag NPs from PE2 (H-Ag NPs)
3	A3	Ag NPs from PE3 (A-Ag NPs)
4	A4	Ag NPs from PE4 (C-Ag NPs)
5	A5	Ag NPs from PE5 (E-Ag NPs)
6	A6	Ag NPs from PE5 (S-Ag NPs)
7	C1	Cu/CuO NPs from PE1 (V-Cu/CuO NPs)
8	C2	Cu NPs from PE2 (H-Cu NPs)
9	C3	Cu NPs from PE3 (A-Cu NPs)
10	C4	Cu NPs from PE4 (C-Cu NPs)
11	C5	Cu NPs from PE5 (E-Cu NPs)
12	C6	CuO NPs from PE5 (S-CuO NPs)

Figure 5. The six Ag NPs (A1, A2, A3, A4, A5 and A6) and six Cu/CuO NPs (C1, C2, C3, C4, C5 and C6) synthesised using the six medicinal plants.

3.6. Characterization Techniques

3.6.1. UV-vis-DRS and UV-vis analysis

Ultraviolet–visible spectroscopy (UV-Vis) denotes absorption spectroscopy or reflectance spectroscopy in the UV-Vis spectral region. UV-vis absorption spectroscopy measures the relative change of transmittance of light, whereas in diffuse reflectance, measures the relative change in the amount of reflected light of a surface. Normally, the former is used for solutions/suspensions or thin films, whereas the latter is used for solids, optically rough films or powders. The working principle of UV-Visible spectroscopy is that absorption of photons promotes the molecule to an excited state and hence this technique is ideal for determining the optical and electronic properties such as the band gap of material (Rocha et al. 2018). The optical band gap energy, Eg, of all nanocomposites will be determined from UV-vis spectra using Tauc's equation: The ultraviolet-visible spectroscopy techniques [Shimadzu UV-vis, SM-1600 (for solution analysis) and Shimadzu UV-vis-DRS, UV-2600 (for powder analysis)] in the range of 200–800 nm were used to study the optical properties of Cu/CuO and Ag NPs.

3.6.2. FT-IR analysis

The FT-IR spectroscopy is a technique used to obtain an infrared spectrum of the absorption of a solid, liquid or gas sample. The term Fourier transform infrared spectroscopy originates from the fact that a Fourier transform (a mathematical process) is required to convert the raw data into the actual spectrum. In infrared (IR) spectroscopy, infrared radiation passes through a sample and while some of it is absorbed by the sample, the rest is transmitted. The resulting spectrum represents the molecular absorption and transmission, creating a molecular fingerprint of the sample. This makes infrared spectroscopy useful for several types of analysis. FTIR can provide much information on the material including, the identification of unknown materials, the determination of the quality or consistency of a sample and the determination of the amount of each component in the mixture. An infrared spectrum represents a fingerprint of the sample with absorption peaks corresponding to the frequencies of vibrations between the bonds of the atoms making up the material. Therefore, infrared spectroscopy can result in a positive identification (qualitative analysis) of various organic and inorganic materials. In addition, the size of the peaks in the spectrum can be an indication of the quantity of a specific compound in the sample. With modern software algorithms, infrared is a good tool for quantitative analysis (Rosi et al. 2019). The Fourier

transform-infrared spectroscopy (Perkin Elmer FT-IR, Spectrum 65) using KBr pellets in the range of 400–4000 cm^{-1} was used to study the chemical bonding behavior of biomolecules surface amalgamated Cu/CuO and Ag NPs.

3.6.3. XRD analysis

The X-ray diffraction (XRD) is a rapid analytical technique used for identifying the atomic as well as molecular structure of crystal. Diffraction effects are observed when an electromagnetic radiation impinges on the structure at the level of the radiation wavelength. XRD is based on the constructive interference of monochromatic X-rays and the crystalline sample. The interaction of the incident rays with the sample produces constructive interference when conditions satisfy Bragg's Law ($n\lambda = 2d\sin\theta$).

The diffracted X-rays are detected, processed and counted. All possible diffraction directions of the lattice should be attained by scanning the sample through a range of 2θ due to the random orientation of the powdered material. The mineral with unique spacing d can be identified by compare the XRD pattern with the standard reference pattern (Day et al. 2016). The X-ray diffraction (XRD, Shimadzu, PXRD-7000) was used to study the actuality and crystallinity of Cu/CuO and Ag NPs.

3.6.4. TGA and DTA analysis

Thermo Gravimetric Analysis (TGA) is a thermal analysis technique which measures the weight change in a material as a function of temperature and time, in a controlled environment. This is very useful to investigate the thermal stability of a material and its fraction of volatile components, or to investigate its behaviour in different atmospheres. Differential thermal analysis (DTA) is a calorimetric technique, recording the temperature and heat flow associated with thermal transitions in a material. This enables phase transitions to be determined (e.g. melting point, glass transition temperature, crystallization etc.). TGA/DTA is a simultaneous thermal analyzer that can characterize multiple thermal properties of a sample in a single experiment. The TGA component measures temperatures where decomposition, reduction or oxidation occurs. It simultaneously measures the weight changes associated with decomposition, oxidation, and any other physical or chemical changes that result in sample weight loss or gain. The DTA component shows whether decomposition processes are endothermic or exothermic. The DTA also measures temperatures corresponding to phase changes where no mass loss occurs, such as melting, crystallization and glass transitions (Rostek and Biernat 2013). The DTG (Shimadzu DTG-

60H) and DSC (Perkin Elmer, DSC 4000, USA) techniques in a nitrogen atmosphere at 20.0 mL min-1 flow rate and 50 °C min^($^{-1}$) hold time were used to study the thermal stability and degradation behavior of the synthesized Cu/CuO and Ag NPs.

3.6.5. SEM-EDAX and TEM-HRTEM-SAED analysis

The scanning electron microscopy (SEM) is a powerful characterization technique for surface analysis and morphology of the materials. The SEM shows very detailed three dimensional images at much high magnifications as compared to light microscope. In SEM, an electron beam from an electron source is focused by a fine probe that raster scans over the surface of the specimen under vacuum. The beam of electrons passes through the electromagnetic lenses and strikes the surface of the sample. As the electrons penetrate the surface, interactions occur that result in the emission of electrons or photons from or through the surface. The detector collects the secondary/backscattered electrons ejected from the sample and passes them onto a photomultiplier which converted them into a signal and directs them towards a displaying screen. The SEMs are used to determine the external morphology (texture), chemical composition, and crystalline structure of the nanomaterials samples. In particular, the measurement of secondary electrons allows studying the morphology of the sample while the measurement of backscattered electrons in addition to producing an image of the sample gives information on its composition because their emission is related to the atomic number of the elements present.

Another application of the electron microscopy is to characterize the elements of a material by Energy Dispersive X-ray Spectroscopy (EDAX). The sample is bombarded with the electrons from the atoms on the surface of the specimens. This results in the electron vacancy which is then filled by another electron from a higher shell. To balance the energy difference between the two electrons, an X-ray is emitted. The EDAX measures the number of emitted X-rays versus their energy, which is the characteristic of the element. Thus, this technique is used for identifying the elemental composition of the specimen, and also used to provide information of atomic distribution (mapping) and semi-quantitative analysis (Rades et al. 2014).

The scanning electron microscopy with energy-dispersive X-ray spectroscopy (SEM-EDX-EVO 18 model with low vacuum facility and ALTO 1000 cryo attachment) was used to study the morphological studies of Cu/CuO and Ag NPs.

The TEM seeks to see beyond the surface and it shows sample as whole. It provides the two dimensional image and also it offers 50 million magnifications. The resolution of TEM is

0.5 Å in which the beam of electron is transmitted through ultrathin specimen and it interact with the specimen as it passes and gives an image. The formed image is magnified and it focused on imaging device. TEM is a very valuable tool for the material's analysis, since it can furnish a variety of information including chemical composition, crystal/surface structure information and image resolutions of up to a few angstroms just by switching the operational mode. TEM has become an important characterization technique due to its high lateral spatial resolution and its capability to provide both image and diffraction information from a single sample. The morphology can be observed on a significantly higher resolution compared to SEM and the crystallization can be analyzed through the selective area electron diffraction (SAED) patterns (Li et al. 2016).

The morphological features and crystalline features of Cu/CuO and Ag NPs with d-spacing values were explored using a high-resolution transmission electron microscopy (JEOL TEM 2100 HRTEM).

3.7. Antibacterial Activity Studies

All the antibacterial tests were conducted at Oromia Public Health Research, Capacity Building & Quality Assurance Laboratory, Adama, Ethiopia. The *in-vitro* antibacterial activity of Cu/CuO and Ag NPs was evaluated using Agar disc-diffusion method against selected one Gram positive bacterial strain (*Staphylococcus aureus*) and three Gram negative pathogenic bacterial strains (*Escherichia coli, Pseudomonas aeruginosa and Enterobacter aerogenes*). Prior to antibacterial activity test, the bacterial strains were cultured in nutrient broth for 24 hrs to obtain logarithmic growth phase of the test bacteria. A standardized inoculum of the bacteria is swabbed onto the surface of Mueller-Hinton Agar (MHA) plate. The actively growing bacterial cultures of 1.3×10^8 CFU/mL concentration were inoculated/spread onto the MHA plate (turbidity was adjusted with TSB to match 0.5 McFarland standard). The nanoparticles extract was prepared with four different concentrations in Dimethyl Sulfoxide. Four concentrations (6.25, 12.5, 25 and 50 µg/µl) of the synthesized nanoparticles were added to the respectively labeled wells.

The antibiotic discs of 6 mm diameter were applied to agar surface using forceps with gentle pressure and then impregnated with the dissolved extract. Chloramphenicol disc was used as a positive control while DMSO was taken as negative control. The plates were incubated at 35 ±2 °C in an ambient air incubator for 18-24 hrs. The antimicrobial activity was evaluated in terms of zone of inhibition, measured to the nearest millimeters (mm) using a ruler and recorded.

4. RESULTS AND DISCUSSION

The selected six medicinal plants namely, *Vernonia amygdalina* Del., *Hagenia abyssinica* (Brace) JF. Gmel., *Artemisia absinthium L*., *Carum copticum L*., *Echinops sp.*, and *Syzygium guineense* (Willd.) DC., have been subjected to phytochemical screening as per the standard procedure and protocol. The scientific names of the identified plant species and their family names are given in Table 5.

Table 5. The botanical and family names of the medicinal plant species.

Sl. No.	Botanical name of the plant	Family name
1	*Vernonia amygdalina* Del.,	Asteraceae
2	*Hagenia abyssinica* (Brace) JF. Gmel.,	Rosaceae
3	*Artemisia absinthium* L.,	Asteraceae
4	*Carum copticum* L.,	Apiaceae
5	*Echinops* sp.,	Asteraceae
6	*Syzygium guineense* (Willd.) DC	Myrtaceae

The phytochemical screening of all the plant extracts for the presence of bioactive components was carried out successfully. The alkaloids, flavonoids, terpenoids, phenolic compounds, tannins, anthraquinone glycosides, saponins and cardiac glycosides were found in plant extracts during the phytochemical analysis. The list of the phytochemicals present in each of the plant extract are as given in Table 6. Three steps involved in the origin of NPs includes: reduction of metal ions, formation of cluster and growth of nanoparticles. Polyphenols are believed to undergo tautomeric enol-keto transformation to release the reactive hydrogen atomic species which play the role of converting metal ions to metal nanoclusters / nanostructures (Din et al. 2017). In addition, the enzymes of leaf extract also assist silver/copper ions to get reduced and form protein capped silver NPs (Roy et al. 2019). It is also natural to know that that the phenolic compounds act as organic ligand (Ramyajuliet 2020) and assist in the reduction of silver ions to form Ag NPs. In addition, these compounds also influence the size of the nanoparticle as reported by the earlier researcher (Azarbani and Shiravand 2020).

Table 6. The details of phytoconstituents screening of medicinal plant extracts.

Sl. No.	Phytochemicals	Test/Reagents	Plant Extracts					
			PE1	PE2	PE3	PE4	PE5	PE6
1.	Alkaloids	Wagner's	-	-	+	+	+	+
2.	Tannins	KOH	+	+	+	+	+	+
3.	Flavonoids	Shinoda test	-	-	+	+	+	-
4.	Terpenoids	Silkowiski	-	-	+	+	+	-
5.	Anthraquinone glycosides	Born Trager's	+	+	+	+	-	+
6.	Cardiac glycosides	Keller Killiani's	+	+	-	-	-	+
7.	Saponins	Foam test	-	-	-	-	-	+

The synthesised Ag NPs have been characterized by all the advanced techniques such as UV-visible, UV-DRS, XRD, FTIR, TGA-DTA, SEM-EDAX, TEM-HRTEM and SAED.

4.1. UV-Vis-DRS analysis of Ag and Cu/CuO NPs

The UV-visible absorbance spectrum of instantaneously synthesised Ag NPs revealed λ_{max} values of 454 nm, 461 nm, 411 nm, 451 nm, 452 nm and 455 nm for A1, A2, A3, A4, A5 and A6 nanoparticles, respectively as shown in Figure 6, just after 10 min of mixing plant extract with silver nitrate solution. The absorbance spectrum (Figure 7) recorded after 20, 30, 40, 50 and 60 minutes of forming homogeneous mixture, exhibited identical absorbance bands with little enhancement in the intensities. The enhanced absorbance in the consecutive bands, clearly confirm the increased concentration of nanoparticles (MEMON et al. 2020). As the time passes on, the reduction of silver ions is followed by nucleation of small cluster of silver atoms to form nanoparticles in the presence of biomolecules of plant extract which are possibly believed to have acted as reducing agent and stabilising agent. Poly phenolic compounds usually help in the reduction of silver ions into silver atoms.

Almost identical results were observed during the analysis of synthesized Ag NPs by using the *Lustrum lucidum* leaf extract and *Persea americana* seed extract (Girón-Vázquez et al. 2019). The surface plasmon absorbance presents a set of different λmax values for NPs

synthesised using different plant extracts which is possibly due to morphological features of the NPs.

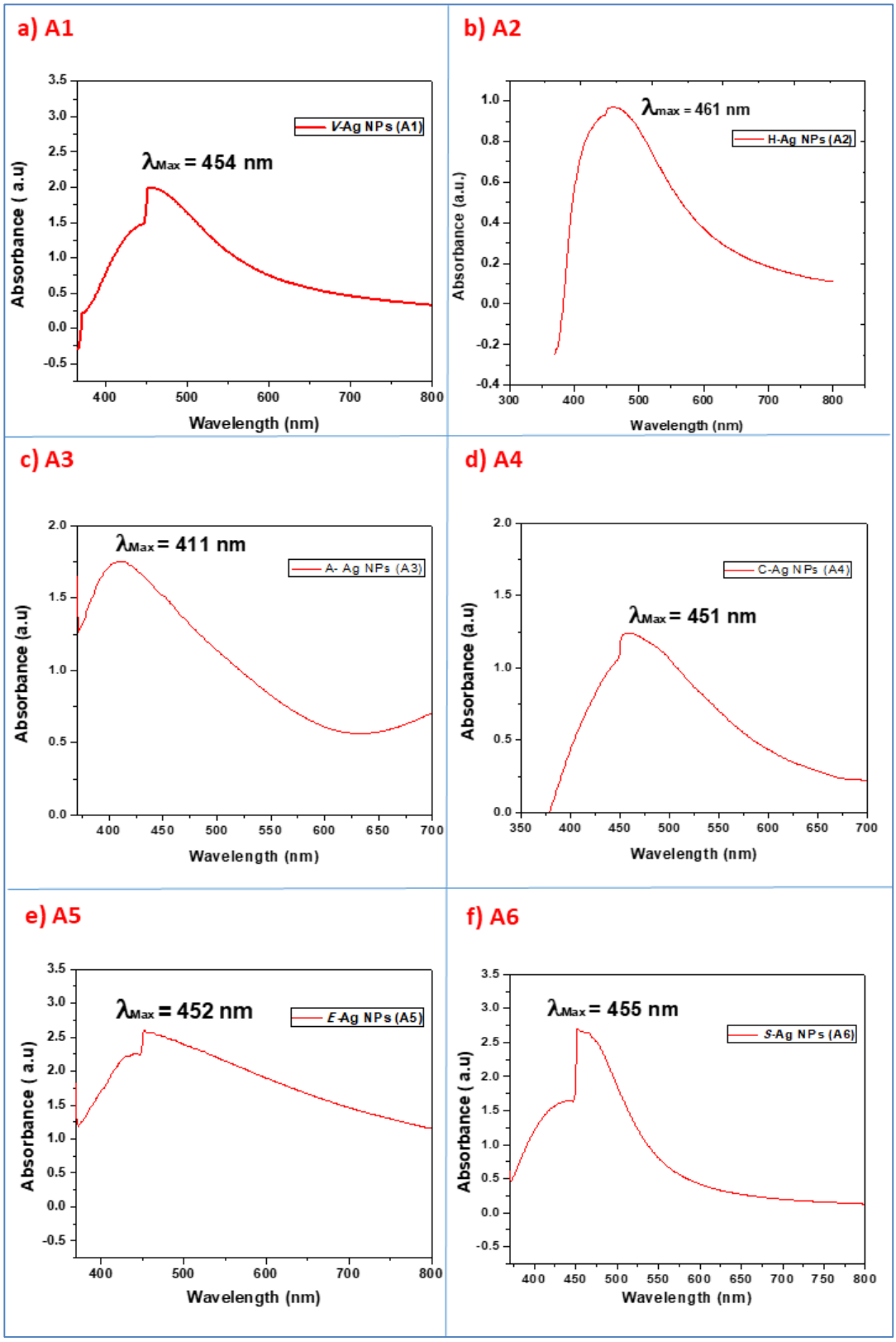

Figure 6. The absorbance spectra of Ag NPs a) A1 b) A2 (c) A3 (d) A4 e) A5 and f) A6.

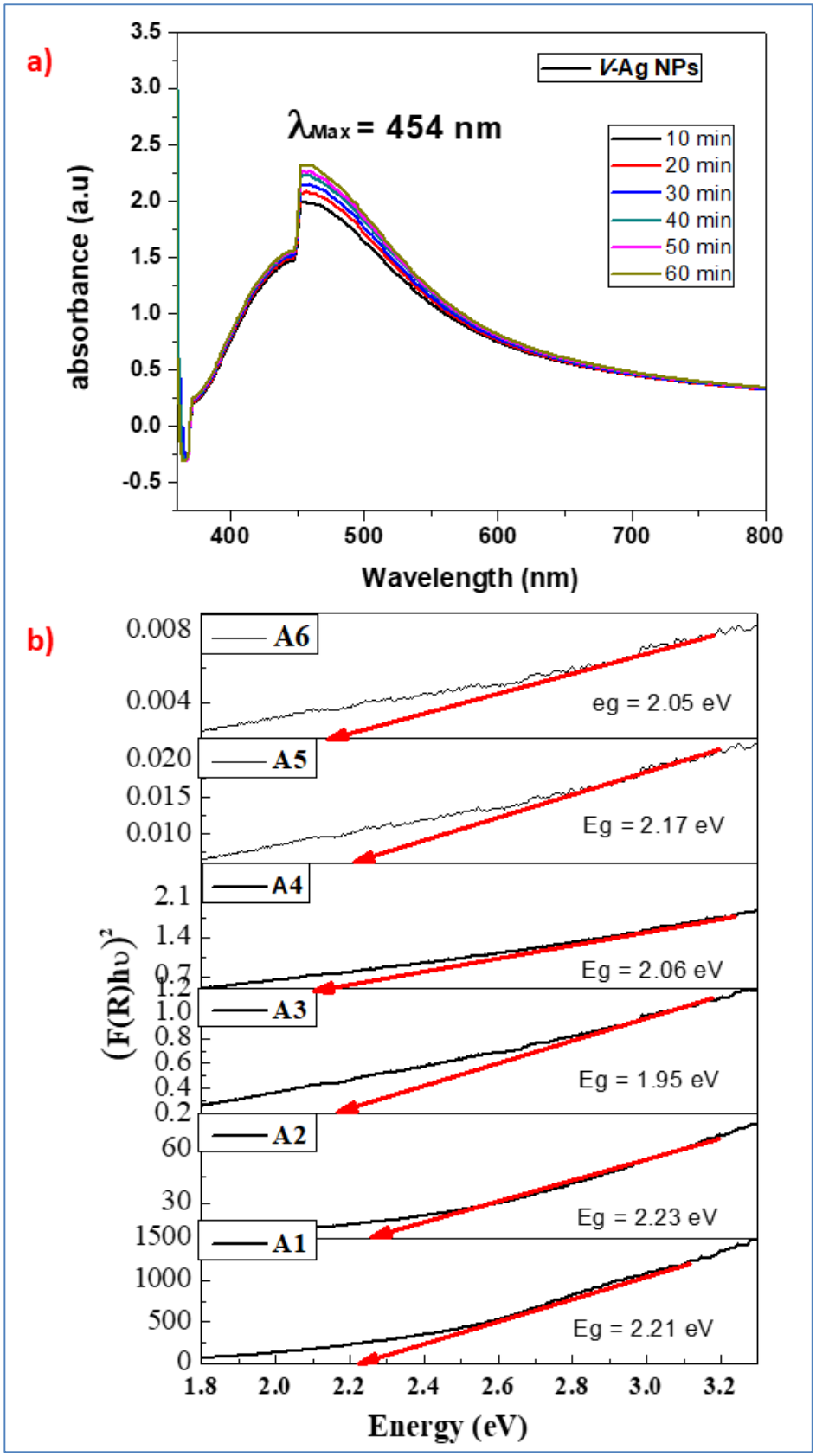

Figure 7. a) The absorbance spectra of Ag NPs (A1) at various time intervals and b) Tauc plots for all the Ag NPs.

The UV-visible-DRS spectra were recorded for all the NPs (Figure 7b). The Tauc plot was utilized to compute the band gap energy of all the Ag NPs with the assistance of Kubelka-Munk function. For a direct band gap, the absorption coefficient near the band edge was given by Wood and Tauc's relation.

$$\alpha = \frac{A}{h\upsilon} (h\upsilon - E_g)^{1/2} \text{ ----- (1)}$$

where a; absorption coefficient; hν; the photon energy, E_g; the energy gap and A; the constant depending on the type of transition. Eq. (1) can be rearranged and written in the form

$$(\alpha h\upsilon)^2 = A^2 (h\upsilon - E_g) \text{-----(2)}$$

From the Eq. (2) αhν=0 and E_g=hν.

The plot of $(\alpha h\nu)^2$ versus hν was utilized to get energy band gap of Ag NPs. The energy gap (E_g) values of 2.21 eV, 2.23 eV, 1.95 eV, 2.06 eV, 2.17 eV and 2.05 eV were deduced for A1, A2, A3, A4, A5 and A6 nanoparticles, respectively.

The synthesised Cu NPs (C1, C2, C3, C4, C5 and C6) have been characterized by all the advanced techniques visible, UV-DRS, XRD, FTIR, TGA-DTA, SEM-EDAX, TEM-HRTEM and SAED to explore their composition, bonding, structural and morphological features. The synthesis of C1 NPs was successful by the application of PE1 (*Vernonia amygdalina Del.* Plant leaf extract) extract to reduce and cap copper ions to copper. The tannins, anthraquinone glycosides, cardiac glycosides and phenols were found in PE1 extract during the phytochemical analysis. The list of the phytochemicals present in the extract are as given in Table 6. These phytoconstituents are expected to a play role as reducing agents, stabilizing agents, capping agents or chelating agents in the formation of NPs. Three steps involved in the origin of NPs includes: reduction of metal ions, formation of cluster and growth of nanoparticles. Polyphenols are believed to undergo tautomeric enol-keto transformation to release the reactive hydrogen atomic species which play the role of converting copper ions to copper nanoclusters / nanoparticles. In addition, the enzymes of PE1 extract also assist copper ions to get reduced and form protein capped copper NPs. It is also natural to know that that the phenolic compounds act as organic ligand and assist in the reduction of copper ions to form copper NPs and later converted to CuO NPs. In this case the stability of copper NPs was considerably lower and hence results in the consequent oxidation to CuO NPs possibly due to the presence of varieties of biomolecules at higher concentration. The UV-visible absorbance spectrum of instantaneously synthesised VeA-

CuO NPs revealed λmax of 412 as shown in Figure 8a, just after 10 min of mixing plant extract with copper nitrate solution.

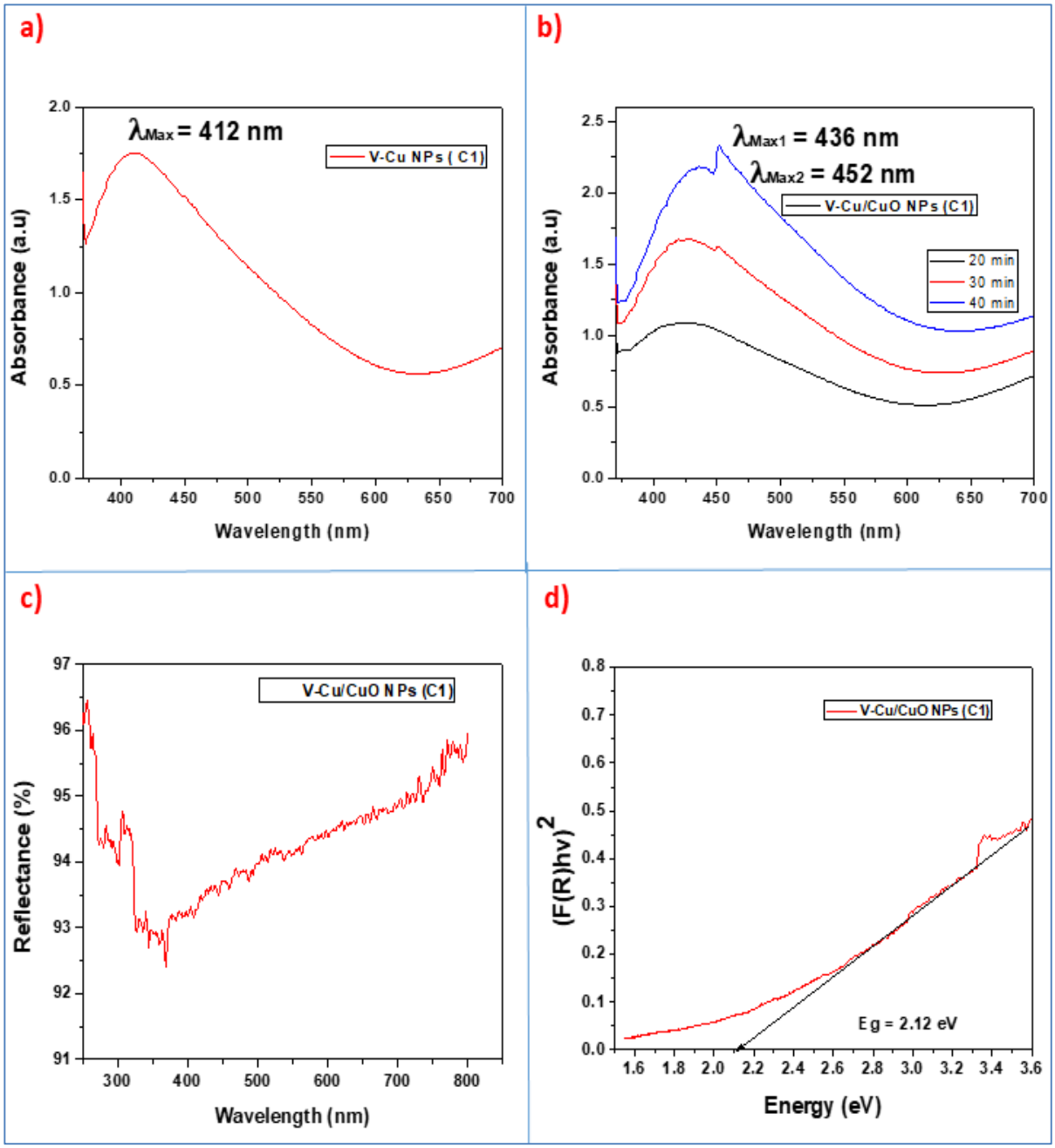

Figure 8. (a) and (b) The absorbance spectrum of C1 (Cu/CuO) NPs at different time intervals (c) UV-DRS spectrum of C1 Cu/CuO) NPs. (d) Tauc plot of C1 (Cu/CuO) NPs (yielding E_g Value).

The absorbance spectrum recorded after 40 minutes of forming homogeneous mixture, exhibited 2 maxima, one λmax at 436 nm and the other at λmax of 452 nm (Figure 8b). The splitting of absorbance band into two, clearly affirm the formation of CuO nanoparticles

with different morphological features. The presence of two maxima clearly substantiates a mixture of differently shaped and sized Cu and CuO NPs.

Almost identical results were observed during the analysis of synthesized CuO NPs by the application of *Zingiber and Allium sp*. (Yaqub et al. 2020)and *Psidiumguajava* (Singha et al. 2020), leaves extract. The surface plasmon absorbance presents a set of different λmax values for NPs synthesised using different plant extracts which is possibly due to morphological features of the NPs. The UV-visible-DRS spectrum was recorded (Figure 8c) for NPs. The Tauc plot (Figure 8d) was utilized to compute the band gap energy of CuO NPs with the assistance of Kubelka-Munk function. The energy gap (E_g) of 2.12 eV was deduced for CuO NPs.

The UV-visible absorbance spectrum recorded for H-Cu NPs (C2) exhibited λ_{max} of 403 as shown in Figure 9a. The surface plasmon absorbance basically depends on the size of NPs and hence every researcher reports a different λmax value for NPs synthesised using different plant extracts. Similarly, the UV-visible diffused reflectance spectrum was recorded (Figure 9c). The band gap energies of all the NPs were evaluated using Tauc plot as shown in Figure 9b by using the data obtained in reflectance spectra utilizing Kubelka-Munk function. The band gap values of all the samples has been presented in the Figure 9c.

The UV-visible absorbance spectrum of instantaneously synthesised Cu NPs (C3 and C4) using *Artemisia absinthium L.* leaf extract and *Carum copticum* seed extract revealed λ_{max} values of 414 nm and 421 nm respectively. The E-Cu NPs (C5) synthesised by using the root extract of *Echinops Sp.* plant were subjected to characterization. The alkaloids, tannins, flavonoids and terpenoids were found in *Echinops Sp.* plant *root extract* (PE5) during the phytochemical analysis.

The UV-visible absorbance spectrum of instantaneously synthesised E-Cu NPs revealed λmax of 441 nm as shown in Figure 10a, just after 10 min of mixing plant extract with copper nitrate solution. The absorbance spectrum recorded after 20, 30, 40, 50 and 60 minutes of forming homogeneous mixture, exhibited identical absorbance bands at λmax of 441 nm (Figure 10b).

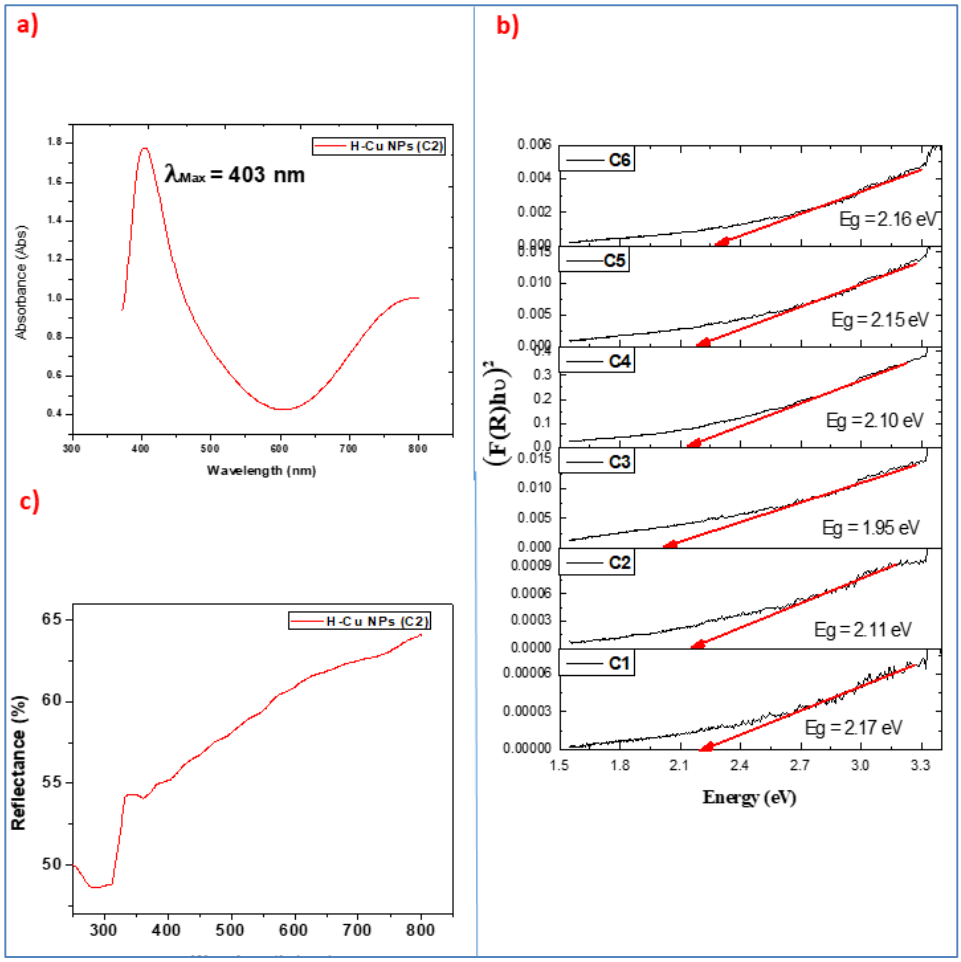

Figure 9. (a) UV-visible absorbance spectrum of H-Cu NPs (C2) (b) UV-visible diffused reflectance spectrum of H-Cu NPs (c) Tauc plot of H-Cu NPs showing its E_g Value (d) XRD diffraction pattern of H-Cu NPs.

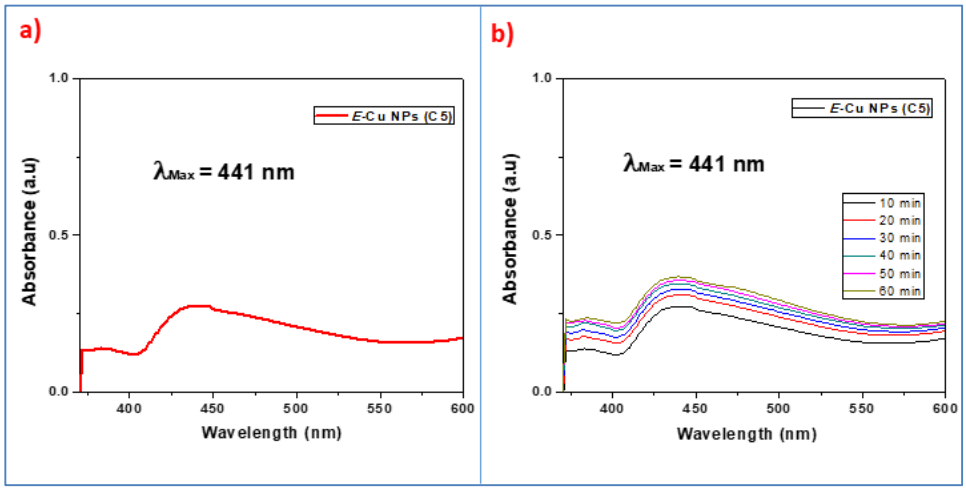

Figure 10. (a) and (b) The absorbance spectrum of *E*-Cu NPs (C5) at different time intervals.

The leaf extract of *Syzygium guineense* plant (PE6) was applied to synthesize Cu NPs but finally resulting nanomaterial was proved to be CuO NPs. The biomolecules present in the extract were alkaloids, phenolic compounds, tannins, saponins, anthraquinone glycosides and cardiac glycosides. The UV-visible absorbance spectrum recorded for instantaneously synthesised S-CuO NPs (C6) exhibited λmax of 423 as shown in Figure 11a, just after 10 min of mixing plant extract with copper nitrate solution. This absorption band is basically due to surface plasmon resonance of S-CuO NPs. The absorbance spectrum recorded after 40 minutes of forming homogeneous mixture, exhibited 2 maxima, one λmax at 423 nm and the other at λmax of 451 nm (Figure 11b).

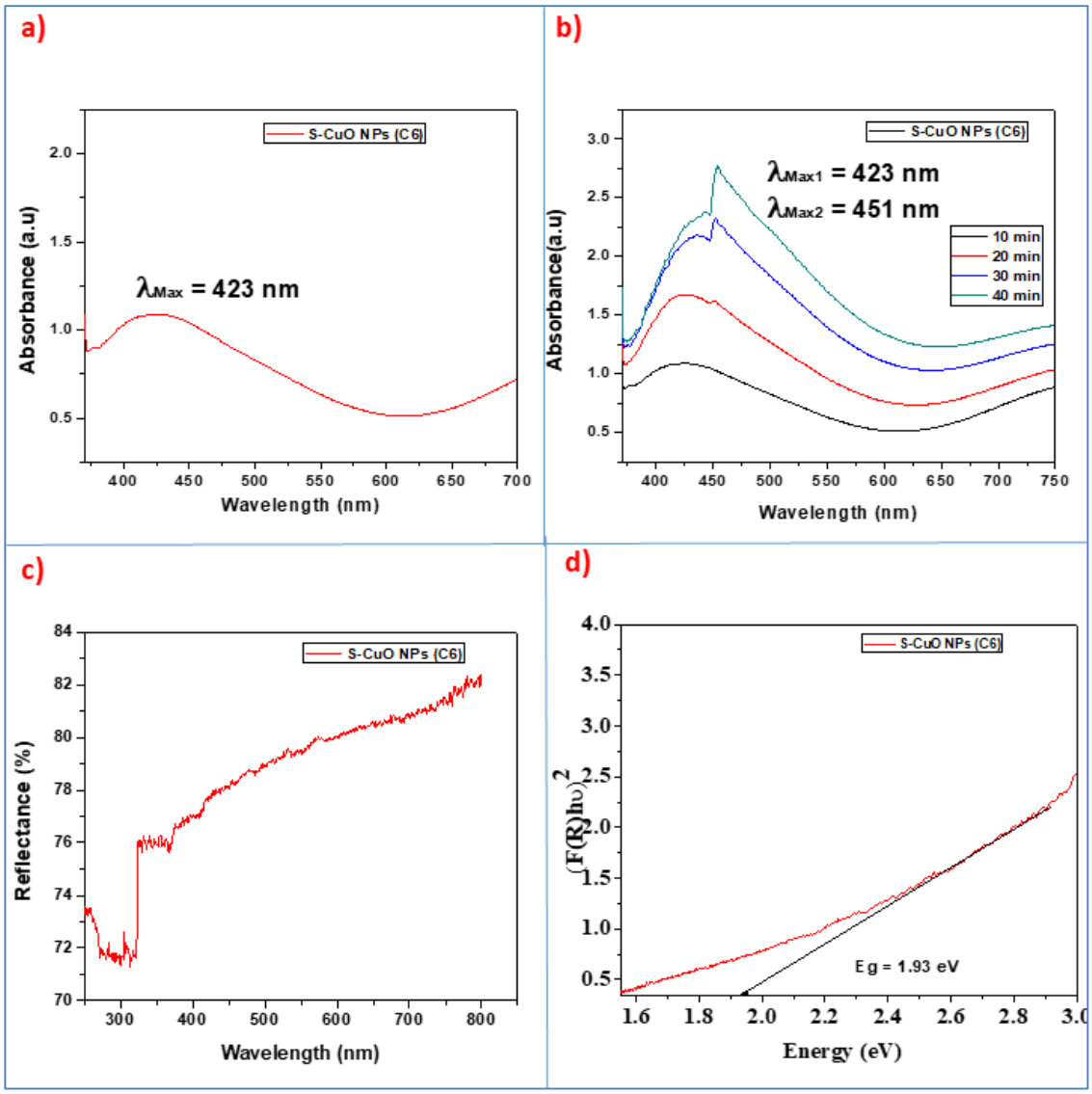

Figure 11. (a) and (b) UV-visible absorbance spectrum of S-CuO NPs (C6) at different time intervals (c) UV-visible diffused reflectance spectrum of S-CuO NPs (C6). (c) Tauc plot of S-CuO NPs (C6) showing E_g Value.

Similarly, the UV-visible diffused reflectance spectrum was recorded (Figure 51c). The band gap energy of S-CuO NSs obtained by Tauc plot using the data obtained in reflectance spectra utilizing Kubelka-Munk function is as shown in Figure 11d. The band gap energy, E_g of S-CuO NPs was found to be 1.93 eV.

4.2. FT-IR analysis of Ag and Cu/CuO NPs

The FTIR spectroscopy was helpful in revealing the bonding features of both the plant extract (*Vernonia amygdalina*) and Ag-NPs (A1). The intense peaks shown in Figure 12 a, respectively at 3375 cm^{-1} and 1262 cm^{-1} corresponds to phenolic –OH stretching and bending vibrational frequencies (Salmen and Alharbi 2020).

The peak at 1650 cm^{-1} arises due to C=O vibration of ketonic groups (Nzekekwu and Abosede 2019). The small peak at 2925 cm^{-1} was correlated to the alkane C−H stretching mode (Widyaningtyas et al. 2019). The vibration of −COO group of carboxylic acid was found to appear at 1405 cm^{-1} (Azarbani and Shiravand 2020).

A less intense band at around 875 cm^{-1} confirms the presence of glycosidic linkage. The presence of prominent peaks at 3375 cm^{-1}, 1650 cm^{-1}, 1405 cm^{-1}, 875 cm^{-1} and 615 cm^{-1} in the FTIR spectra of both plant extract and NSs, clearly indicate the presence of bioactive molecules around the NPs. These bioactive molecules had been confirmed to have performed a sizable function in the nucleation and growth of V-Ag NPs.

The C-O-C vibration displays at 1068 cm^{-1}. The bending vibrations of Ag–O–H bonds resulted in a small peak at 896 cm^{-1} which is possibly due to Ag–O bond (Dessie et al. 2020). A peak at 615 cm^{-1} correlates to bending vibrations of C–H bond. FTIR spectral inspection confirmed the presence of phytochemicals (phenolics, tannins, glycosides and proteins) in plant extract and their roles as reducing agent and stabilizing agent during the synthesis of V-Ag NPs. Especially, the phenolics were reported to be strong candidates for binding with Ag NPs (Mat Yusuf et al. 2020).

The FTIR spectrum, as shown in Figure 12 b, clearly demonstrates, less intense peak for A2 sample, corroborating weak surface amalgamation of biomolecules of PE2 extract with H-Ag NPs. But in case of A3 (Figure 12c) and A4 (Figure 12d) samples, the spectra appear to exhibit the similar trends as observed for A1 sample. The intense peaks shown in Figure 12e, respectively at 3395 cm^{-1} corresponds to–OH stretching frequencies.

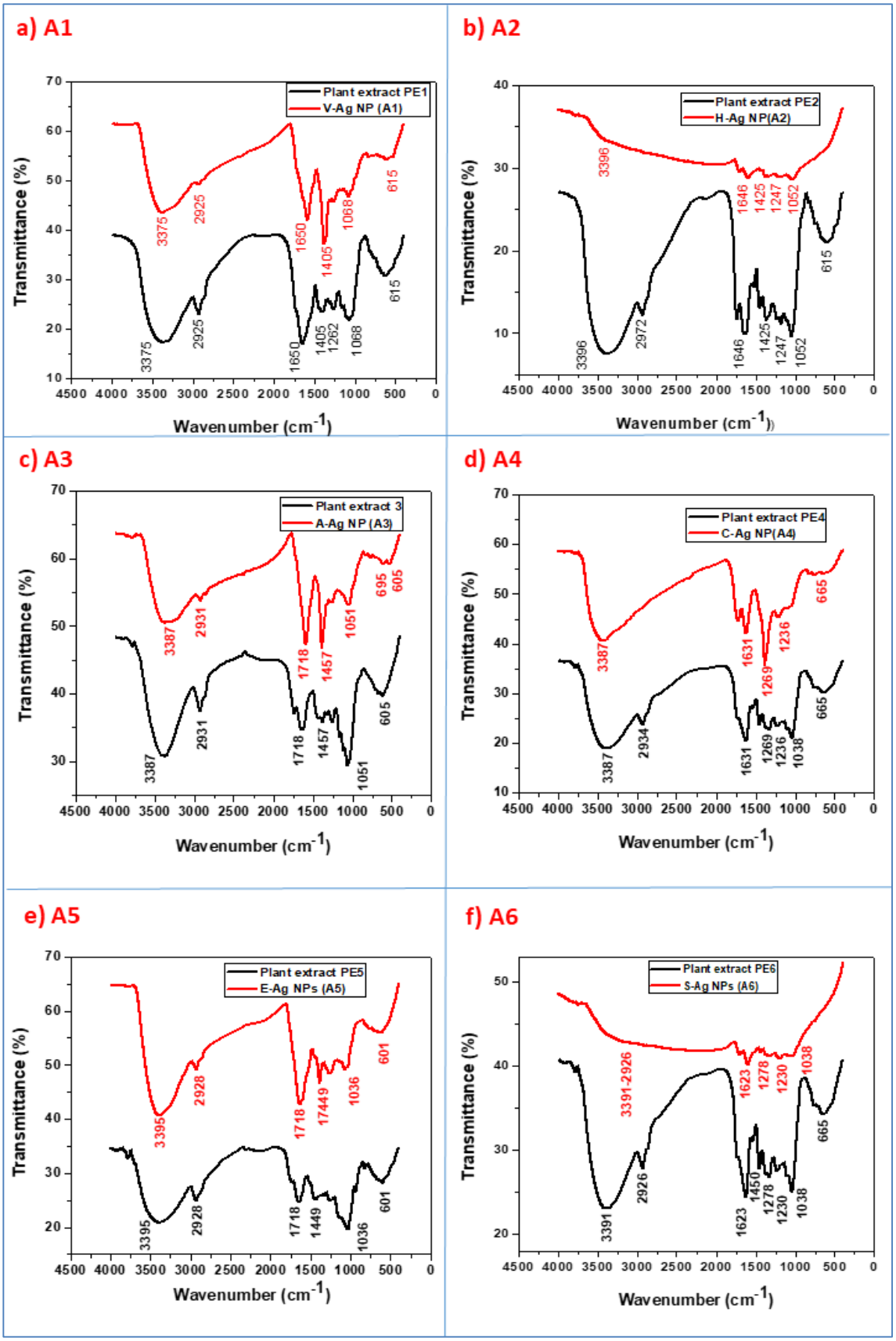

Figure 12. The FTIR spectra of plant extracts (PE1, PE2, PE3, PE4, PE5 and PE6) and Ag-NPs (A1, A2, A3, A4, A5 and A6).

The peak at 1718 cm^{-1} arises due to C=O vibration of ketonic groups. The small peak at 2925 cm^{-1} was correlated to the alkane C−H stretching mode. The vibration of −COO group of carboxylic acid was found to appear at 1449 cm^{-1}. A moderately intense band at around 1035 cm^{-1} confirms the stretching of C-O-C bond. The presence of prominent peaks at 3395 cm^{-1}, 1718 cm^{-1}, 1449 cm^{-1}, 1035 cm^{-1} and 601 cm^{-1} in the FTIR spectra of both plant root extract and NPs, clearly indicate the presence of bioactive molecules around the NPs. These bioactive molecules had been confirmed to have performed a sizable function in the nucleation and growth of *E*-Ag NPs. The bending vibrations of Ag–O–H bonds resulted in a small peak at 601 cm^{-1} which is possibly due to Ag–O bond. The FTIR spectra of plant extract PE6 and *A6* Ag NPs is presented in Figure 12f. FTIR spectra confirmed the presence of biomolecules in the extract and NPs. The broad peaks appeared in the region between 3391 and 2926 cm^{-1} corresponds to –OH stretching vibration and sp^3 C-H stretching vibrations, respectively. The peak at 1623 cm^{-1} corresponds to C=O stretching of carbonyl groups. The sharp peak around 1450 cm^{-1} shows the presence of −COO group of carboxylic acid. It is also believed that the amine and carboxylate group present in the PE6 plant leaf extract responsible for the binding of proteins with the surface of Ag and thereby leading to the stabilization of the biosynthesized nanoparticles.

The peaks represented by 1350 cm^{-1} shows C-N stretching of amide. The medium peak at 1160 cm^{-1} corresponds to C-O stretching of phenolic compounds. The C-O-C stretching appears at 1038 cm^{-1}. The bending vibrations of Ag–O–H bonds resulted in a small peak at 800 cm^{-1} which can be attributed to the presence of the Ag–O bond. The last peak at 665 cm^{-1} corresponds to bending modes of vibrations of C–H bond. The small shift in the IR bands indicates the possible reaction of silver ions and synthesis of nanoparticles in the extract. FTIR analysis results confirmed the presence of various phytochemicals of plant extracts such as alkaloids, phenolic compounds, tannins, saponins, anthraquinone glycosides and cardiac glycosides involved in the synthesis of Ag NPs. This provides the effective role of phytoconstituents in the process of reduction of silver ions and stabilization silver NPs.

The FTIR spectroscopy was helpful in revealing the bonding features of both PE1 extract and V-CuO NPs. The intense peaks shown in Figure 13, respectively at 3375 cm^{-1} and 1262 cm^{-1} corresponds to phenolic –OH stretching and bending vibrational frequencies. The peak at 1650 cm^{-1} arises due to C=O vibration of ketonic groups. The small peak at

2925 cm^{-1} was correlated to the alkane C−H stretching mode. The vibration of −COO group of carboxylic acid was found to appear at 1405 cm^{-1}.

A less intense band at around 875 cm^{-1} confirms the presence of glycosidic linkage. An intense peak at 615 cm^{-1} substantiates the formation of CuO and its stretching (Zaman et al. 2020). The presence of prominent peaks at 3375 cm^{-1}, 1650 cm^{-1}, 1405 cm^{-1} and 875 cm^{-1} in the FTIR spectra of both plant extract and NPs, clearly indicate the presence of bioactive molecules around the NPs. These bioactive molecules had been confirmed to have performed a sizable function in the nucleation and growth of V-CuO NPs.

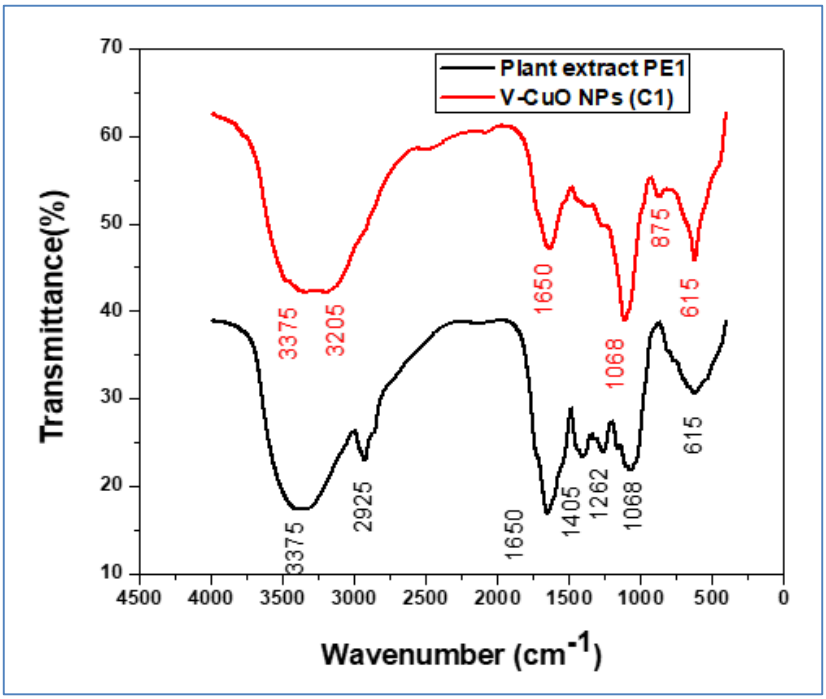

Figure 13. The FTIR spectra of PE1 plant extract and V-CuO NPs (C1)

The C-O-C vibration displays at 1068 cm^{-1}. The bending vibrations of Cu–O–H bonds resulted in a small peak at 896 cm^{-1} which is possibly due to Cu–O bond. A peak at 615 cm^{-1} correlates to bending vibrations of C–H bond. FTIR spectral inspection confirmed the presence of phytochemicals (phenolics, tannins, glycosides and proteins) in plant extract and their roles as reducing agent and stabilizing agent during the synthesis of V-CuO NPs. The FTIR spectra of H-Cu NPs (C2) showed peaks at 3351, 3284, 2920, 2350, 1720, 1625, 1342, 1160, 1058, 740 and 590 cm^{-1} (Figure 14). From those indicated peaks, the broad absorption peaks of Cu NPs observed at 3351 cm^{-1} and 3254 cm^{-1} represents the presence of higher concentration of alcohols, with O-H stretches and N-H stretches of amines (Ghosh et al. 2020).

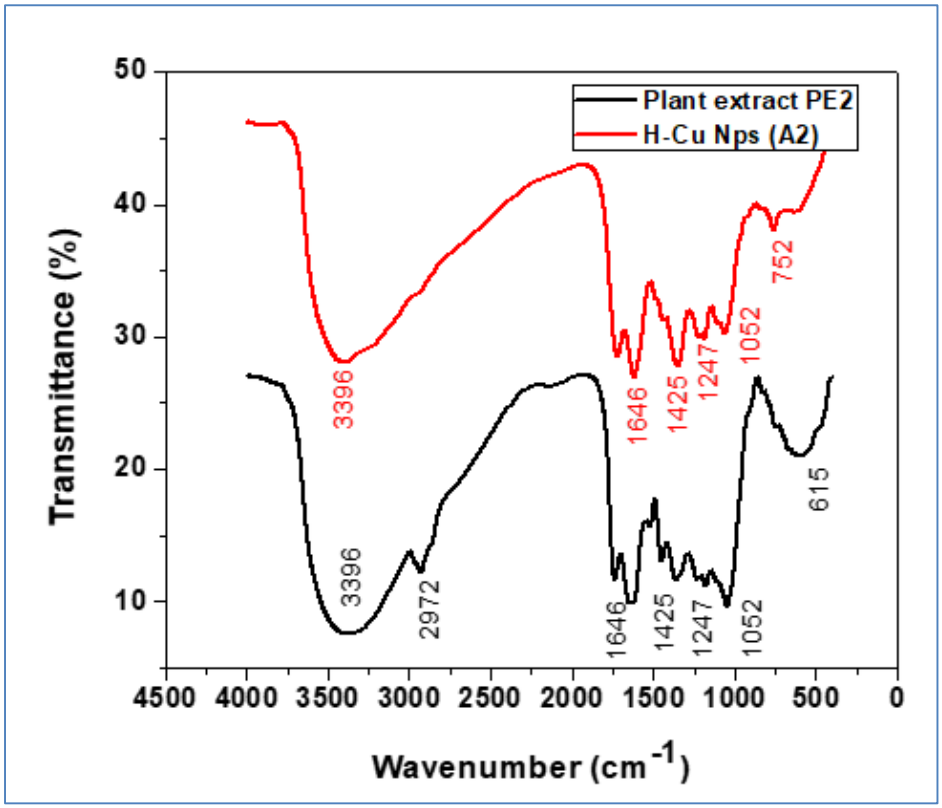

Figure 14. The FTIR spectra of *Hagenia abyssinica* plant extract and H-Cu NPs (C2).

The intense peaks shown at 2929.0 cm^{-1} and 2890.6 cm^{-1} corresponds to asymmetric C–H stretching of $–CH_2$ and $–CH_3$ groups respectively. The presence of atmospheric CO_2 resulted in a stretching vibration located at wave number of 2350 cm^{-1}. It is also believed that the amine and carboxylate group present in the leaf extract of *Hagenia abyssinica* responsible for the binding of proteins with the surface of Cu and thereby leading to the stabilization of the biosynthesized nanoparticles. The absorption peaks represented at 1720 cm^{-1} and 1625 cm^{-1} indicates the presence of C=O and C=C bending mode of vibrations. The peaks represented by 1350 cm^{-1} shows C-N stretching of amide. The medium peak at 1160 cm^{-1} corresponds to C-O stretching of phenolic compounds. The C-O-C stretching appears at 1058 cm^{-1}. The last peak at 590 corresponds to bending modes of vibrations of C–H bond. In addition to this, the FTIR spectrum of Cu NPs shows peaks corresponding to the broad band centered at 752 cm^{-1} which represents a characteristic peak believed to be due to interaction of Cu with biomolecules of extract.

The FT-IR spectra of instantaneously synthesised Cu NPs (C3 and C4) using *Artemisia absinthium L.* leaf extract and *Carum copticum* seed extract also revealed almost identical results and hence not reproduced here. The FT-IR spectra of E-Cu NPs (C5) is as shown in Figure 15. The FTIR spectroscopy was helpful in revealing the bonding

features of both extract and Cu NPs. The intense peaks shown in Figure 15, respectively at 3379 cm^{-1} corresponds to–OH stretching frequencies. The peak at 1709 cm^{-1} arises due to C=O vibration of ketonic groups. The small peak at 2934 cm^{-1} was correlated to the alkane C−H stretching mode. The vibration of −COO group of carboxylic acid was found to appear at 1456 cm^{-1}. A moderately intense band at around 1039 cm^{-1} confirms the stretching of C-O-C bond. The presence of prominent peaks at 3379 cm^{-1}, 1709 cm^{-1}, 1456 cm^{-1}, 1039 cm^{-1} and 601 cm^{-1} in the FTIR spectra of both plant root extract and NPs, clearly indicate the presence of bioactive molecules around the NPs.

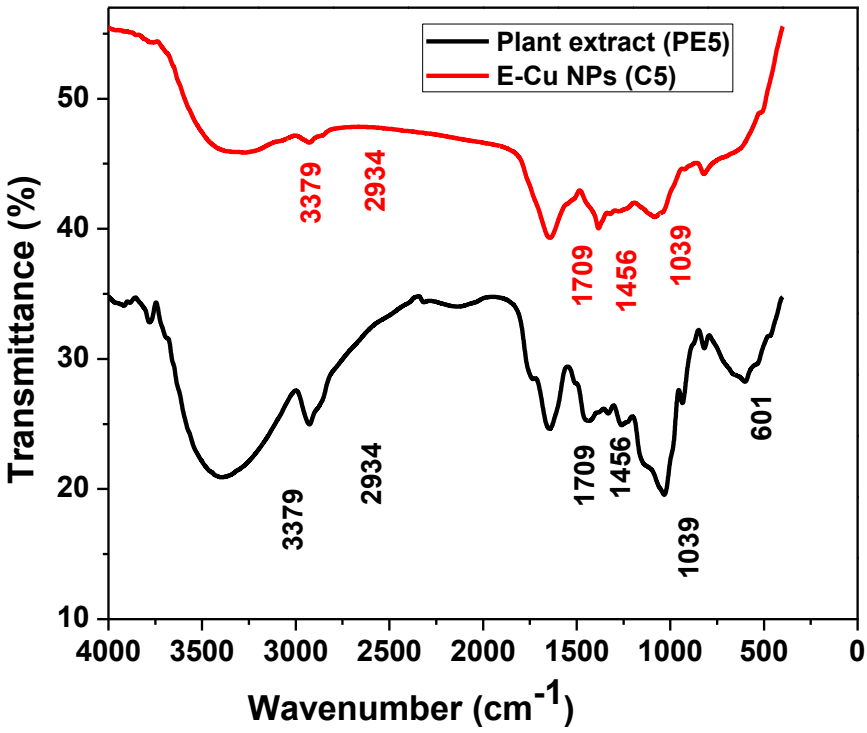

Figure 15. The FT-IR spectra of E-Cu NPs (C5)

These bioactive molecules had been confirmed to have performed a sizable function in the nucleation and growth of *E*-Cu NPs. The bending vibrations of Cu–O–H bonds resulted in a small peak at 601 cm^{-1} which is possibly due to Cu–O bond. FTIR spectral inspection confirmed the presence of phytochemicals (phenolics, tannins, glycosides and proteins) in extract and their roles as reducing agent and stabilizing agent during the synthesis of *E-Cu* NPs. Especially the phenolics were reported to be strong candidates for binding with copper NPs. The FTIR spectra of PE6 plant extract and S-CuO NPs are shown in Figure 16. The intense peaks shown at 3391 cm^{-1} 1278 cm^{-1} and 1230 cm^{-1} corresponds to phenolic –OH stretching and bending vibrations.

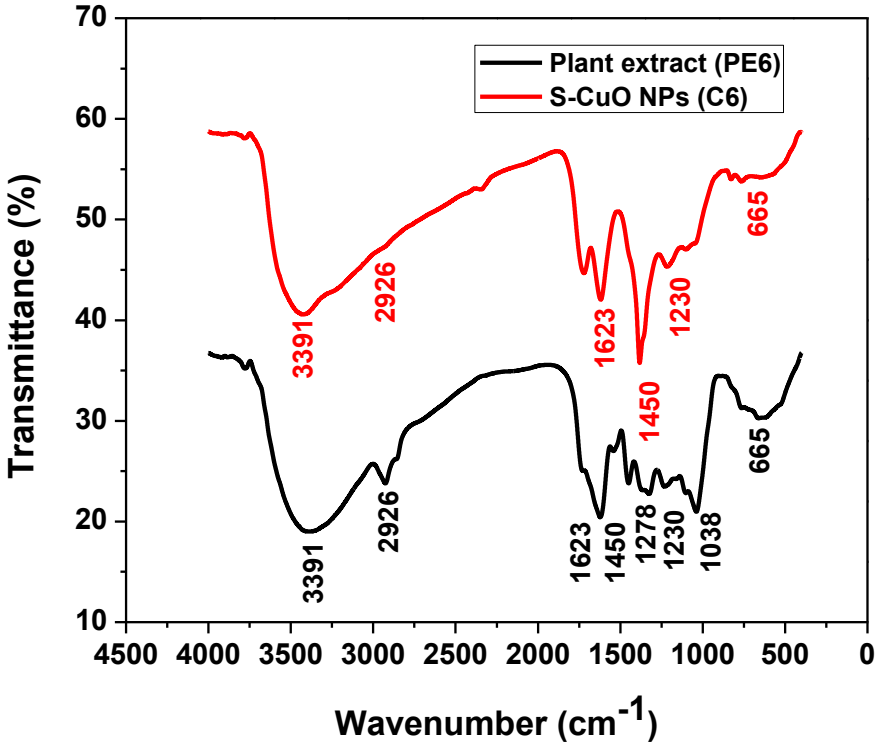

Figure 16. The FT-IR spectra of S-CuO NPs (C6)

The FTIR analysis results confirmed the presence of various phytochemicals of Syzygium guineense leaf extract such as phenolics, tannins, glycosides and proteins which played the roles of reducing agent and stabilizing agent during the synthesis of S-CuO NPs.

4.3. XRD analysis of Ag and Cu/CuO NPs

The XRD analysis was executed to explore the in-depth details of crystal structure of Ag NPs. The XRD spectrum of Ag NPs (Figure 17) demonstrates a total of 4 prominent peaks. These peaks with 2θ values of 38.14º, 44.7º, 64.50º, and 77.42º conform to 111, 200, 220 and 311 crystal lattice planes of silver (face centred cubic structure) and the diffraction data is in compliance with the data of ICSD card No. 004-7383 (Fm3m) (Sadeghi and Gholamhoseinpoor 2015). The Ag NPs (A2, A3, A4, and A5) synthesised by using all the other plant extracts too exhibited highly crystalline nature with fcc lattice structure. Figure 18 presents the XRD pattern of Ag NPs obtained using PE2, PE3, PE4 and PE5 plant extracts. Unlike the XRD pattern of A1, the XRD patterns of A2, A3, A4 and A5 exhibited two additional peaks at 2θ values of 27º and 32º which is reported to

be due to the crystallization of plant metabolite on the surface of the Ag NPs (Pirtarighat et al. 2019). The yiled of A6 Ag NP obtained after the synthesis was very less and hence its XRD is not presented as large amount of sampe is needed to record the XRD diffractogram.

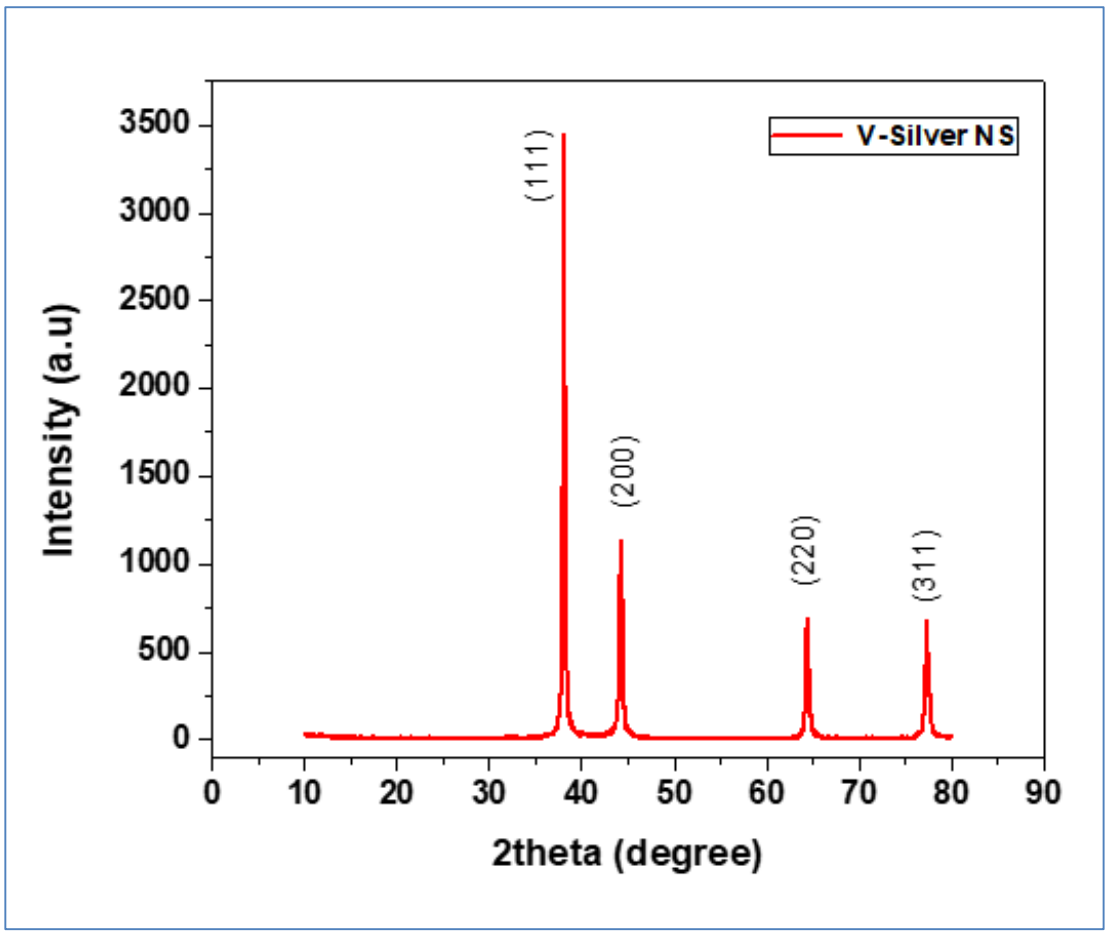

Figure 17. The XRD pattern of V-Ag NPs (A1).

The XRD analysis was executed to explore the in-depth details of crystal structure of V-CuO NPs (C1). The XRD spectrum of V-CuO NPs (Figure 19) demonstrates a total of 11 prominent peaks (Udayabhanu et al. 2015) (Hussain et al. 2019). The peaks at 2θ values of 32.46°, 35.52°, 38.73°, 48.81°, 53.42°, 58.01°, 61.53°, 66.09° 67.98°, 72.48° and 75.13° correlates to (110), (002), (111), (20-2), (020), (202), (11-3), (31-1), (113) and (400) planes of CuO (fcc) (ICSD card No. 00-048-1548, Tenorite-C2/c) (Fuku et al. 2020). This confirms the formation of crystalline CuO from the plant extract via green synthetic route. It has been observed usually during the environment friendly biosynthesis of copper nanoparticles that the rapid oxidation in air yield CuO (Rabiee et

al. 2020)(Sánchez-Sanhueza et al. 2016). It is believed that, Cu and Cu_2O formed at the initial stages of biosynthesis would have oxidized on exposure to air after a longer period of time.

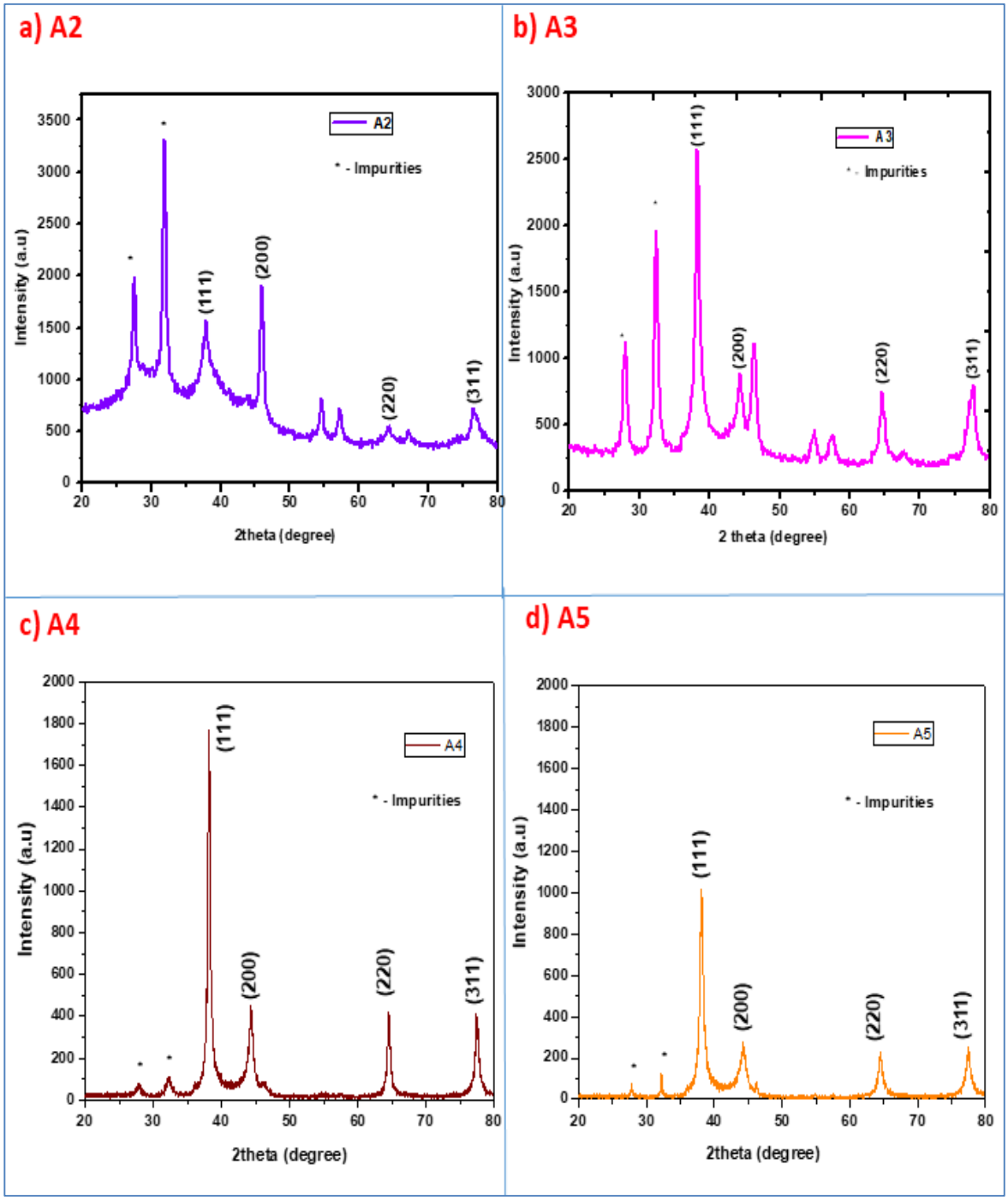

Figure 18. The XRD patterns of A2, A3, A4 and A5 Ag NPs.

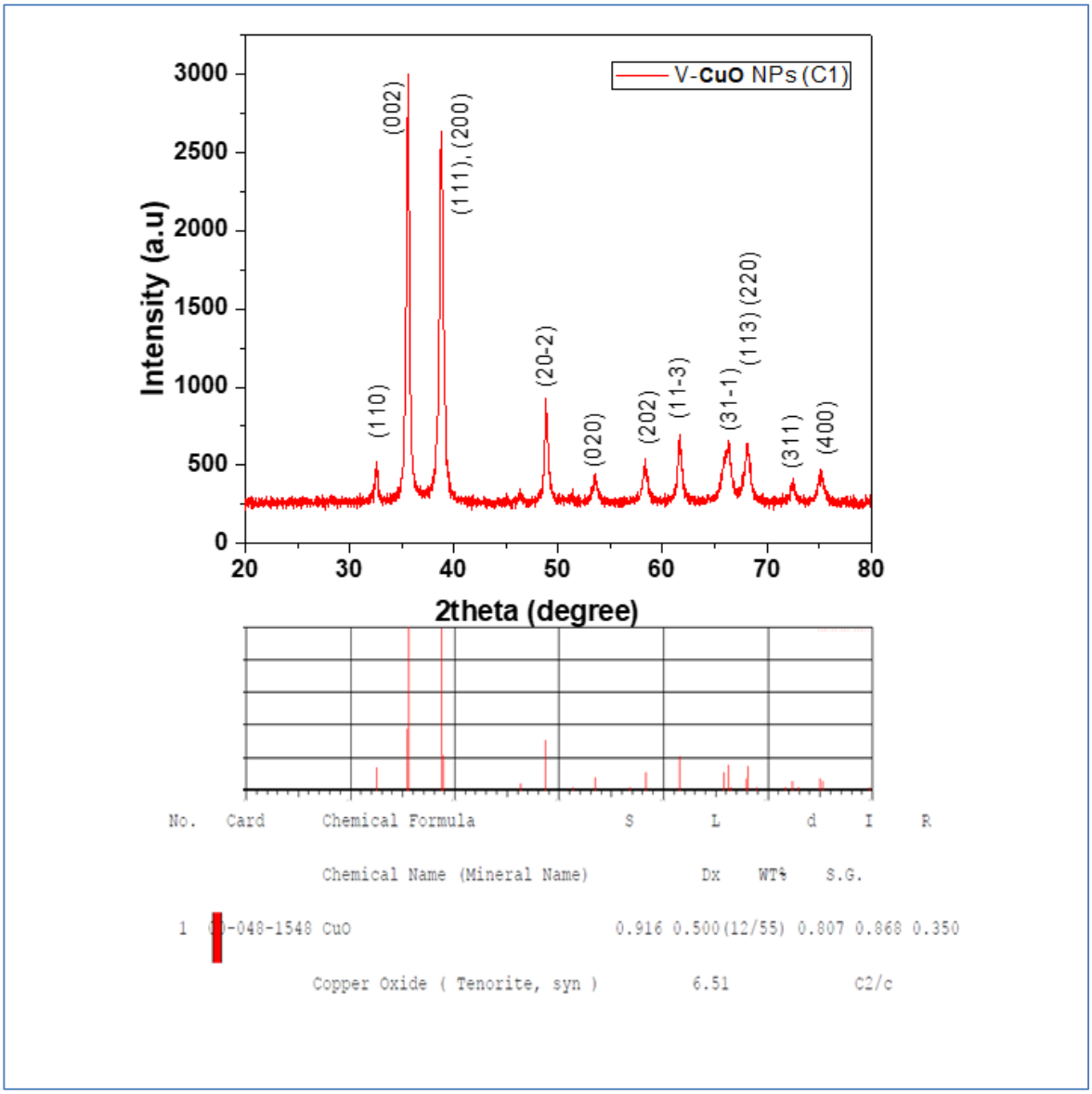

Figure 19. The XRD spectrum of V-CuO NPs (C1) with peak list.

The XRD diffraction patterns of C2 and C3 are presented in Figure 20a and b. The peaks observed in the pattern at 2θ values = 43º, 51º and 70º corresponds to (111), (200) and (220) lattice planes of face centred cubic structure of Cu NPs and the diffraction data were in good agreement with ICSD file No. 04-0836 (Khatami et al. 2017). The amount of Cu NPs obtained in the case PE4 plant extract was very less and hence XRD spectrum has not been recorded. The XRD analysis was executed to explore the in-depth details of crystalline nature of E-Cu NPs. The XRD spectrum of E-Cu NPs (C5) (Fig 20c) demonstrates a very weak broad band which signifies amorphous nature of NPs. But it can also be concluded that small percentage for Cu NPs formed may have crystalline nature otherwise XRD pattern would have been very much flat. It can be understood from the XRD results that the obtained Cu NPs were mostly amorphous signifying inefficiency

of the bioactive molecules to reduce and cap copper ions quickly. This is in consistent with results published by the researcher in the recent past (Ramyajuliet 2020).

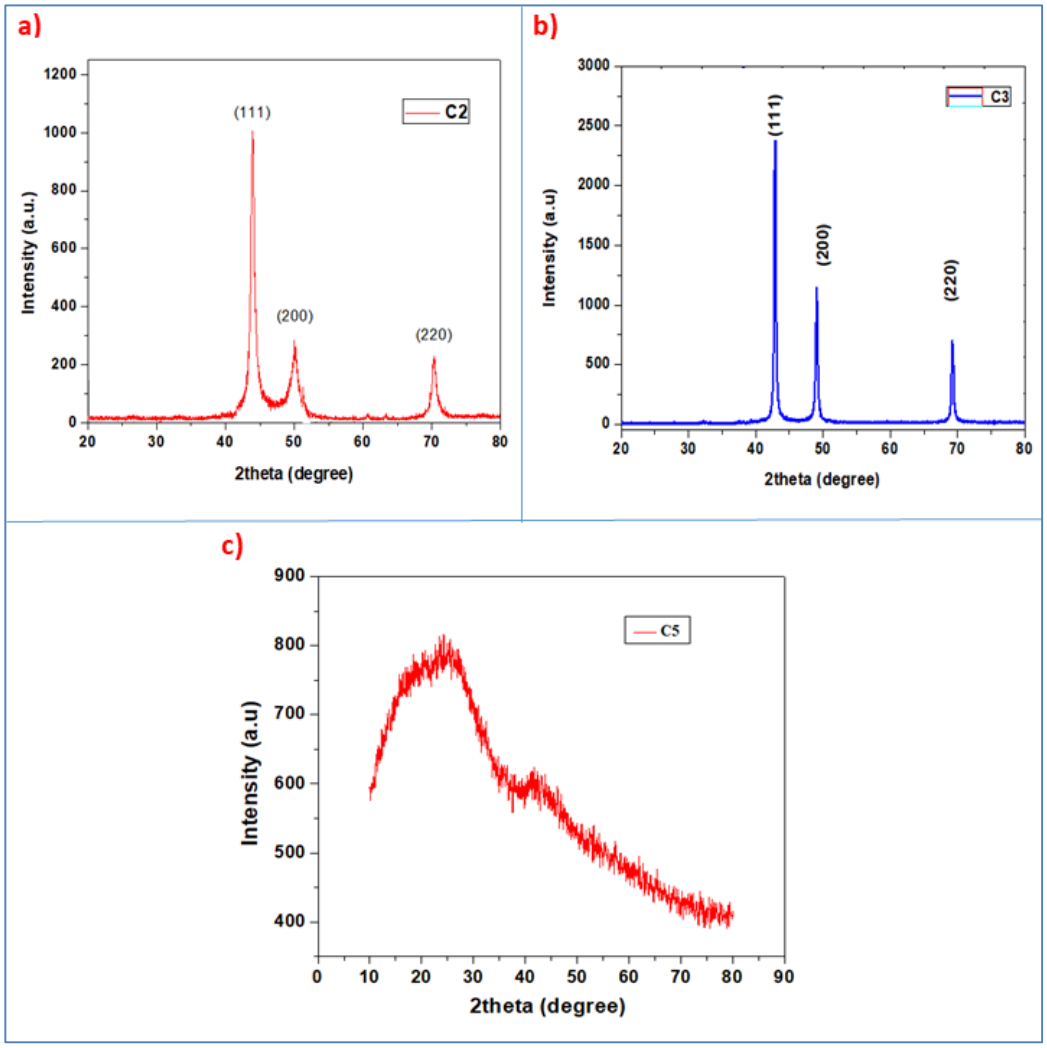

Figure 20. The XRD spectra of C2, C3 and C5 NPs.

4.4. TGA and DTA analysis of Ag, Cu/CuO NPs

Figure 21 presents the TGA-DTA curves for the thermal transformation of V-Ag NPs on heating from 0 to 800 °C under oxygen. The TGA curve revealed the two-step decomposition of Ag NPs, with the weight loss occurring in the temperature ranges of 30−180 ºC and 180−570 ºC. About 5 % weight loss was observed in the first temperature region due to usual water evaporation from the V-Ag NPs. Similarly, 2nd weight loss was recorded to an extent of 26 % corresponding to the decomposition of capped biomolecules on the NPs. The presence of different types of capped biomolecules around the Ag NPs is believed to be responsible for a single stage decomposition during TGA studies.

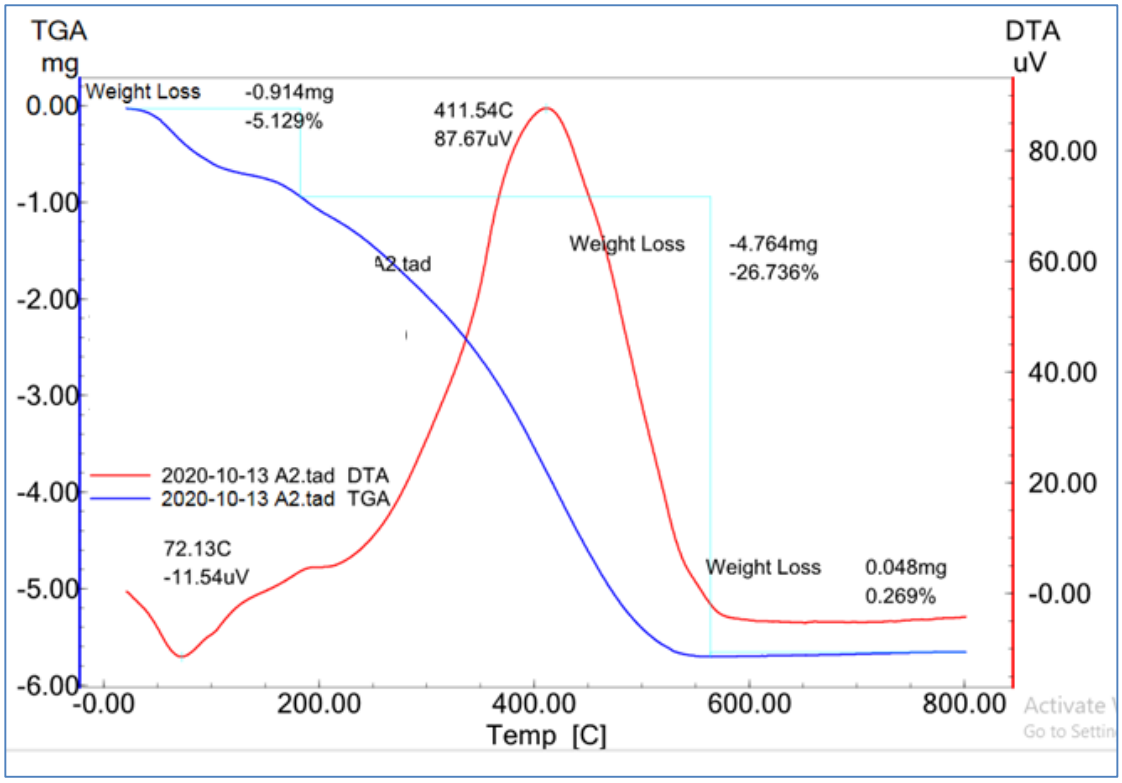

Figure 21. The TGA and DTA curves of V-Ag NPs (A1).

Figure 21 also shows a small endothermic DTA peak at the region of 72 °C, which corresponds to the first mass loss in the TGA curve. The second weight loss occurring in the temperature range between 180 and 570 ºC in TGA is associated with a prominent DTA exothermic peak at 411 °C. No significant weight loss is observed for V-Ag NPs after 570 ºC, confirming that the Ag NP is thermally stable above 570 ºC.

Figure 22 presents the TGA-DTA curves for the thermal transformation of V-CuO NPs on heating from 0 to 800 °C under oxygen. The TGA curve revealed the three-step decomposition of CuO NPs, with the weight loss occurring in the temperature ranges of 30−160 ºC, 160−270 ºC and 270−480 °C. About 16 % weight loss was observed in the first temperature region due to usual water evaporation from the NPs. Similarly, 2nd and 3rd weight losses were recorded to an extent of 17 % and 48 % corresponding to the decomposition of capped biomolecules on the NPs. The presence of different types of capped biomolecules are believed to be responsible for two stages of decomposition during TGA studies.

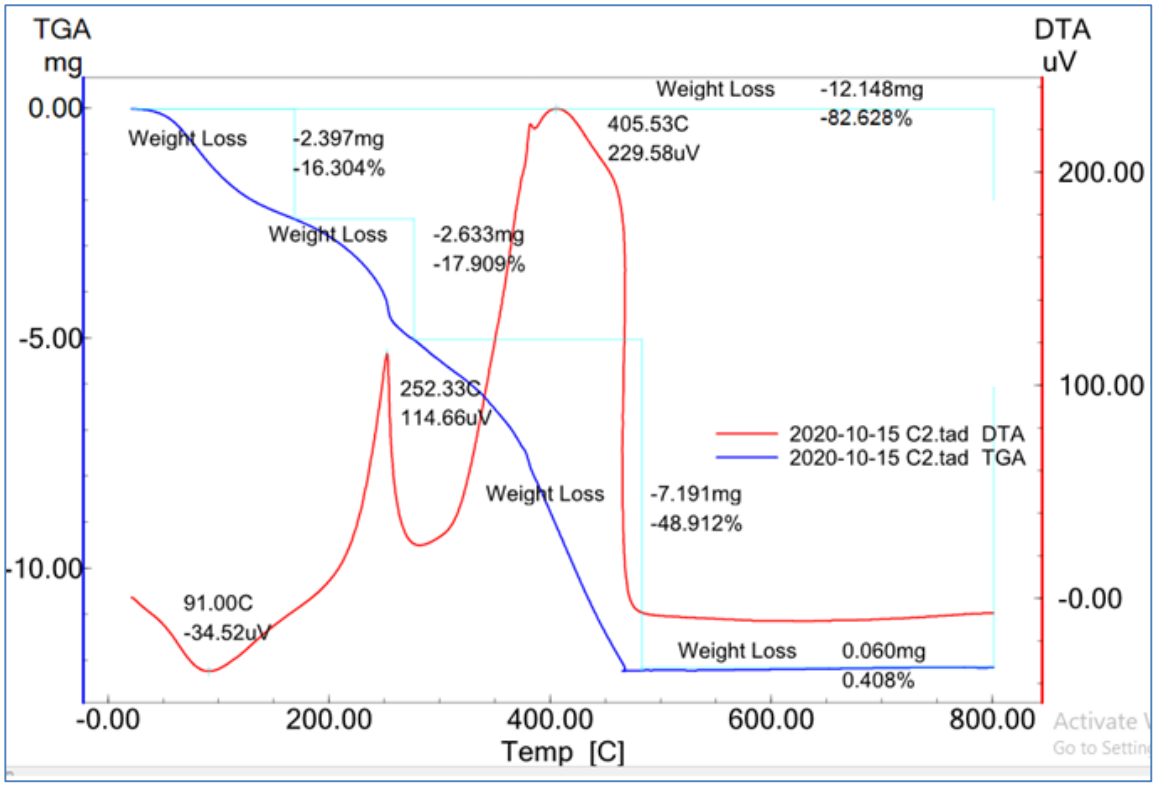

Figure 22. The TGA and DTA curves of V-CuO NPs (C1).

The first mass loss observed on TGA curve as shown in Figure 22 appeared as endothermic DTA peak at the region of 91 °C. The appearance of prominent DTA exothermic peak at 252 °C refers to the second weight loss occurred in the range between 160 and 270 °C in TGA. The third major weight loss of 48 % at 405 ^{o}C (DTA exothermic peak) corresponds to complete decomposition of bioorganic phytoconstituents present around CuO NPs.

4.5. *SEM-EDAX and TEM-HRTEM-SAED analysis*

The electron microscopy was applied to delve into the morphological features of Ag NPs. The SEM micrographs of NPs along with their EDAX spectra are presented as Figure 23, 24, 25, 26, 27 and 28 for A1, A2, A3, A4, A5 and A6 silver NPs, respectively.

The presence of mixed type of NPs is possibly due to the nature and amount of capping agents around the particles. The average particle size of Ag NPs was found to be in the range of 5–50 nm. Identical values were reported by the past researcher for silver NPs (Velgosova et al. 2019). The presence of less agglomerated Ag NPs due to high surface area yielded small sized particles. The Ag NPs were found to be as small as 5 nm in their

dimension which clearly confirms the efficient role of biomolecules as stabilizing agents preventing the growth of clusters of silver atoms to bigger nanoparticles.

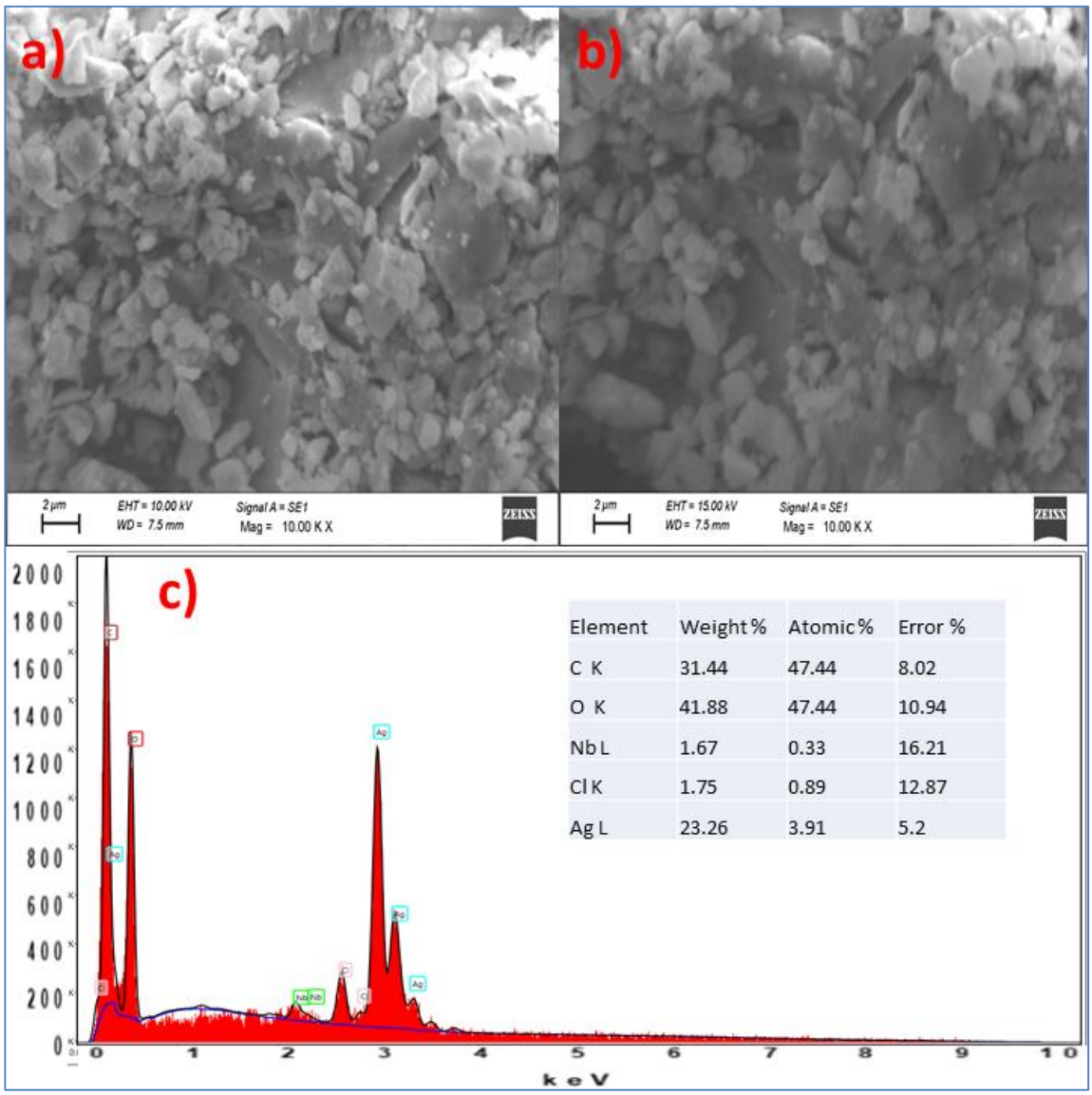

Figure 23. (a) and (b) SEM micrographs of A1 sample (c) EDAX spectrum of A1 sample.

EDAX analysis revealed the elemental composition of the V-Ag NPs as depicted in Figure 23c. The elements, Ag, C and Cl have been identified in the spectrum signifying the purity of the nanostructures and additional peak for Au appeared due to the usage of standard during the analysis.

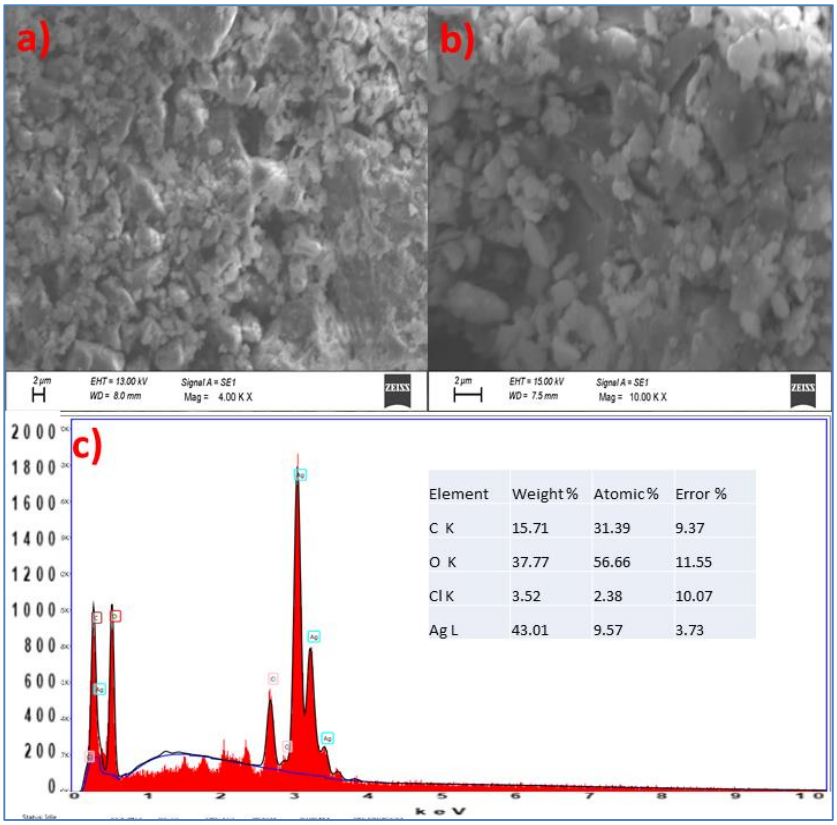

Figure 24. (a) and (b) SEM micrographs of A2 sample (c) EDAX spectrum of A2 sample.

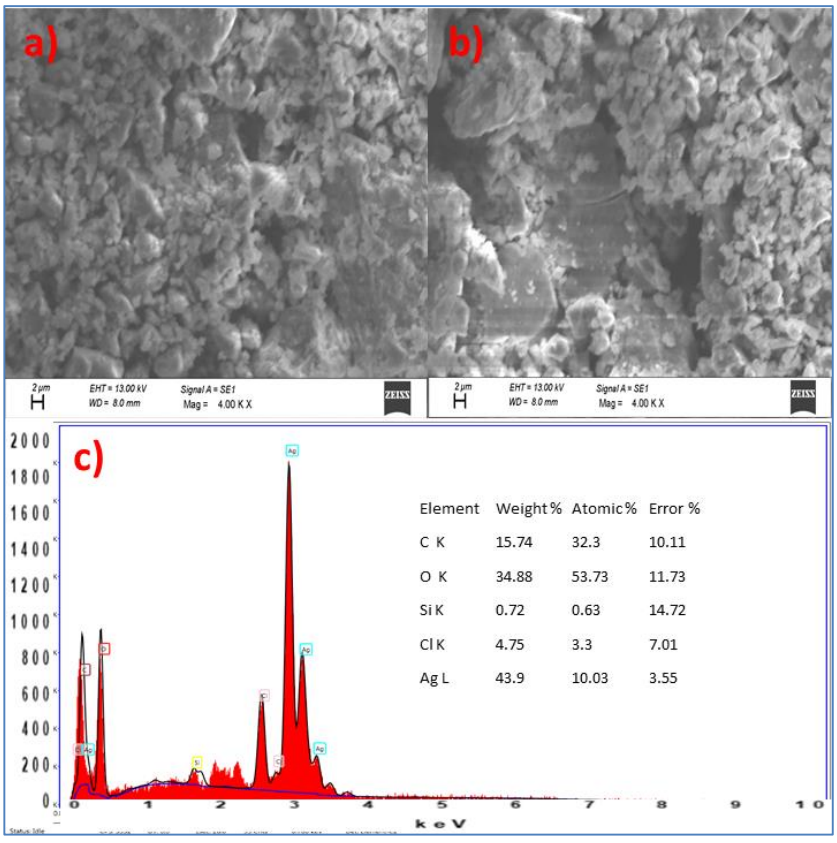

Figure 25. (a) and (b) SEM micrographs of A3 sample (c) EDAX spectrum of A3 sample.

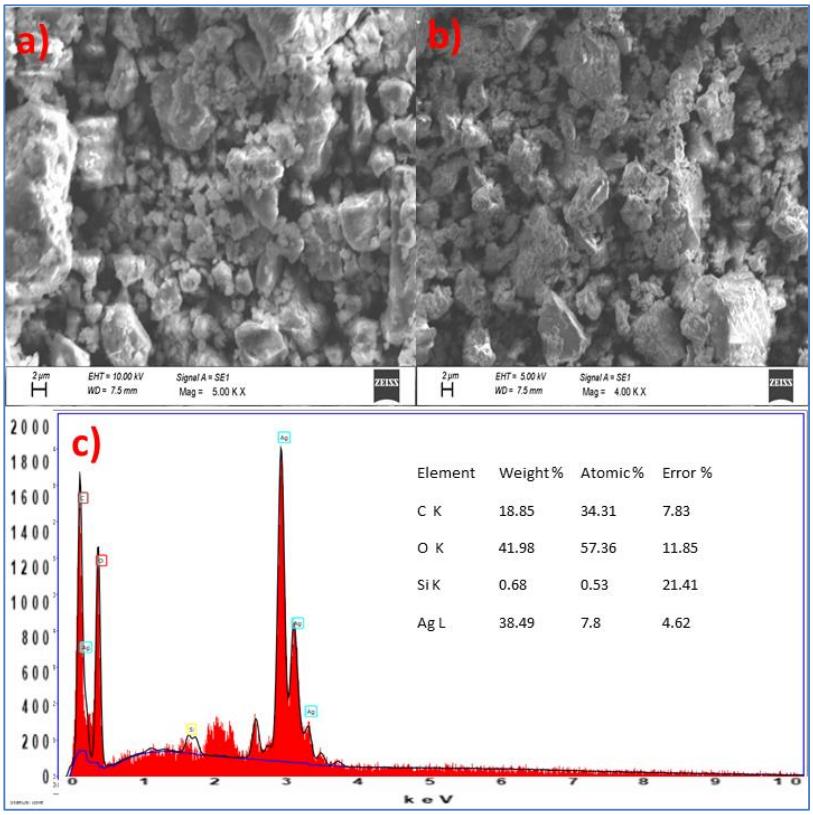

Figure 26. (a) and (b) SEM micrographs of A4 sample (c) EDAX spectrum of A4 sample.

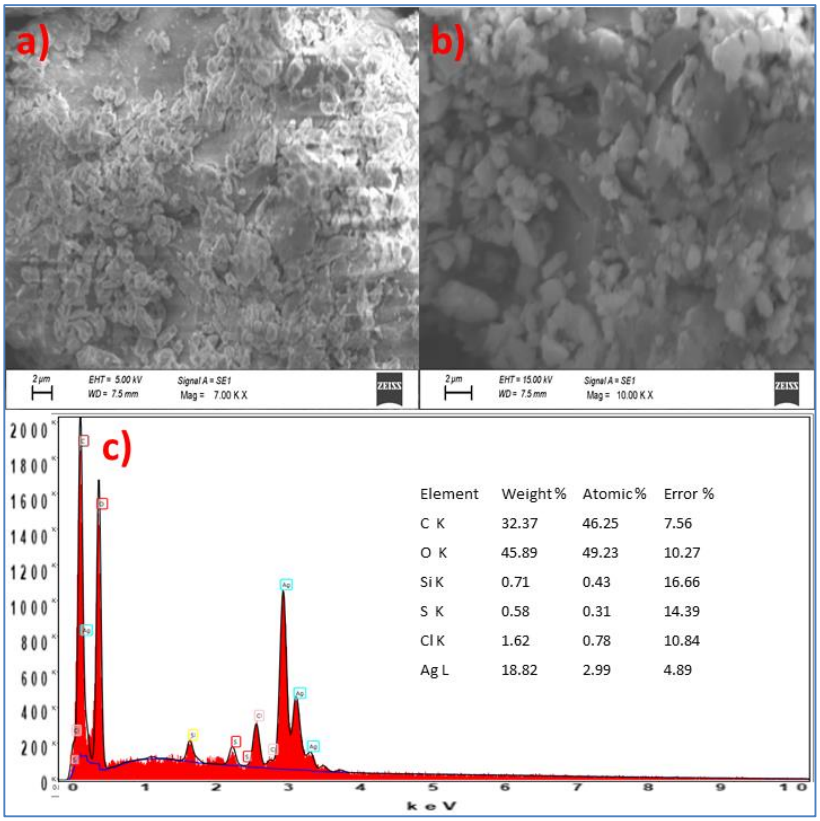

Figure 27. (a) and (b) SEM micrographs of A5 sample (c) EDAX spectrum of A5 sample.

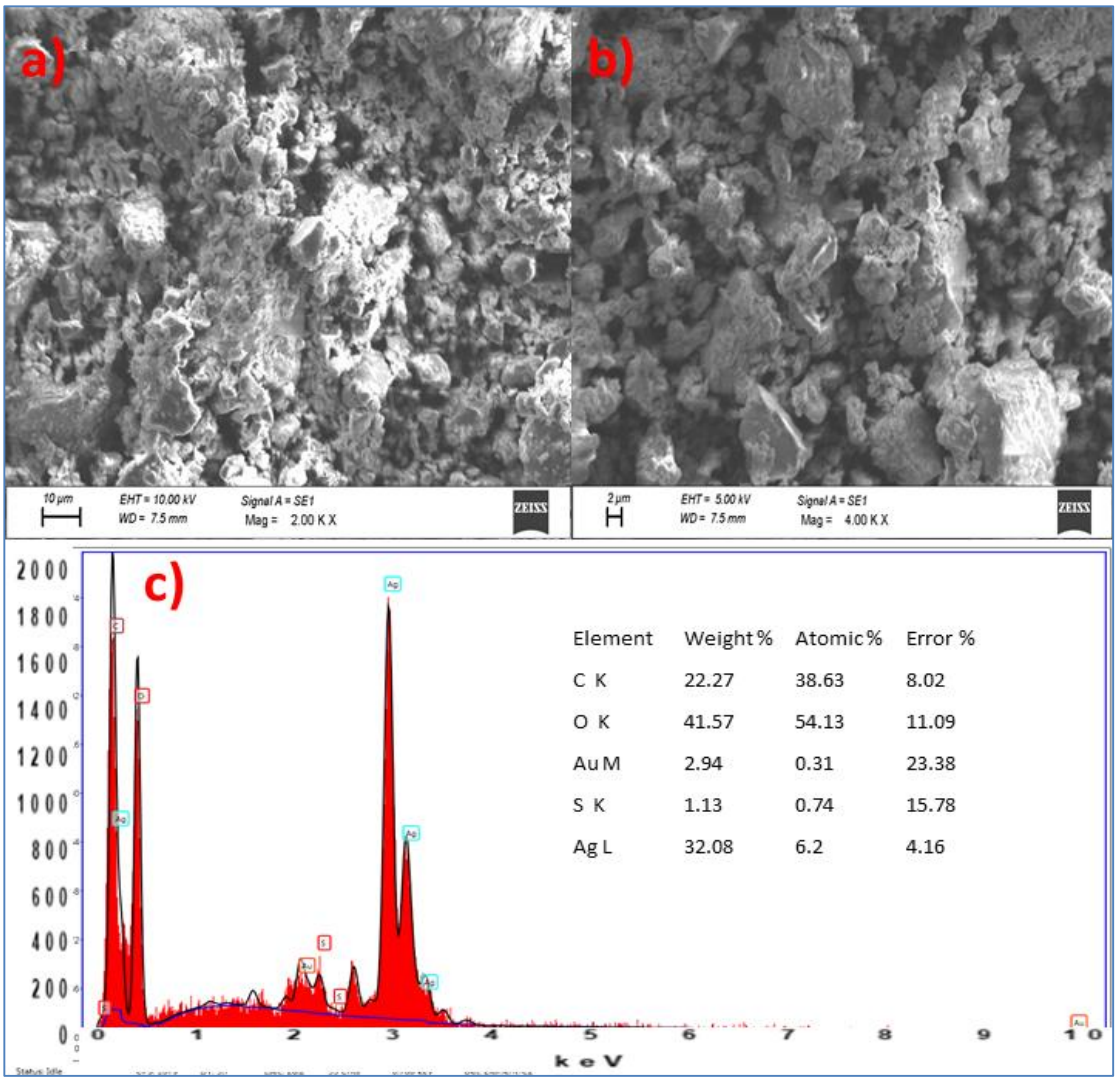

Figure 28. (a) and (b) SEM micrographs of A6 sample (c) EDAX spectrum of A6 sample.

Finally, to conclude that the presence of major elements in the EDAX spectra of all the Ag NPs confirmed the formation of particles of silver which was also proved previously by Uv-Vis, FTIR and XRD techniques. In order to discover the deep insights on the shape, size and structure of silver NPs, TEM-HRTEM-SAED technical micrographs and patterns had been well utilized. The TEM images of Ag-NPs as shown in Figure 29 (a-d) depicted varieties of nanostructures in terms of their diverse shapes and sizes. A mixture of diversely shaped particles including cylindrical, hexagonal, triangular shapes were found in these images. It is worth to note that the particle size and shape control still remains a great challenge as no external constraints were imposed during the experimentation. The HRTEM images as shown in Figure 30 affirms that as-synthesized Ag NPs (A1) are mostly spherical but also with regular as well as irregular geometries. This is possibly due to the dual role (Reduce

and stabilize) played by the bioactive molecules of medicinal plant extracts. The existence of nanosized particles of the dimension less than 5 nm substantiate the efficient role of bioactive components of the extract

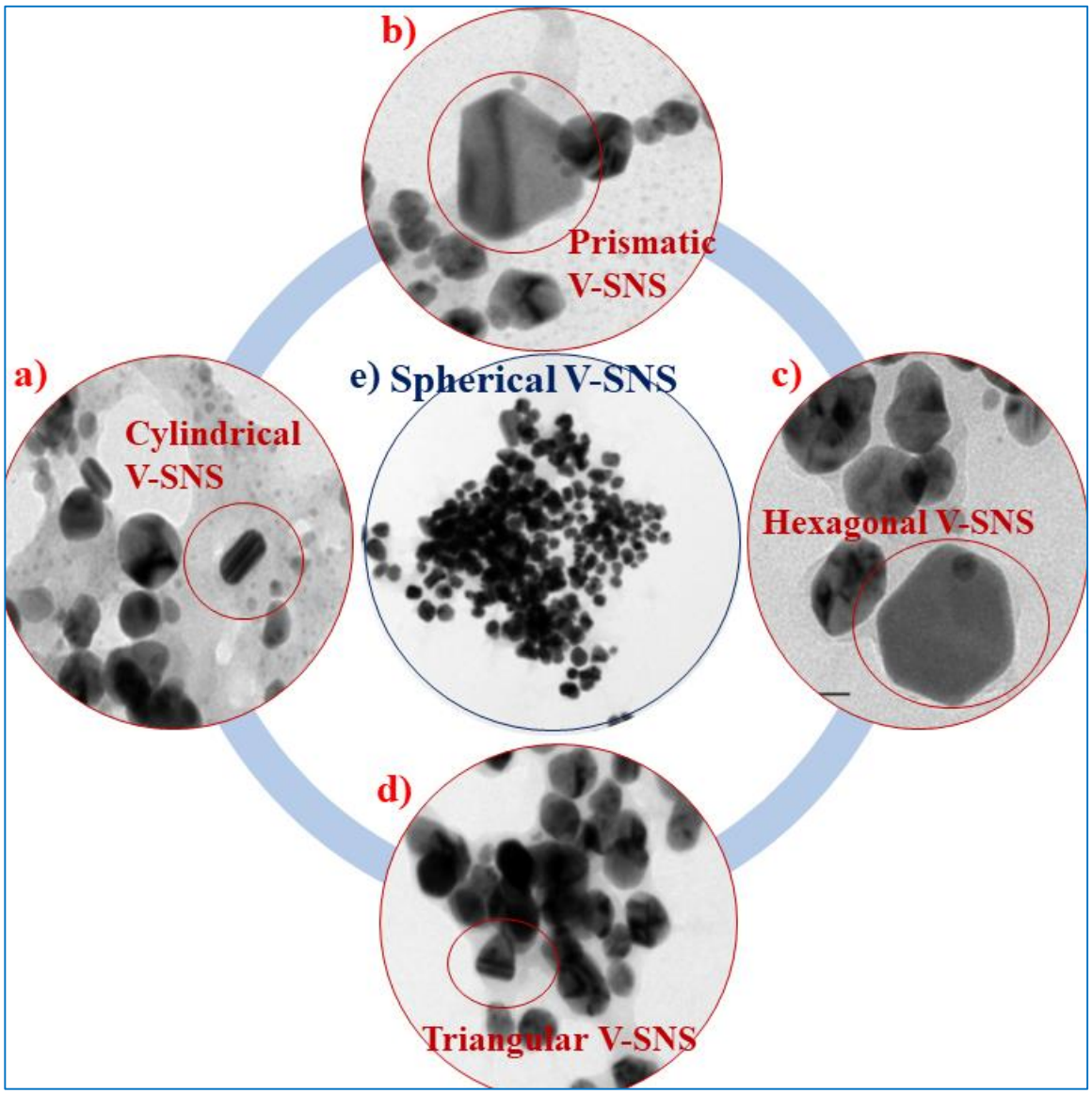

Figure 29. The TEM images of Ag NPs with a) cylindrical, b) prismatic c) hexagonal, d) triangular shapes with nearly spherical shapes (e).

as capping and stabilizing agents otherwise agglomerated particles would have formed. This result indicating formation of various size and shape is in close agreement with the report published earlier (Marassi et al. 2018). The almost spherical structures with various size ranging from 8.2 nm to 52.4 nm with an average particle size of 36.88 nm are as shown in Figure 30 a-b.

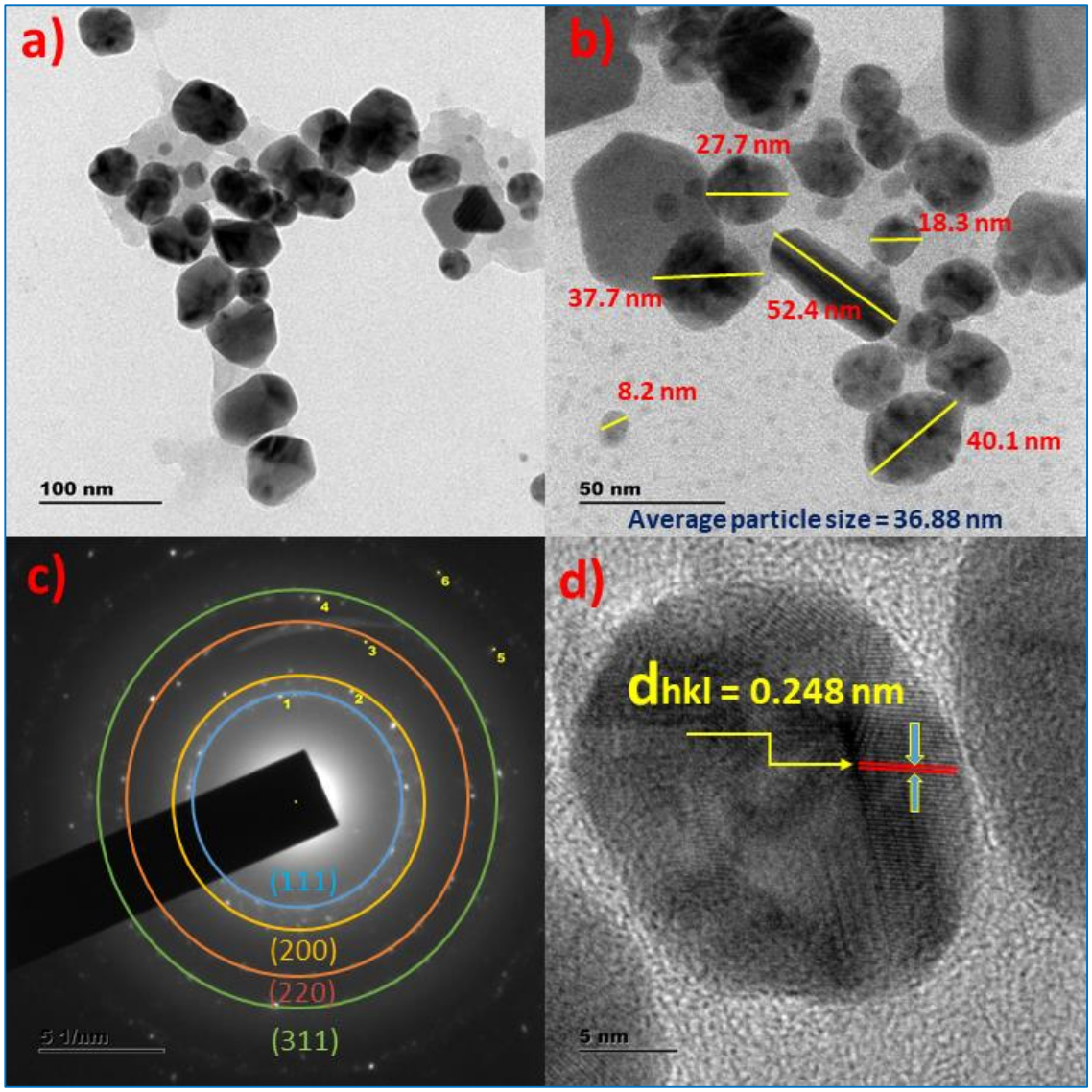

Figure 30. TEM micrographs of Ag NPs (A1) at (a) weak magnification (100 nm) and (b) strong magnification (50 nm) (c) SAED pattern (6 spots) and (d) HRTEM micrographs of lattice fringes of Ag NPs (A1) with IPS value of 0.248 nm.

The six spots appeared on the SAED pattern, were correlated to specific crystal planes of Ag NPs as shown in Figure 30. The most prominent 4 spots were represented in colored concentric circles which represents (111), (200), (220) and (311) planes. The interplanar spacing (IPS) value of 0.248 nm for Ag (111) plane is deduced from Figure 30d. The Figure 31a, 31b and 31c presents the HRTEM micrographs of Ag NPs with enhanced lattice fringes, IFFT and profile of IFFT with interplanar spacing (IPS) value for a specified plane respectively. The IPS values for a specific parallel crystal planes on the surface of Ag NSs was deduced to be 0.248 nm and 0.243 nm at two different sizes.

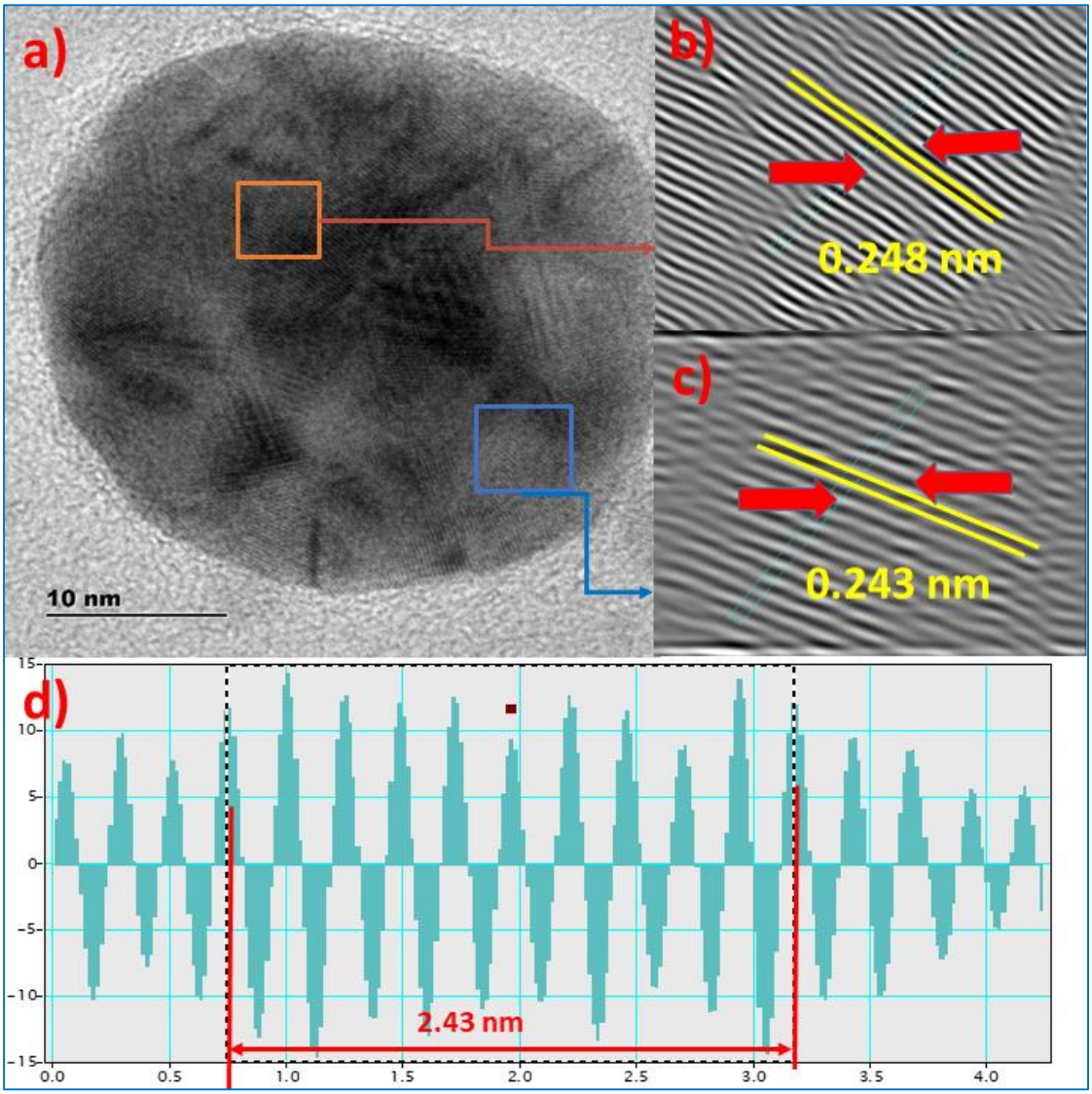

Figure 31. HRTEM morphology of Ag NPs (A1) (a) Magnified lattice fringes (b) and (c) IFFT patterns (d) Profile of IFFT with d-spacing distance.

Table 7 provides the IPS values for the 6 spots appeared on the SAED pattern (Figure 30c) of Ag NPs (A1). Each spot on the SAED pattern corresponds to specific set of lattice planes. The IPS values of 0.2417 nm, 0.2056 nm, 0.1471 nm, 0.2040 nm and 0.1254 nm derived for spot 1, 3, 4 and 5 corresponding to crystal planes, 111(Ag), 200(Ag), 220(Ag) and 311(Ag) are in accordance with the IPS values of Ag crystal structure (Dhand et al. 2016). The other two spots (2 and 6) are possibly due to trace amount of crystalline AgCl. The presence of Cl peak in the EDAX spectrum of Ag NPs further confirms the possibility of formation of AgCl. This SAED analysis using HRTEM images is in compliance with the previously discussed XRD results for the silver nanostructures. The IPS value of lattice fringes at the surface of the Ag NPs was found to be 0.2427 nm.

Table 7. The interplanar spacing values for V-Ag NPs from SAED pattern.

Spot No.	Interplanar spacing (nm)	Rec. Pos. (1/nm)	Degrees to Spot 1	Degrees to x- axis	Amplitude
1	0.2417	4.137	0.00	80.37	2839.10
2	0.2141	4.671	2.04	78.33	4168.58
3	0.2056	4.865	52.10	28.27	4484.95
4	0.1471	6.796	6.11	74.26	1295.65
5	0.1254	7.974	5.87	86.24	5564.48
6	0.09527	10.50	19.92	60.45	4062.21

Similar observations were made with respect to other Ag NP samples. Near spherical particles with varying sizes from 8.51 nm to 42.1 nm with an average particle size of 24.08 nm as determined by imageJ application is presented in Figure 32a-d for Ag NPs (A2) synthesised by using *Hagenia abyssinica* plant leaf extract.

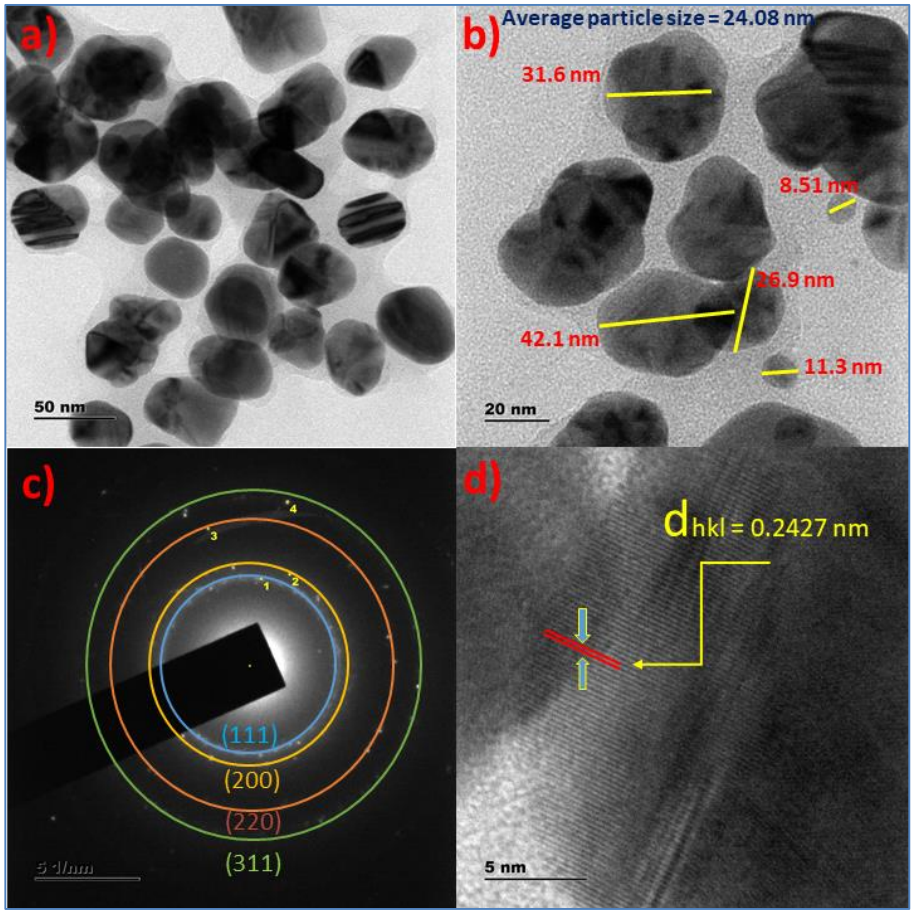

Figure 32. TEM micrographs of Ag NPs (A2) at (a) weak magnification (50 nm) and (b) strong magnification (20 nm) (c) SAED pattern (4 spots) and (d) HRTEM micrographs of lattice fringes of Ag NPs (A1) with IPS value of 0.2427 nm.

HRTEM morphology of Ag NPs with magnified lattice fringes, IFFT patterns and Profile of IFFT with d-spacing value for a specified plane (Figure 32d) are presented in Figure 33a, b, c and d respectively. The analysis of d-spacing values has been carried out by using Gatan Digital Micrograph Software application which resulted in dhkl values of 0.2427 nm and 0.2431 nm for a set crystal planes at different sites on the surface of Ag NPs. HRTEM micrographs exhibited well-defined lattice fringes of d_{111}Ag plane (Figure 33b and c) confirming the clear crystalline nature of prepared g-Ag NPs.

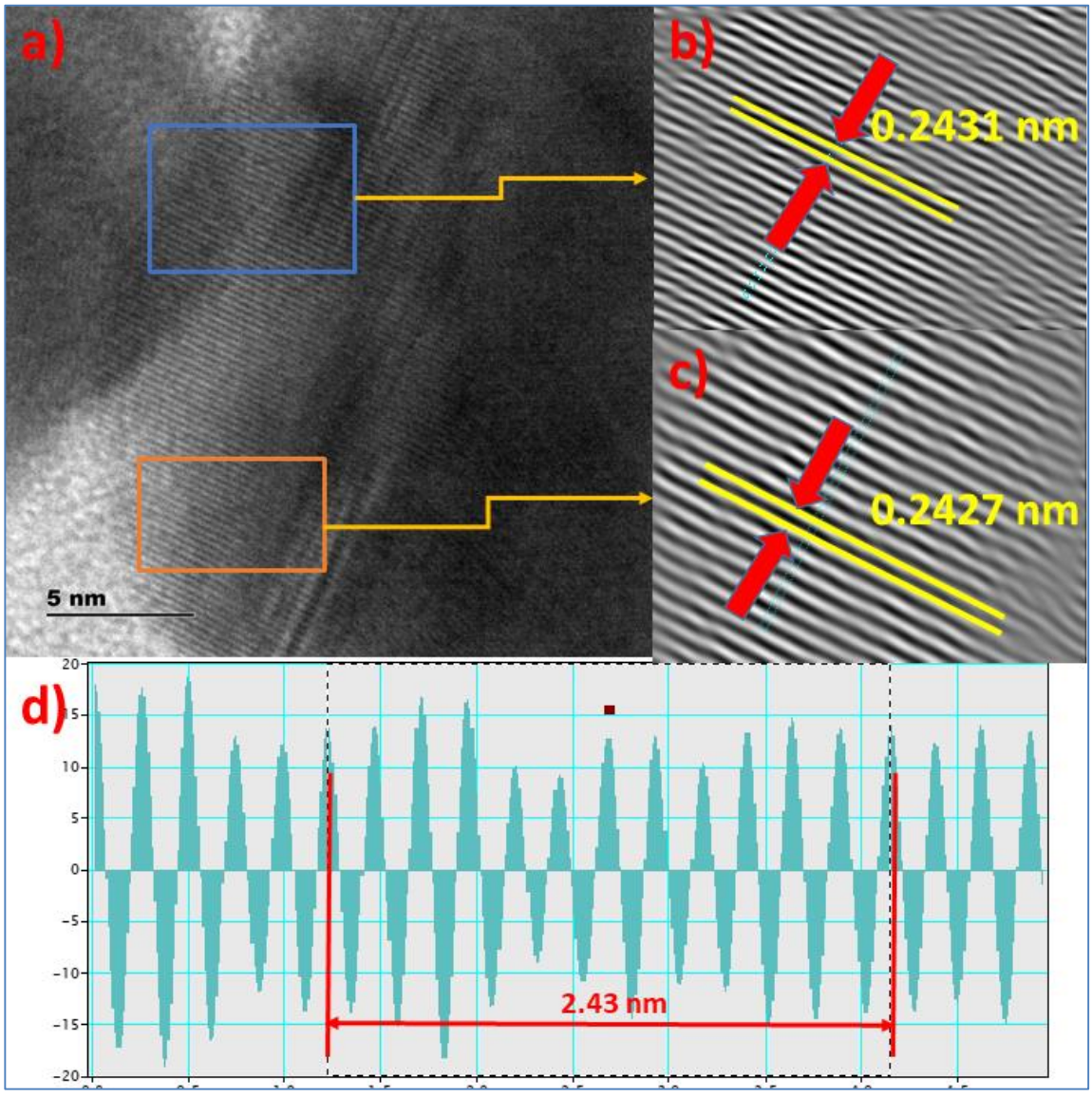

Figure 33. HRTEM morphology of Ag NPs (A2) (a) Magnified lattice fringes (b) and (c) IFFT patterns (d) Profile of IFFT with d-spacing distance.

The d-spacing values for all the spots depicted in the SAED pattern of Ag NPs (Figure 32c) are presented in Table 8.

Table 8. The d-spacing values for Ag NPs (A2) from SAED pattern.

Spot No.	d- spacing (nm)	Rec. Pos. (1/nm)	Degrees to Spot 1	Degrees to x-axis	Amplitude
1	0.2428	4.119	0.00	82.42	311.93
2	0.2126	4.703	16.47	65.95	433.50
3	0.1483	6.742	24.79	107.21	339.25
4	0.1263	7.917	5.72	76.71	500.83

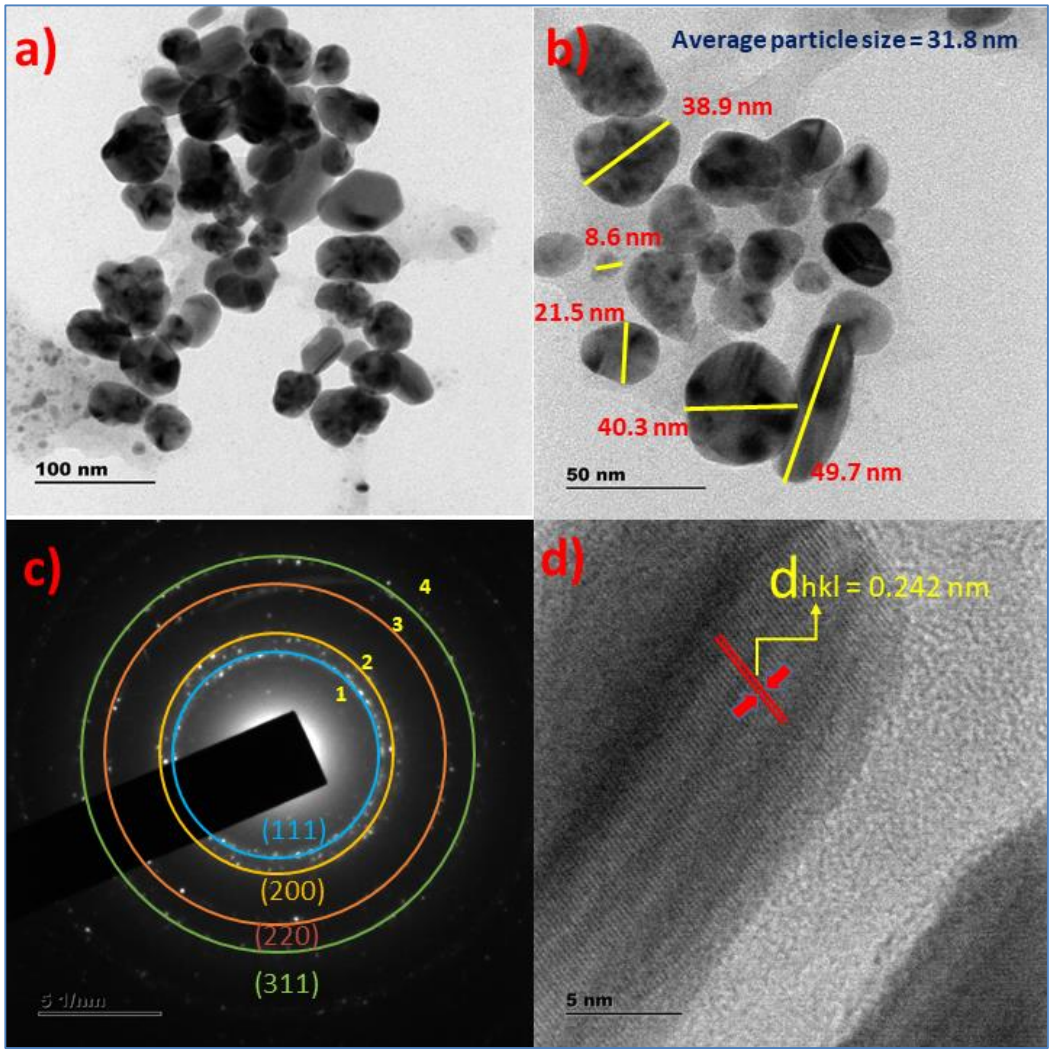

Figure 34. TEM micrographs of Ag NPs (A3) at (a) weak magnification (100 nm) and (b) strong magnification (50 nm) (c) SAED pattern (4 spots) and (d) HRTEM micrographs of lattice fringes of Ag NPs (A3) with IPS value of 0.242 nm.

Each spot on the SAED pattern corresponds to specific set of lattice planes. The XRD pattern of Ag NPs presented earlier in Figure 18a, revealed 4 major peaks corresponding to (111), (200), (220) and (311) planes of fcc structure of pure Ag (ICSD file no. 00-004-7383 (Fm3m)). Thus the results observed on the crystalline nature of Ag NPs by the application of image analysis and XRD technique are mutually in compliance with each other. The d-spacing values of the derived diffraction planes from spot 1 to spot 4; d_{111}Ag = 0.2428 nm, d_{200}Ag = 0.2126 nm, d_{220}Ag = 0.1483 nm and d_{311}Ag = 0.1263 nm, are in good agreement with XRD diffraction pattern of g-Ag NPs. On the similar patterns, TEM-HRTEM-SAED analysis has been conducted for the remaining samples and the corresponding images are presented for A3, A4, A5 and A6 Ag NPs in Figure 35, 36, 37, 38, 39, 40 and 41 respectively.

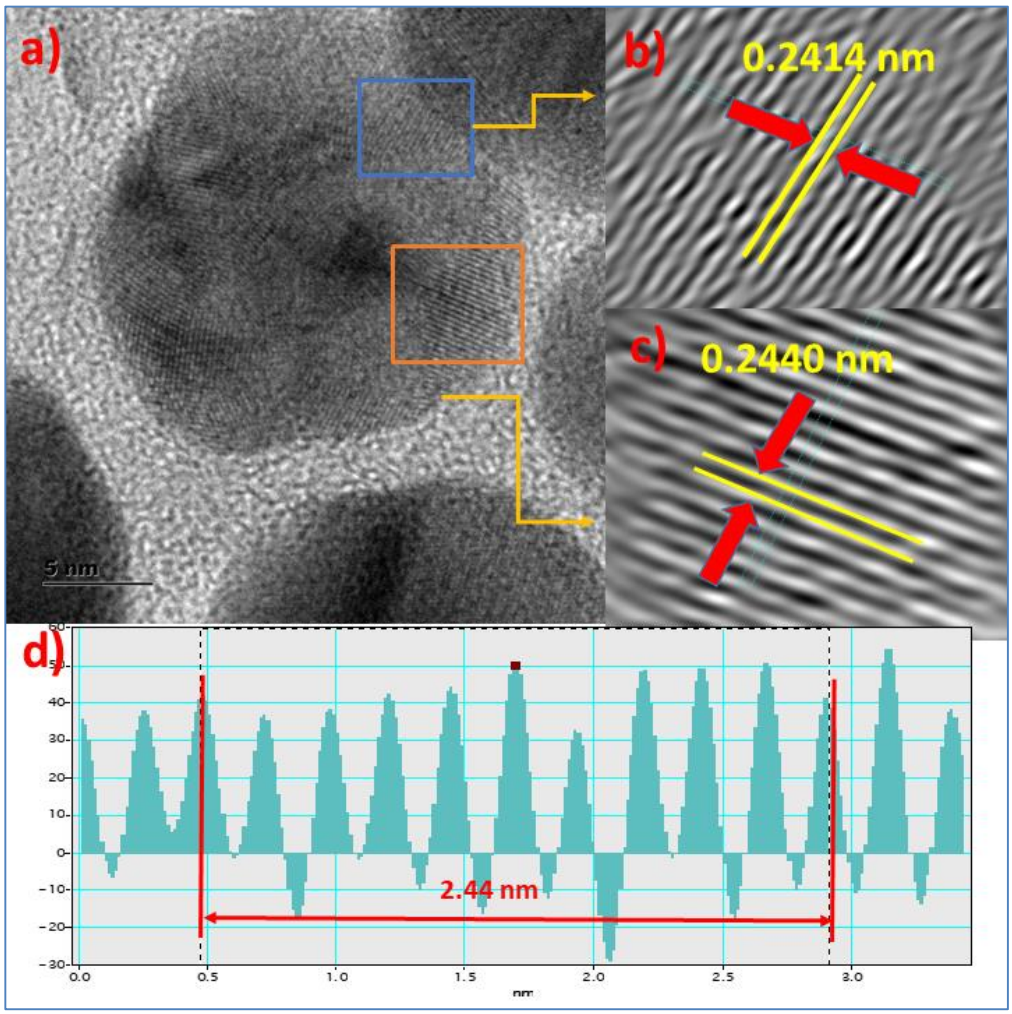

Figure 35. HRTEM morphology of Ag NPs (A3) (a) Magnified lattice fringes (b) and (c) IFFT patterns (d) Profile of IFFT with d-spacing distance.

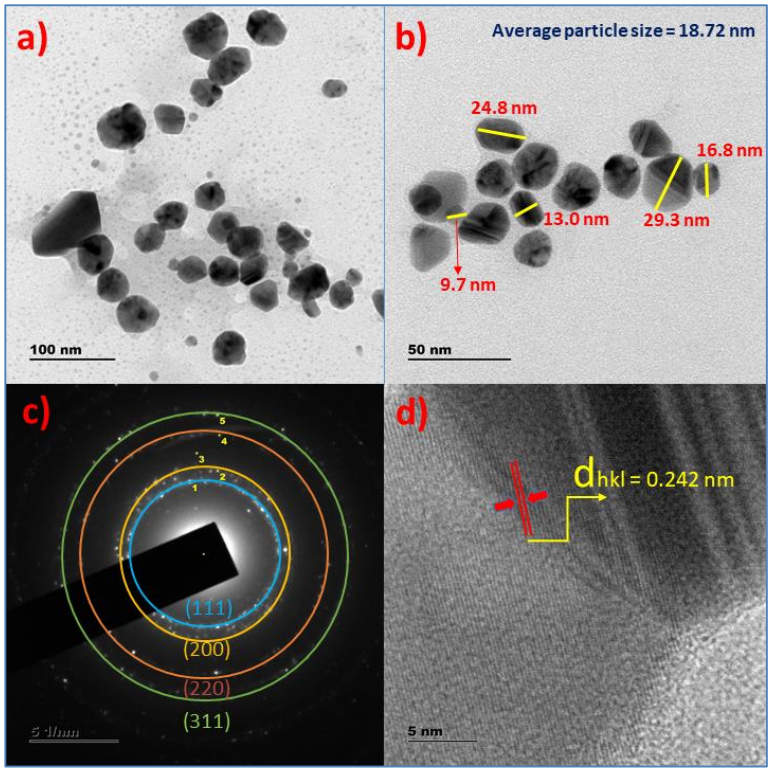

Figure 36. TEM micrographs of Ag NPs (A4) at (a) weak magnification (100 nm) and (b) strong magnification (50 nm) (c) SAED pattern (5 spots) and (d) HRTEM micrographs of lattice fringes of Ag NPs (A4) with IPS value of 0.242 nm.

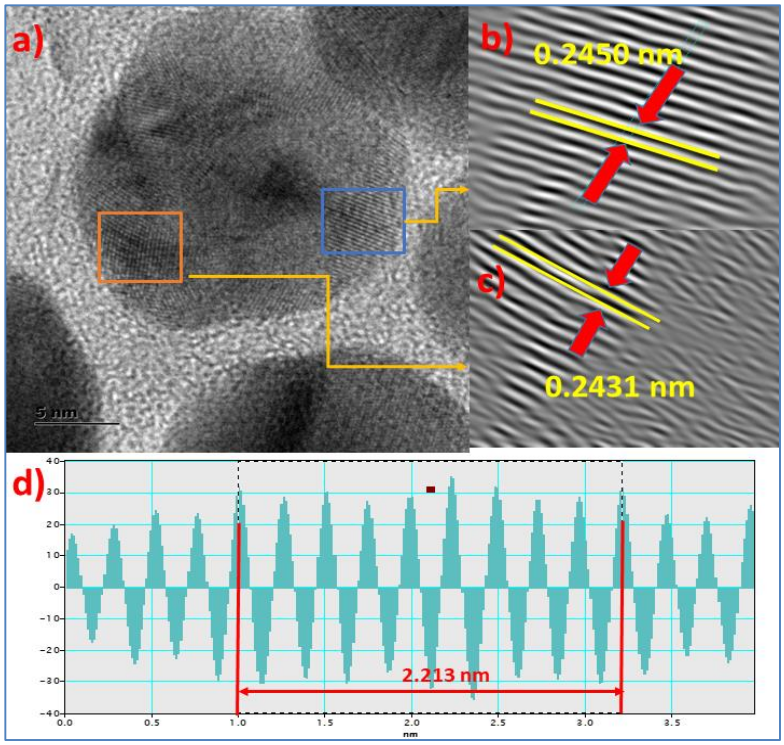

Figure 37. HRTEM morphology of Ag NPs (A4) (a) Magnified lattice fringes (b) and (c) IFFT patterns (d) Profile of IFFT with d-spacing distance.

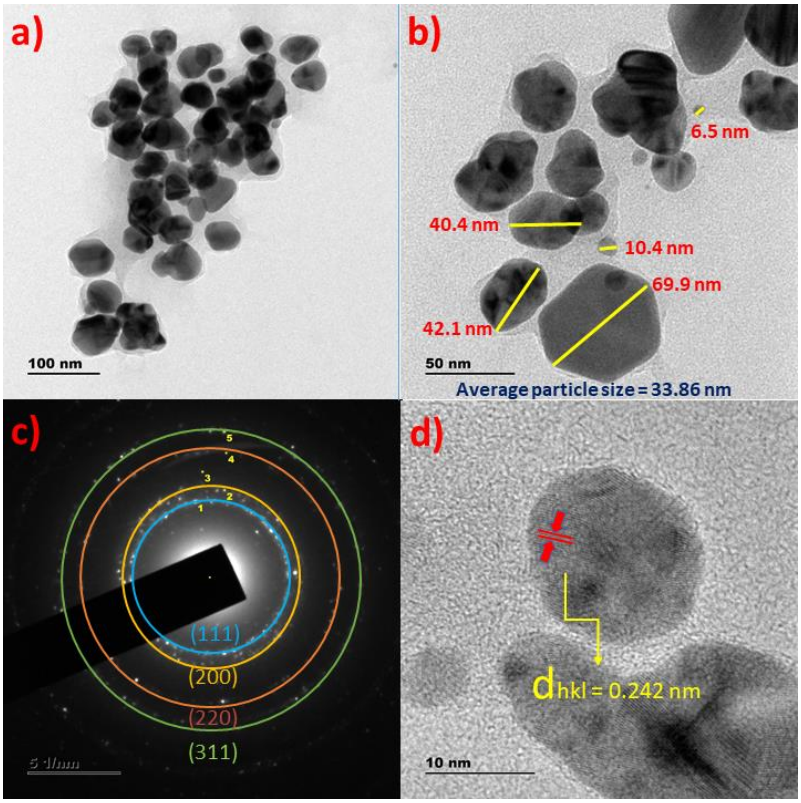

Figure 38. TEM micrographs of Ag NPs (A5) at (a) weak magnification (100 nm) and (b) strong magnification (50 nm) (c) SAED pattern (5 spots) and (d) HRTEM micrographs of lattice fringes of Ag NPs (A5) with IPS value of 0.242 nm.

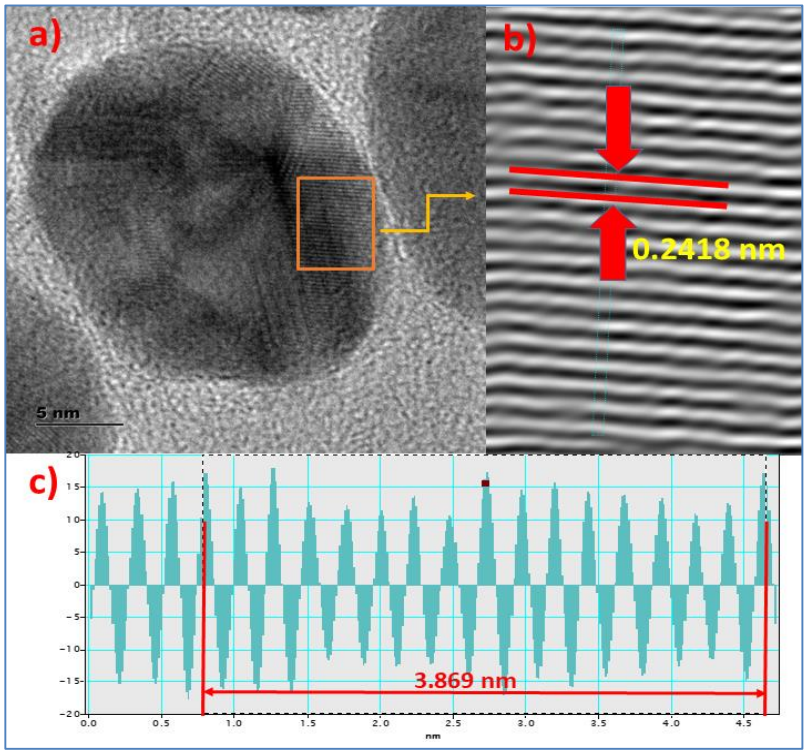

Figure 39. HRTEM morphology of Ag NPs (A5) (a) Magnified lattice fringes (b) and (c) IFFT patterns (d) Profile of IFFT with d-spacing distance.

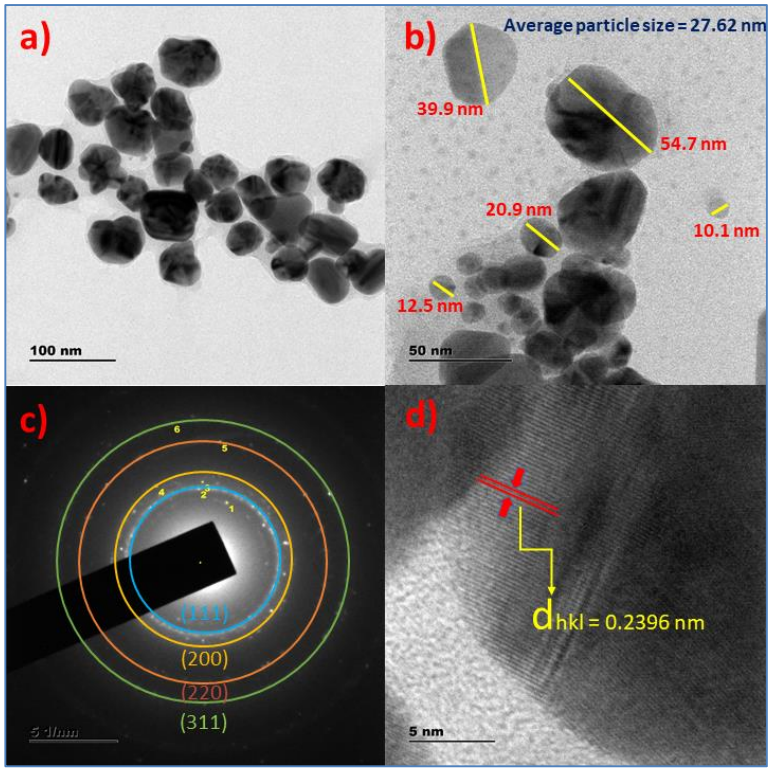

Figure 40. TEM micrographs of Ag NPs (A6) at (a) weak magnification (100 nm) and (b) strong magnification (50 nm) (c) SAED pattern (6 spots) and (d) HRTEM micrographs of lattice fringes of Ag NPs (A6) with IPS value of 0.2396 nm.

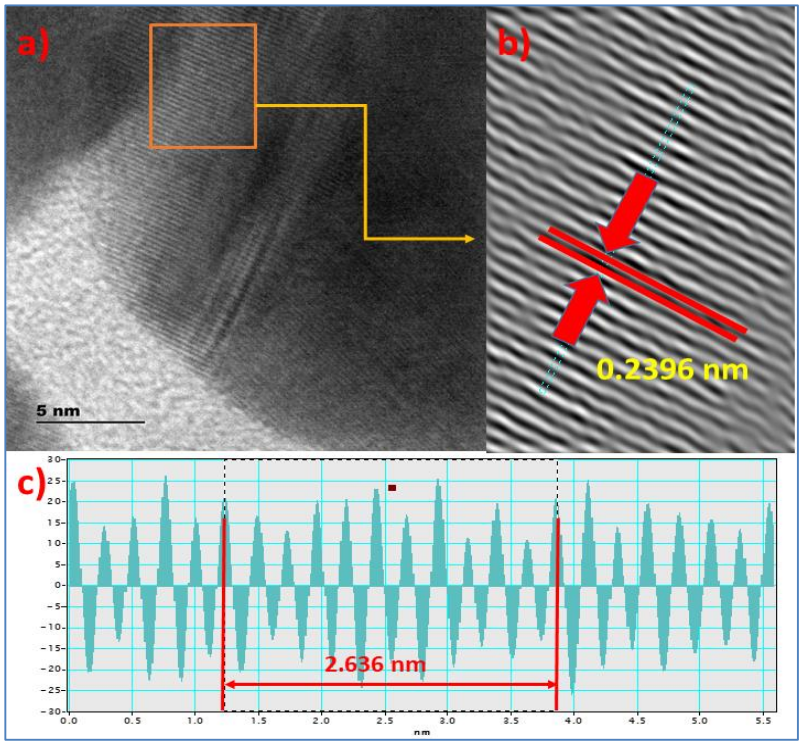

Figure 41. HRTEM morphology of Ag NPs (A6) (a) Magnified lattice fringes (b) and (c) IFFT patterns (d) Profile of IFFT with d-spacing distance.

The complete characterization of A1, A2, A3, A4, A5 and A6 Ag NPs using all the advanced techniques substantiated the structure, crystallinity, purity, bonding, and surface morphological features of silver NPs. It is significant to note that all the Ag NPs obtained from the 6 plant extracts exhibited highly crystalline nature with average particle size varying between 5 nm and 50 nm as confirmed by XRD and HRTEM-SAED studies. But slight variation in the characteristic morphological features among all the 6 Ag NPs, can be attributed to the presence of different set of phytochemicals in the plant extracts. Thus the surface amalgamated biomolecules around the Ag NPs are believed to influence the properties of Ag NPs.

The electron microscopy was applied to delve into the morphological features of V-CuO NPs. The SEM micrographs of NPs are presented as Figure 42a and 42b, which depicted differently sized NPs.

The presence of mixed type of NPs is possibly due to the nature and amount of capping agents around the particles (Nadagouda et al. 2014). EDAX analysis revealed the elemental composition of the V-CuO NPs as depicted in Figure 42c.

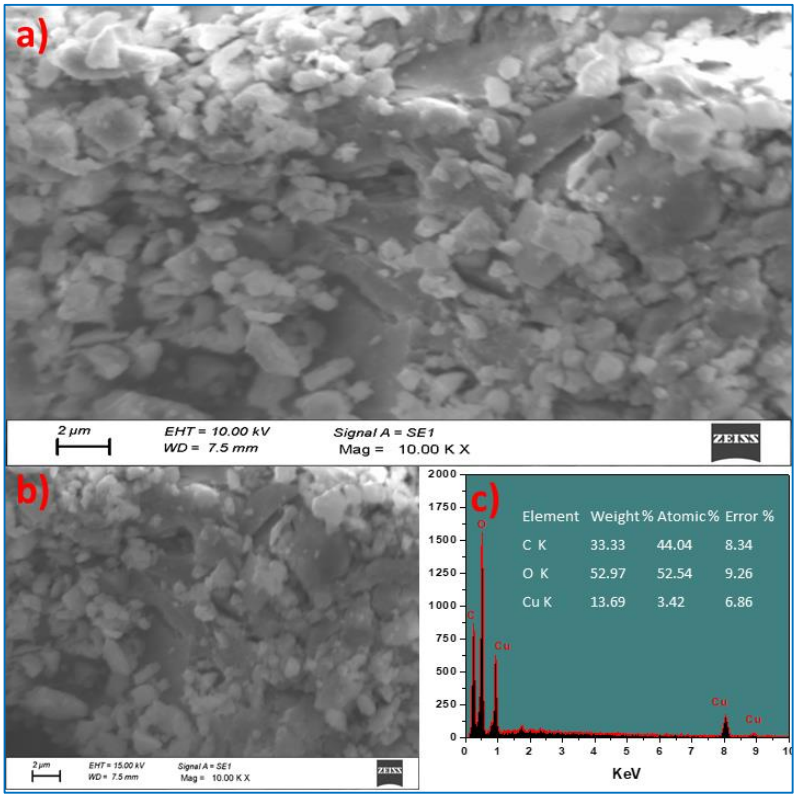

Figure 42. (a) and (b) SEM micrographs of V-CuO NPs (c) EDAX spectrum of V-CuO NPs (C1).

The elements, Cu, C and O have been identified in the spectrum signifying the purity of the NPs. The presence of elements, C and O is most possibly due to bioactive compounds. In addition, it is also apprehended that copper present at the surface had been converted into CuO. In order to discover the deep insights on the shape, size and structure of the V-CuO NPs, TEM-HRTEM-SAED technical micrographs and patterns had been well utilized. The HRTEM images as shown in Figure 43 affirms that as-synthesized V-CuO NPs are mostly spherical but also with regular as well as irregular geometries. This is possibly due to the dual role (Reduce and stabilize) played by the bioactive molecules of PE1 extract. Figure 43a-d shows the TEM images of V-CuO NPs. A mixture of diversely shaped particles including cylindrical, hexagonal, triangular shapes were found in these differently magnified images (Figure 44a-d). It is worth to note that the particle size and shape control still remains a great challenge as no external constraints were imposed during the experimentation. The existence of nanosized particles of the dimension, 8.6 nm (Figure 45) substantiate the efficient role of bioactive components of the extract as capping and stabilizing agents otherwise agglomerated particles would have formed.

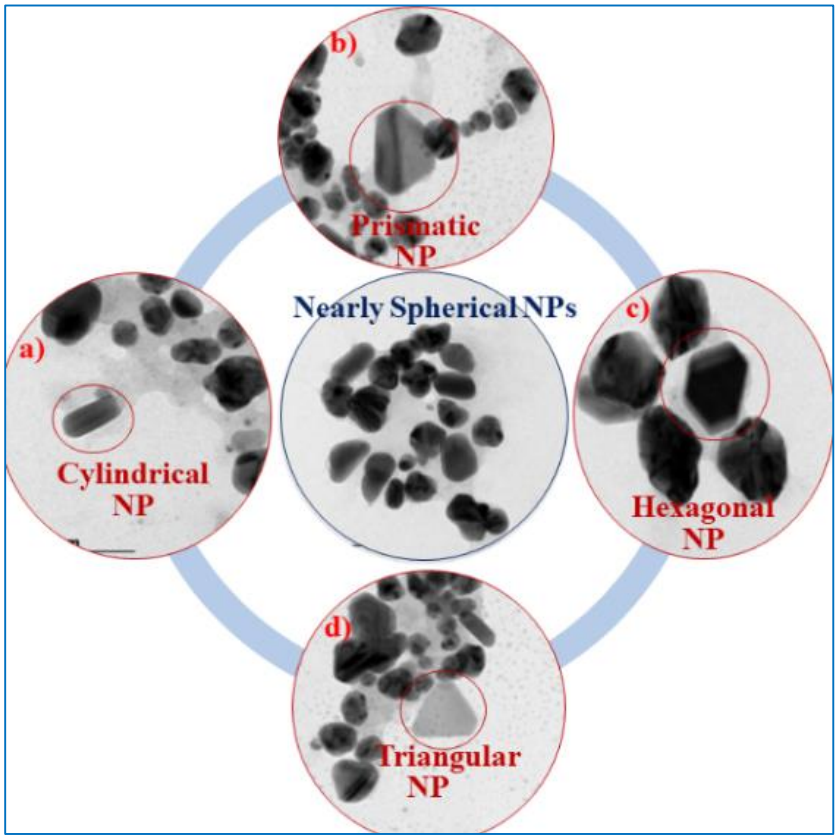

Figure 43. The TEM images of V-CuO NPs with a) cylindrical, b) prismatic c) hexagonal, d) triangular shapes with nearly spherical shapes.

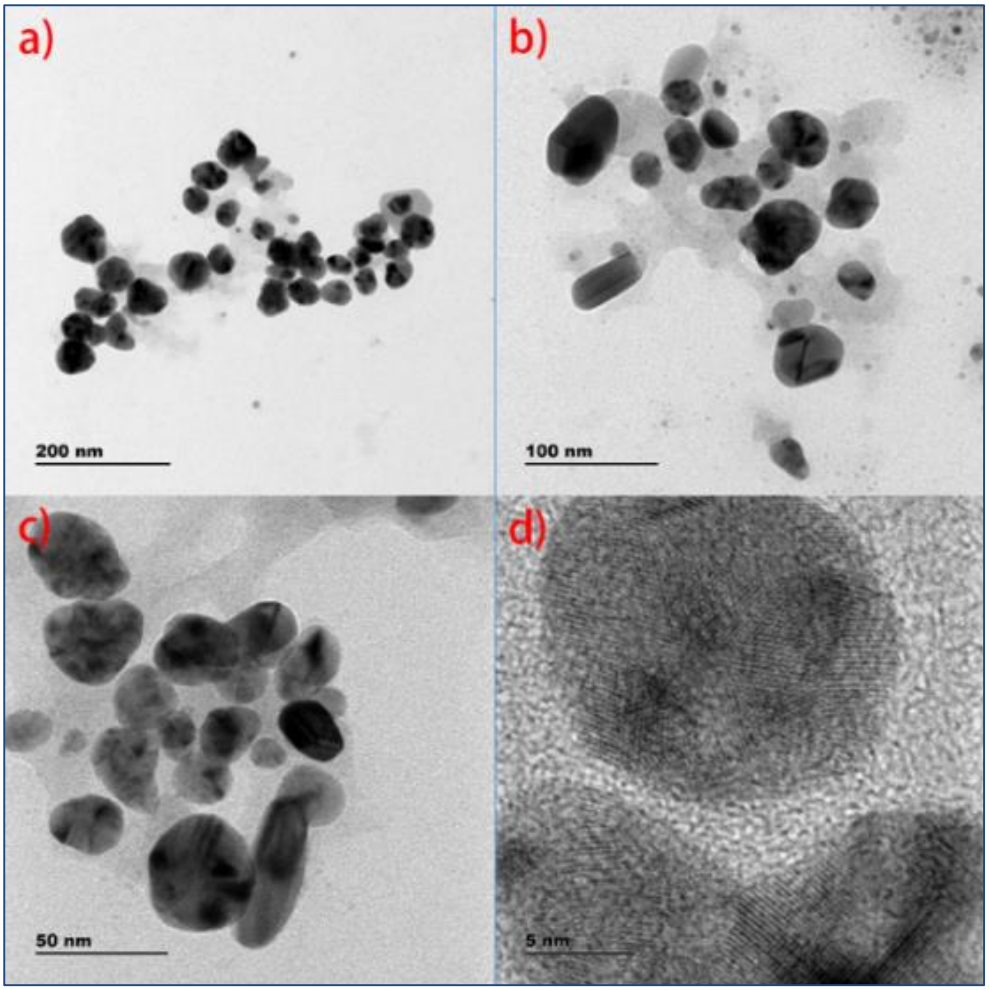

Figure 44. TEM images of *V*-CuO NPs with nearly spherical shapes at various magnifications a) 200 nm, b) 100 nm c) 50 nm d) 5 nm.

The mechanism of green synthesis of CuO NPs is quite challenging especially from the natural plant extracts as they contain varieties of phytoconstituents. These compounds are possibly believed to have played role as reducing agents, stabilizing agents, capping agents or chelating agents in the formation of CuO NPs. It is extremely difficult to arrive at exactly which component of phytoconstituents will reduce or stabilize the NPs even though few studies suggested that antioxidants such as polyphenols act as better reducing agents.

The almost spherical structures with the size ranging from 8.6 nm to 27.5 nm with a median particle size of 19.68 nm are as shown in Figure 45a and 45b. The dark shade on the NPs is believed to be due to the surficial biomolecules. The six spots appeared on the SAED pattern, were correlated to specific crystal planes of V-CuO NPs as shown in Figure 45c. One of such planes is presented with interplanar spacing (IPS) value of 0.2395 nm in Figure 45d.

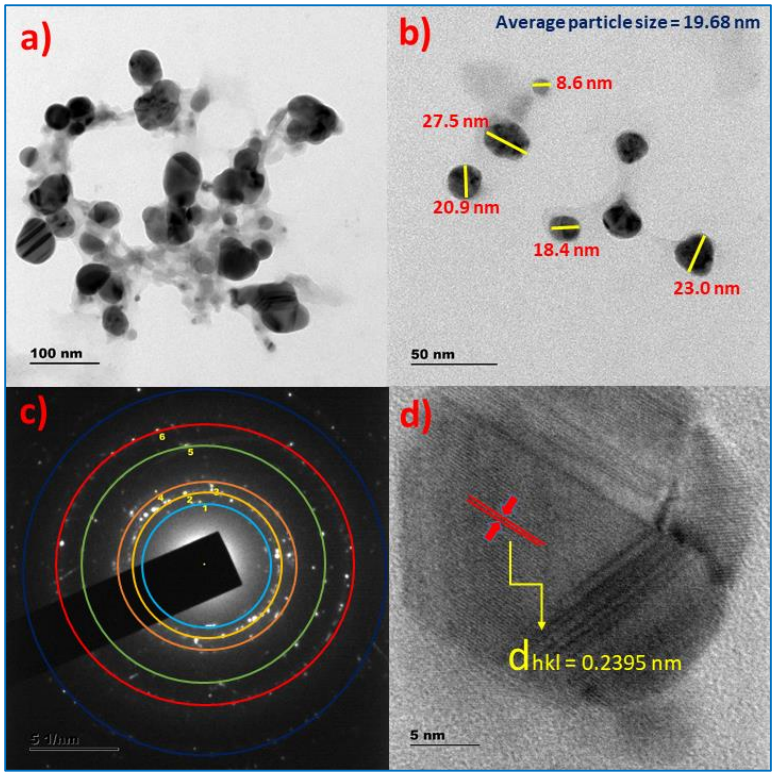

Figure 45. TEM micrographs of V-CuO NPs at (a) weak magnification (100 nm) and (b) strong magnification (50 nm) (c) SAED pattern (6 spots) and (d) HRTEM micrographs of lattice fringes of V-CuO NPs with IPS value of 0.2395 nm.

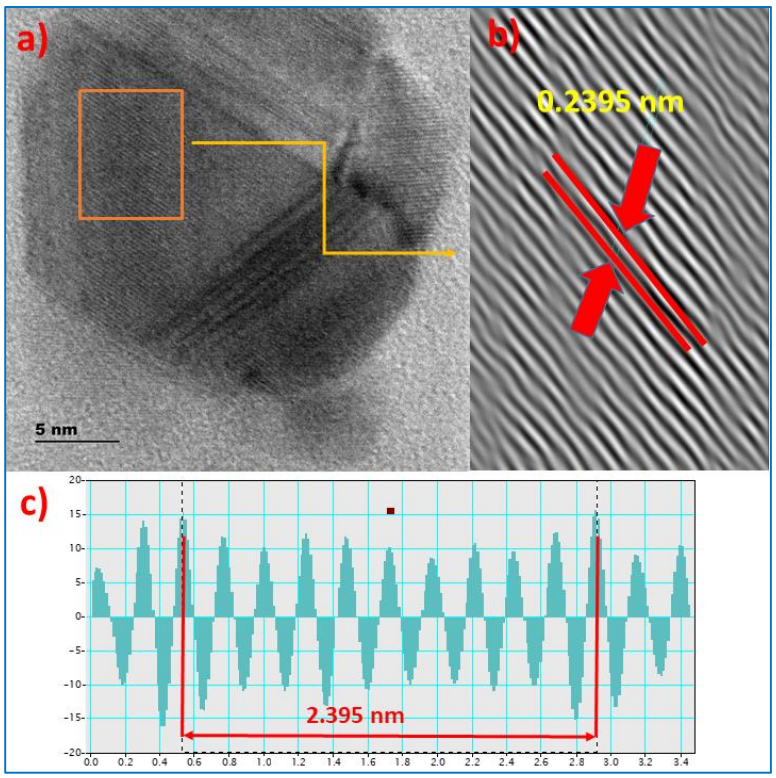

Figure 46. HRTEM morphology of V-CuO NPs (C1) (a) Enhanced lattice fringes (b) IFFT pattern (c) Profile of IFFT with IPS value.

Figure 46a, 46b and 46c presents the HRTEM micrographs with V-CuO NPs with enhanced lattice fringes, IFFT and profile of IFFT with IPS value for a specified plane respectively. The IPS value for a specific parallel crystal planes on the surface of Cu NPs was deduced to be 0.2395 nm. Table 9 provides the IPS values for the 6 spots appeared on the SAED pattern (Figure 45c) of V-CuO NPs. Each spot on the SAED pattern corresponds to specific set of lattice planes. The IPS values of 0.2854 nm, 0.2432 nm, 0.2271 nm, 0.2040 nm, 0.1491 nm and 0.1261 nm, derived for spot 1 to spot 6 corresponding to crystal planes clearly confirms the crystallinity of CuO NPs and dominant presence of CuO NPs. This SAED-HRTEM analysis exhibited results which are in concurrence with XRD results for the V-CuO NPs. The IPS value of lattice fringes at the surface of the V-CuO NPs was found to be 0.2395 nm, which is similar to the dhkl value of 0.24 nm for (111) plane of fcc structured CuO obtained in the previous reported work (Cheirmadurai et al. 2014).

Table 9. The interplanar spacing values for V-CuO NPs (C1).

Spot No.	Interplanar spacing (nm)	Rec. Pos. (1/nm)	Degrees to Spot 1	Amplitude
1	0.2854	3.504	0.00	284.20
2	0.2432	4.112	11.68	1093.93
3	0.2271	4.404	9.20	612.11
4	0.2040	4.903	30.11	178.68
5	0.1491	6.707	5.14	316.22
6	0.1261	7.928	15.73	440.04

The visual display of size and shape of synthesized H-Cu NPs (C2) as depicted by SEM micrographs are shown in Figure 47a and 47b. The SEM images also demonstrated the non-homogeneity of the particles in terms of their shape and size. All the possible spherical and irregular shapes such as truncated hexagonal, cylindrical, triangular, prismatic shapes of Cu NPs with varying particle sizes were found in the micrographs.

The average grain size of Cu NPs was found to be in the range of 10–50 nm. It seems particles were found to agglomerate moderately due to high surface area resulting in the formation of medium sized particles. The chemical composition of the NPs was studied by EDAX analysis. The Figure 47c shows the EDAX spectrum obtained for the H-Cu NPs.

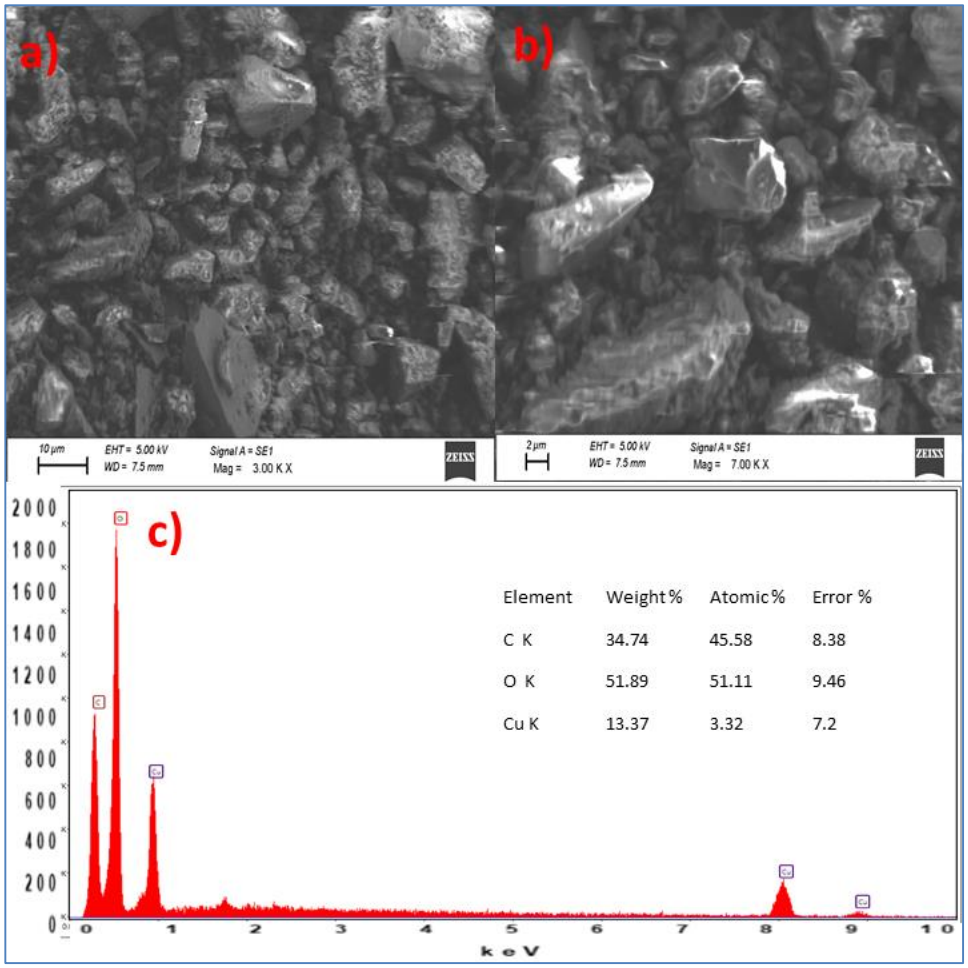

Figure 47. (a) and (b) SEM micrographs of H-Cu NPs (c) EDAX spectrum of H-Cu NPs (C2).

The peaks corresponding to elemental Cu, C and O were clearly identified and no additional peaks were present, which demonstrates the purity of the synthesized NPs and this was consistent with the XRD studies.

The image analysis of C2 revealed spherical morphology for the particles. All these near spherical particles with varying sizes from 14.4 nm to 43.1 nm with an average particle size of 34.76 nm as determined by imageJ application are as shown in Figure 48a and 48b.

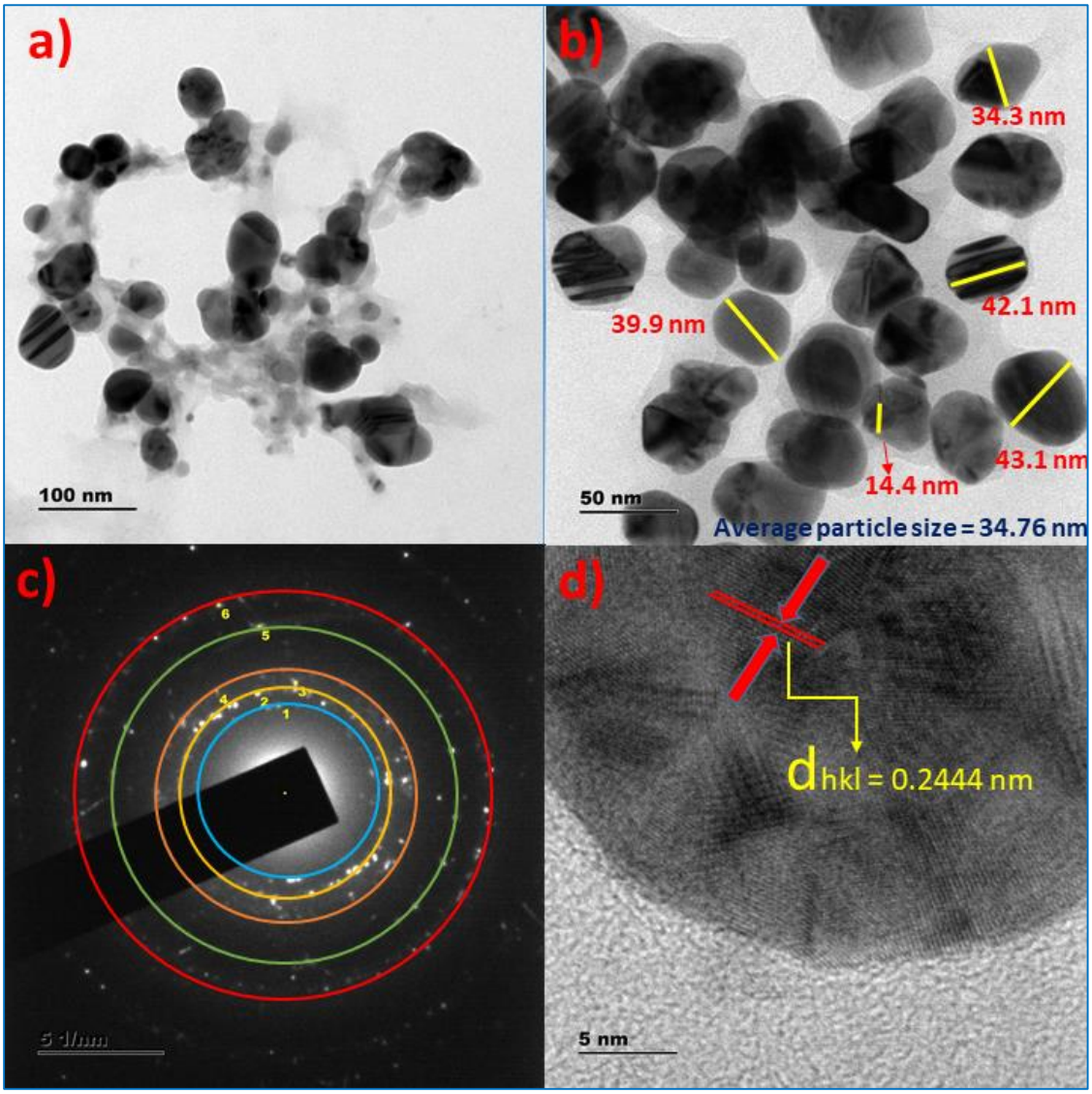

Figure 48. TEM images of as-synthesized H-Cu NPs (C2) at (a) lower magnification (100 nm) and (b) higher magnification (50 nm) (c) SAED pattern with 1 to 6 spots and (d) HRTEM image showing lattice fringes of H-Cu NPs with d-spacing of 0.2444 nm.

The SAED pattern of H-Cu NPs (Figure 48c) contained six spots each corresponding to specific crystal planes. One of such planes is presented with d-spacing of 0.2444 nm as shown in Figure 47d.

HRTEM morphology of H-Cu NPs with magnified lattice fringes, IFFT patterns and profile of IFFT with d-spacing value for a specified plane (Figure 48d) are presented in Figure 49a, 49b and 49c respectively. The analysis to arrive at d-spacing value resulted in d_{hkl} value of 0.2444 nm for a set crystal planes at the surface of Cu NPs.

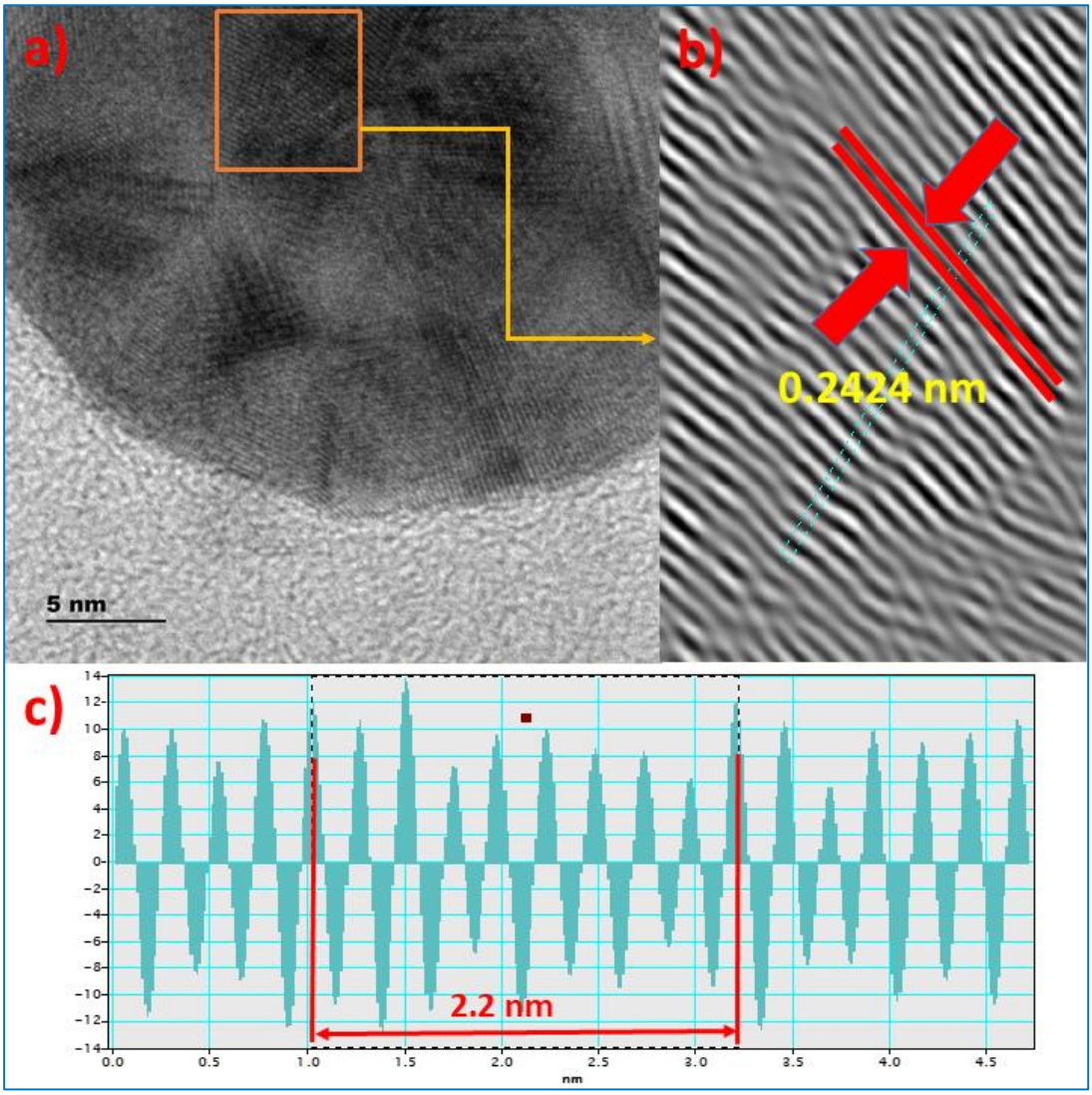

Figure 49. HRTEM morphology of H-Cu NPs (a) magnified lattice fringes (b) IFFT patterns (c) Profile of IFFT with d-spacing distance.

Each spot on the SAED pattern corresponds to specific set of lattice planes. The XRD pattern of H-Cu NPs presented earlier in Figure 20, revealed 3 major peaks corresponding to (111), (200) and (220) planes of fcc structure of pure Cu (ICSD No. 04-0836). The similar result was reported in the recent work (Cheirmadurai et al. 2014).

The estimated d-spacing value of lattice fringes at the surface of the Cu NPs is 0.2444 nm, which is comparable to the d_{hkl} value of (111) plane of fcc structured Cu_2O. It can be concluded that few copper atoms at the surface of NPs possibly reacted with air to form their oxides, Cu_2O and CuO.

TEM-HRTEM-SAED technical micrographs and patterns had been well utilized to explore the features related to particle size and shapes. The HRTEM images as shown in Figure 50

affirms that as-synthesized A-Cu NPs (C3) are mostly spherical but also with regular as well as irregular geometries.

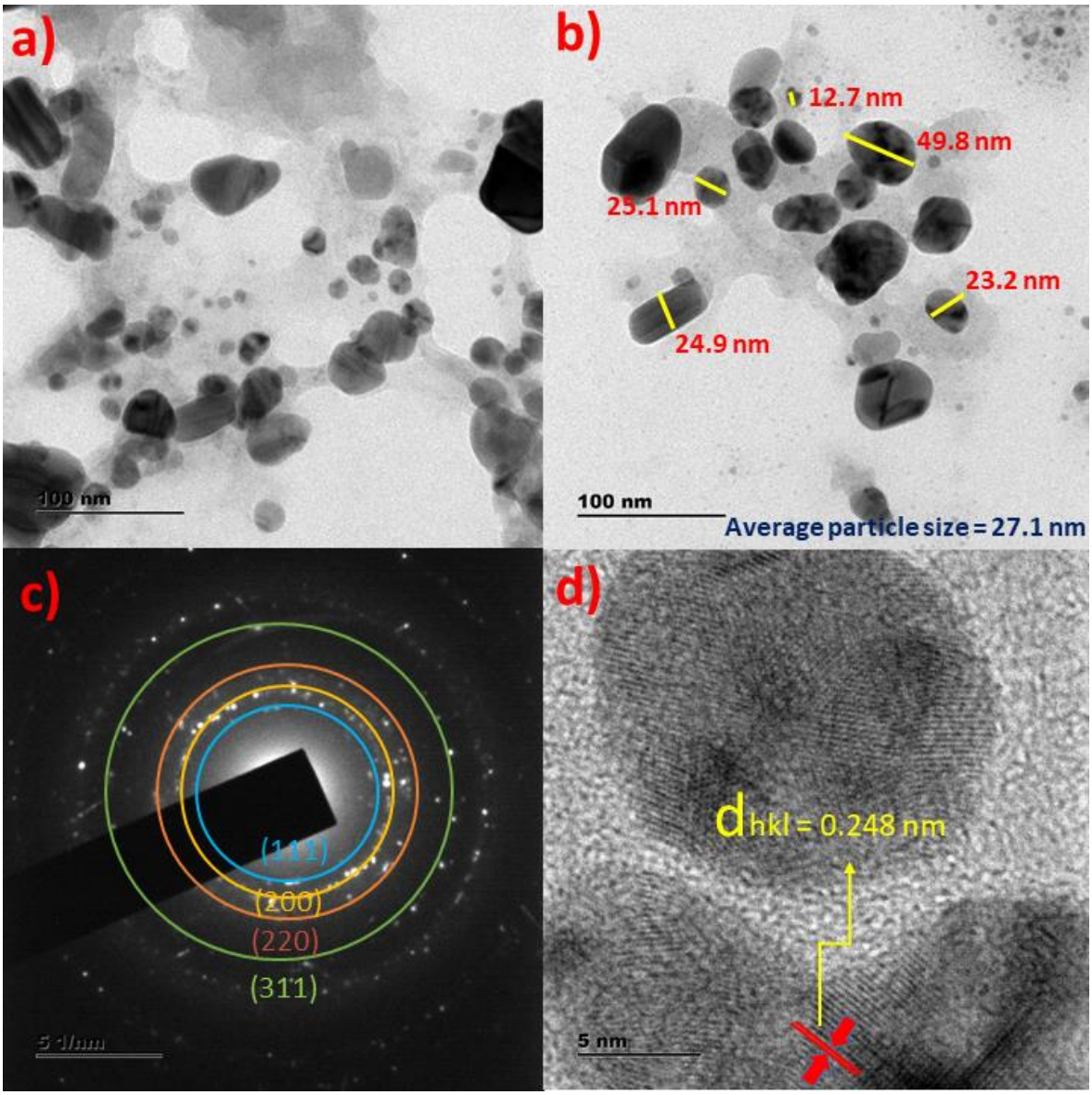

Figure 50. TEM micrographs of A-Cu NPs (C3) at (a) weak magnification (100 nm) and (b) strong magnification (50 nm) (c) SAED pattern (6 spots) and (d) HRTEM micrographs of lattice fringes of A-Cu NPs (C3) with IPS value of 0.248 nm.

The existence of nanosized particles of the dimension, 12.7 nm substantiate the efficient role of bioactive components of the extract as capping and stabilizing agents otherwise agglomerated particles would have formed.

The almost spherical structures with the size ranging from 12.7 nm to 49.8 nm with a median particle size of 27.1 nm are as shown in Figure 50a and 50b. The corresponding SAED pattern is present in Figure 50c.

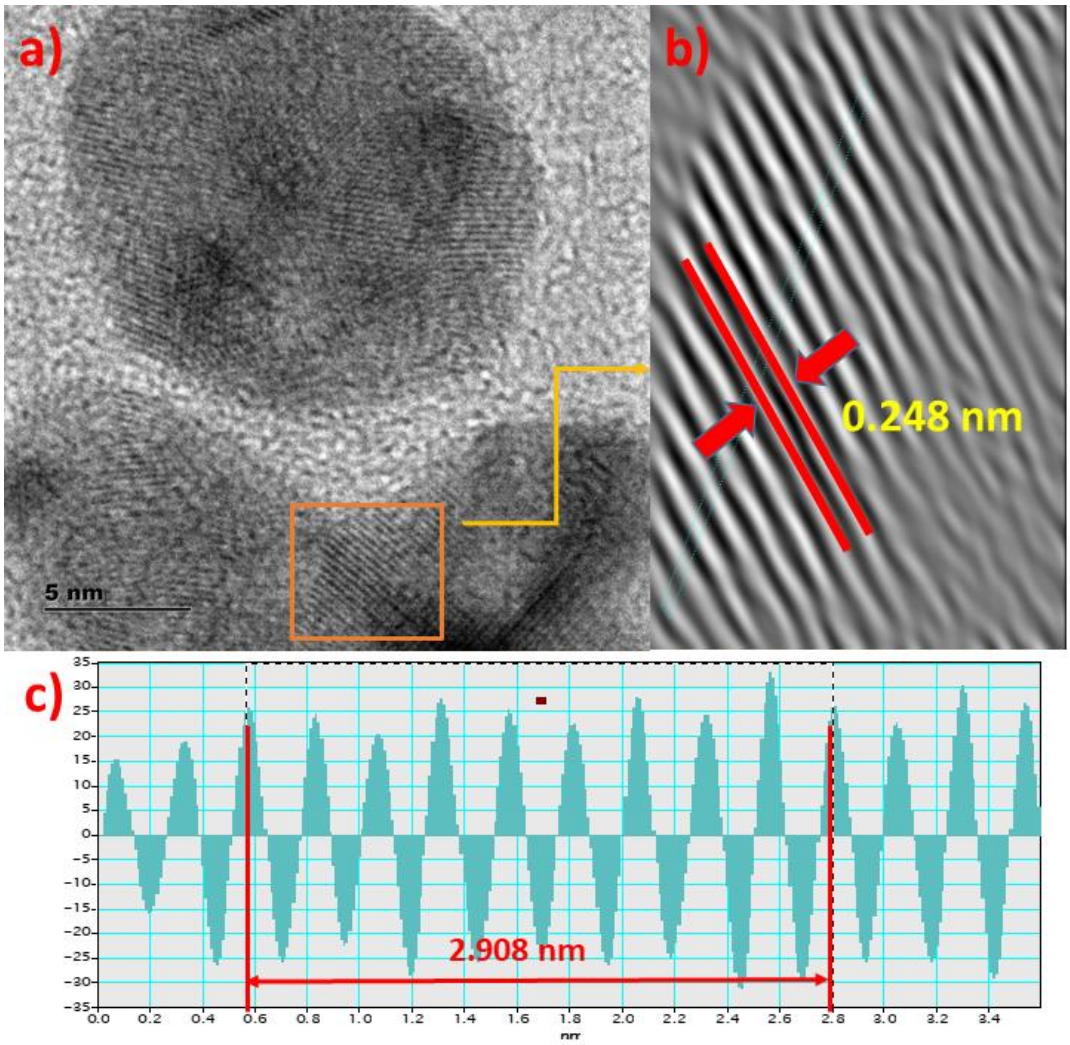

Figure 51. HRTEM morphology of A-Cu NPs (C3) (a) Enhanced lattice fringes (b) IFFT pattern (c) Profile of IFFT with IPS value.

HRTEM morphology of A-Cu NPs with magnified lattice fringes, IFFT patterns and profile of IFFT with d-spacing value for a specified plane (Figure 50d) are presented in Figure 51a, 52b and 53c respectively.

This SAED-HRTEM analysis exhibited results which are in concurrence with XRD results for the Cu NPs The IPS value of lattice fringes at the surface of the Cu NPs was found to be 0.248 nm.

Similarly, the HRTEM images as shown in Figure 52 affirms that as-synthesized C-Cu NPs (C4) nanoparticles also exhibited spherical morphology.

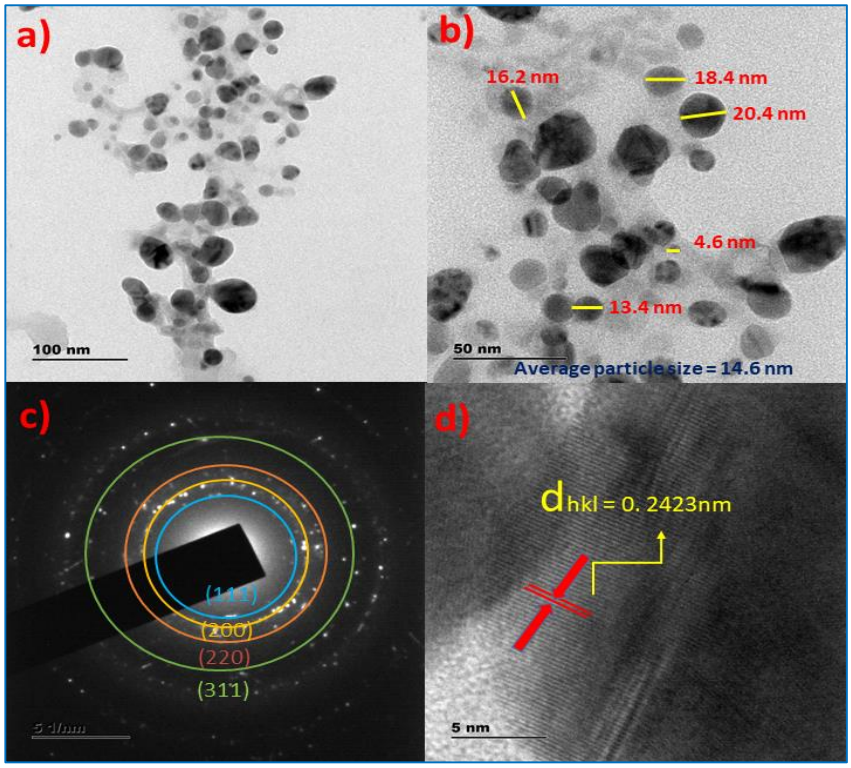

Figure 52. TEM micrographs of C-Cu NPs (C4) at (a) weak magnification (100 nm) and (b) strong magnification (50 nm) (c) SAED pattern (6 spots) and (d) HRTEM micrographs of lattice fringes of C-Cu NPs (C4) with IPS value of 0.2423 nm.

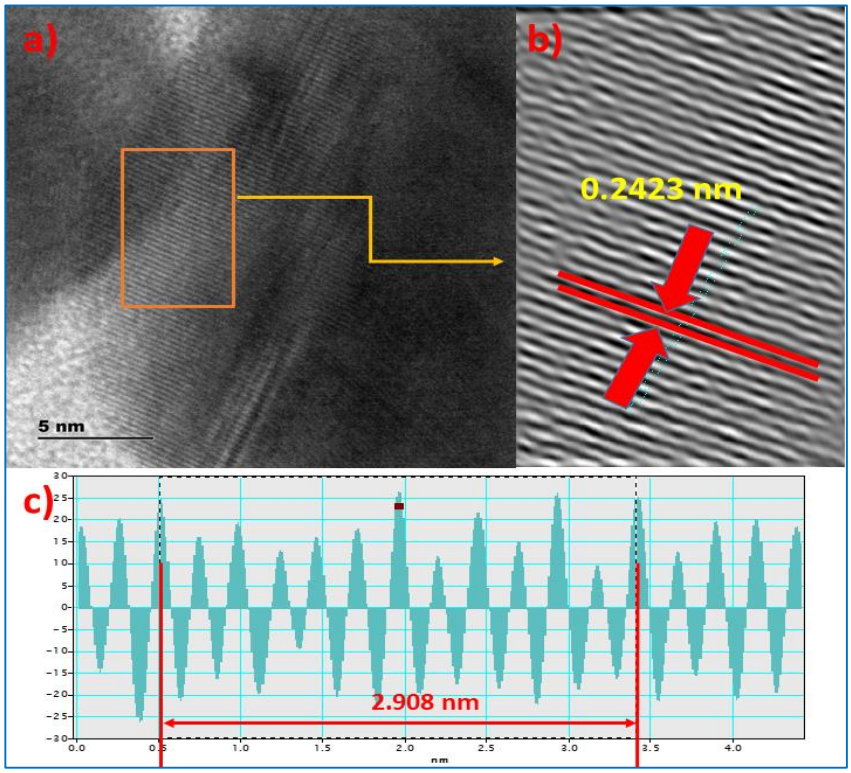

Figure 53. HRTEM morphology of C-Cu NPs (C4) (a) Enhanced lattice fringes (b) IFFT pattern (c) Profile of IFFT with IPS value.

HRTEM morphology of C-Cu NPs with magnified lattice fringes, IFFT patterns and profile of IFFT with d-spacing value for a specified plane (Figure 52d) are presented in Figure 53a, 53b and 53c respectively.

The E-Cu NPs (C5) synthesised by using the root extract of *Echinops Sp.* plant were subjected to all the planned characterization. The alkaloids, tannins, flavonoids and terpenoids were found in *Echinops Sp.* plant *root extract* (PE5) during the phytochemical analysis.

The SEM micrographs of NPs are presented as Figure 54a and 54b, which depicted nanoparticles with agglomerated nature (Fuku et al. 2020).

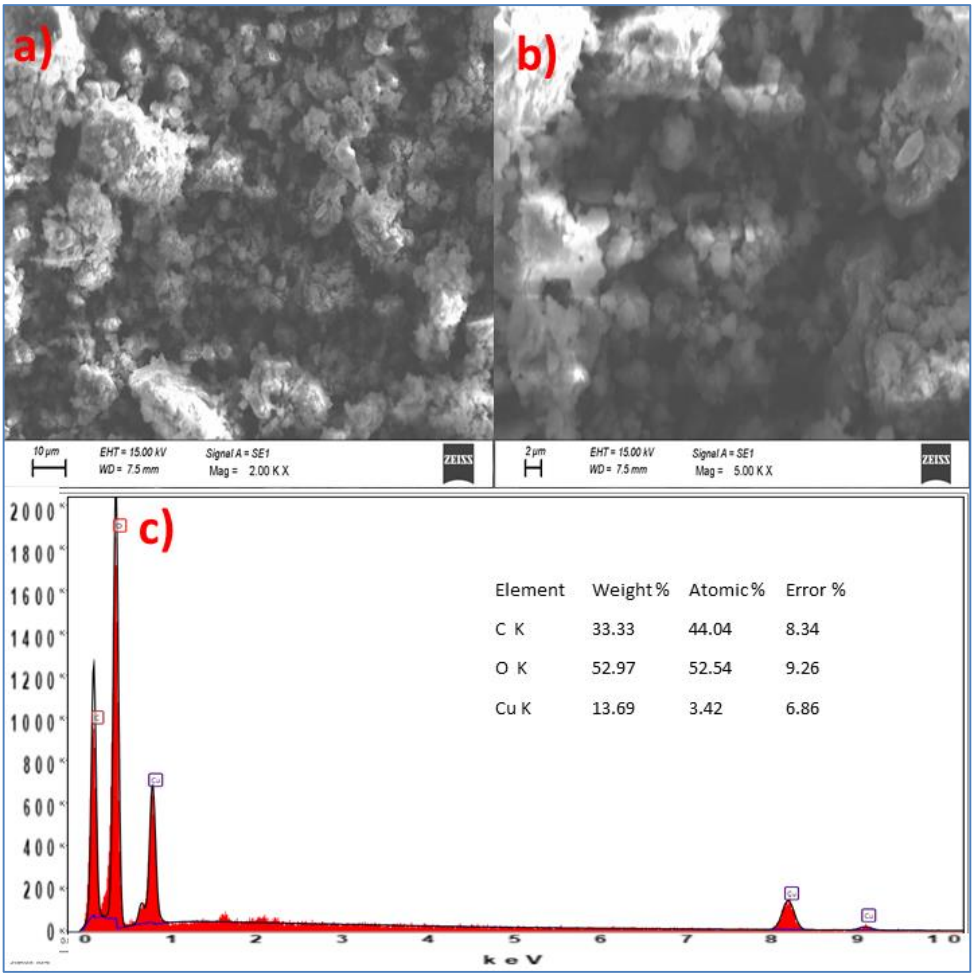

Figure 54. (a) and (b) SEM micrographs of *E*-Cu NPs (C5) (c) EDAX spectrum of *E*-Cu NPs (C5).

TEM images clearly substantiates the absence of crystalline NPs as there are only spherical particles spread over the wide range of distances. The HRTEM images (at different magnifications) as shown in Figure 55 (a, b and d) affirms that as-synthesized E-Cu NPs are mostly spherical but also with irregular geometries.

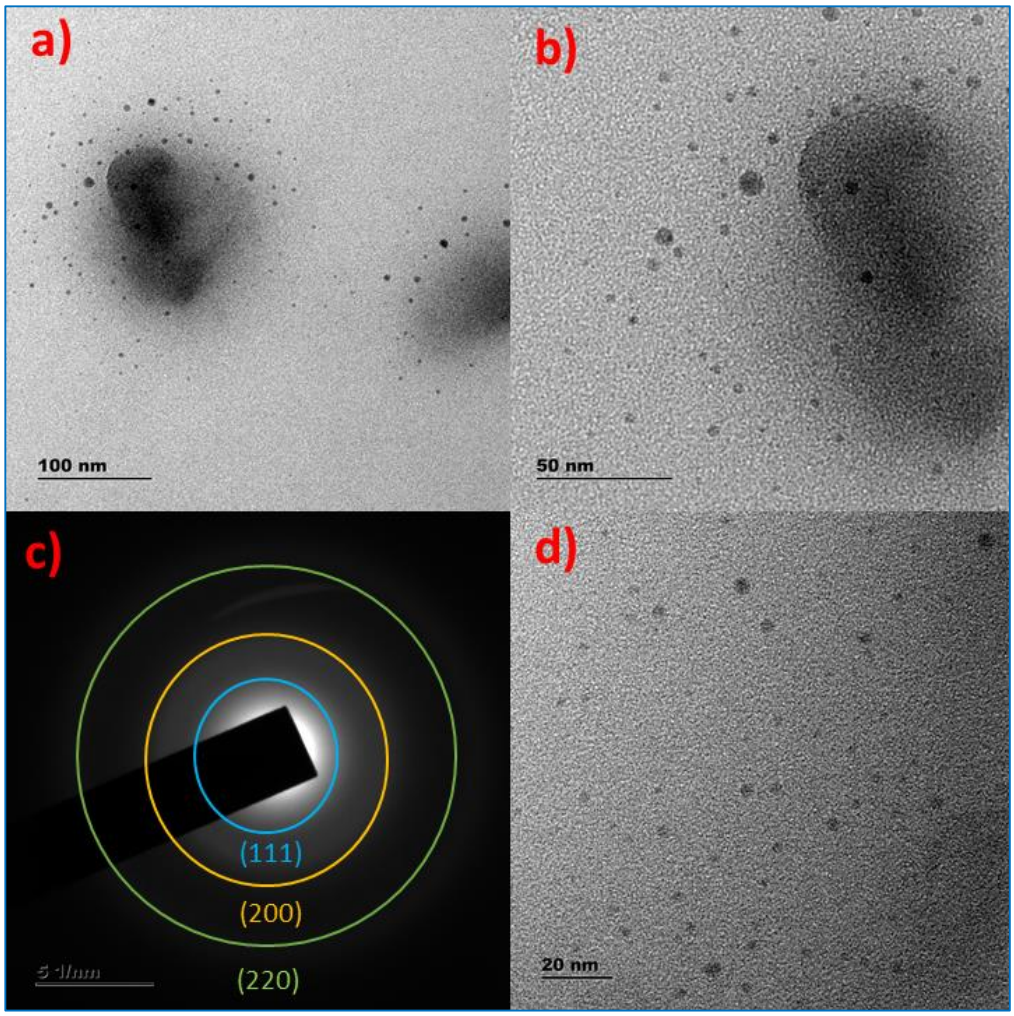

Figure 55. The TEM images of *E*-Cu NPs (C5) with nearly spherical shapes at various magnifications a) 100 nm, b) 50 nm d) 20 nm along with SAED pattern (c)).

A few bright dispersed concentric circles appeared on the SAED pattern (Figure 55c) of Cu NPs. The most prominent 3 concentric circles represent (111), (200), and (220) planes of crystalline face centered cubic Cu. Since the percentage of crystallinity was found to be less, the SAED rings exhibited obscured concentric patterns for the crystal planes of copper.

This SAED analysis using HRTEM images is in compliance with the previously discussed XRD results for the E-Cu NPs. It can be concluded that both XRD and SAED ring analysis confirms the partially crystalline nature of amorphous Cu NPs.

The leaf extract of *Syzygium guineense* plant (PE6) was applied to synthesize Cu NPs but the final product obtained was CuO NPs. The biomolecules present in the extract were alkaloids, phenolic compounds, tannins, saponins, anthraquinone glycosides and cardiac glycosides.

The morphological features of synthesized S-CuO NSs as depicted by SEM micrographs are shown in Figure 56a and 56b. The SEM images also presented various types of nanoparticles in terms of their shape and size.

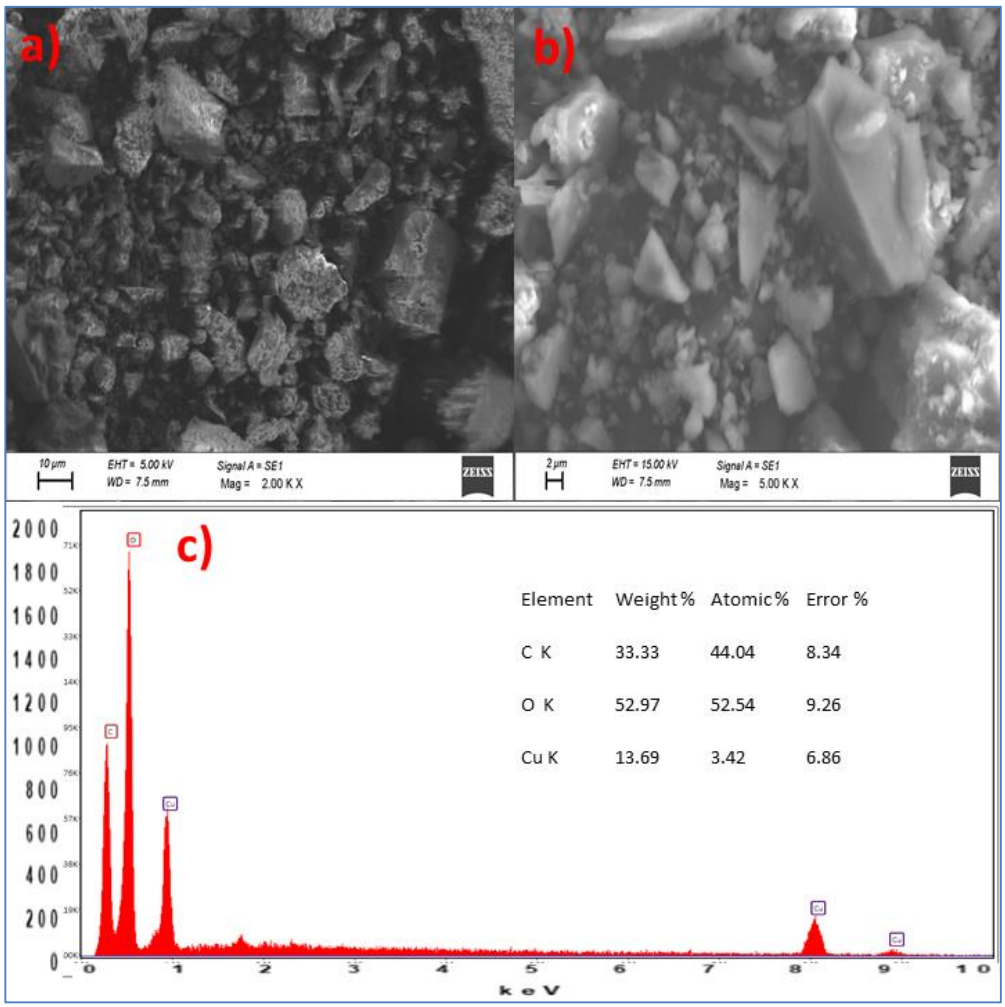

Figure 56. (a) and (b) SEM micrographs of S-CuO NPs (C6) (c) EDAX spectrum of *S*-Cu NPs (C6).

EDAX analysis revealed the elemental composition of the S-CuO NPs as depicted in Figure 56c. The peaks corresponding to elemental Cu, C and O were clearly identified demonstrating the purity of the synthesized NSs and this is consistent with the XRD studies. No additional impurity peaks were observed.

The presence of elements, C and O can be attributed to capped bioactive compounds. In addition, it is also apprehended that copper present at the surface had been converted into CuO. The reduction of copper ions to Cu NPs is facilitated by the biomolecules of plant extract containing surface hydroxyl groups. The HRTEM images of as-synthesized S-CuO (C6) NPs (Figure 57) shows that the synthesized NPs are nearly spherical but aggregated.

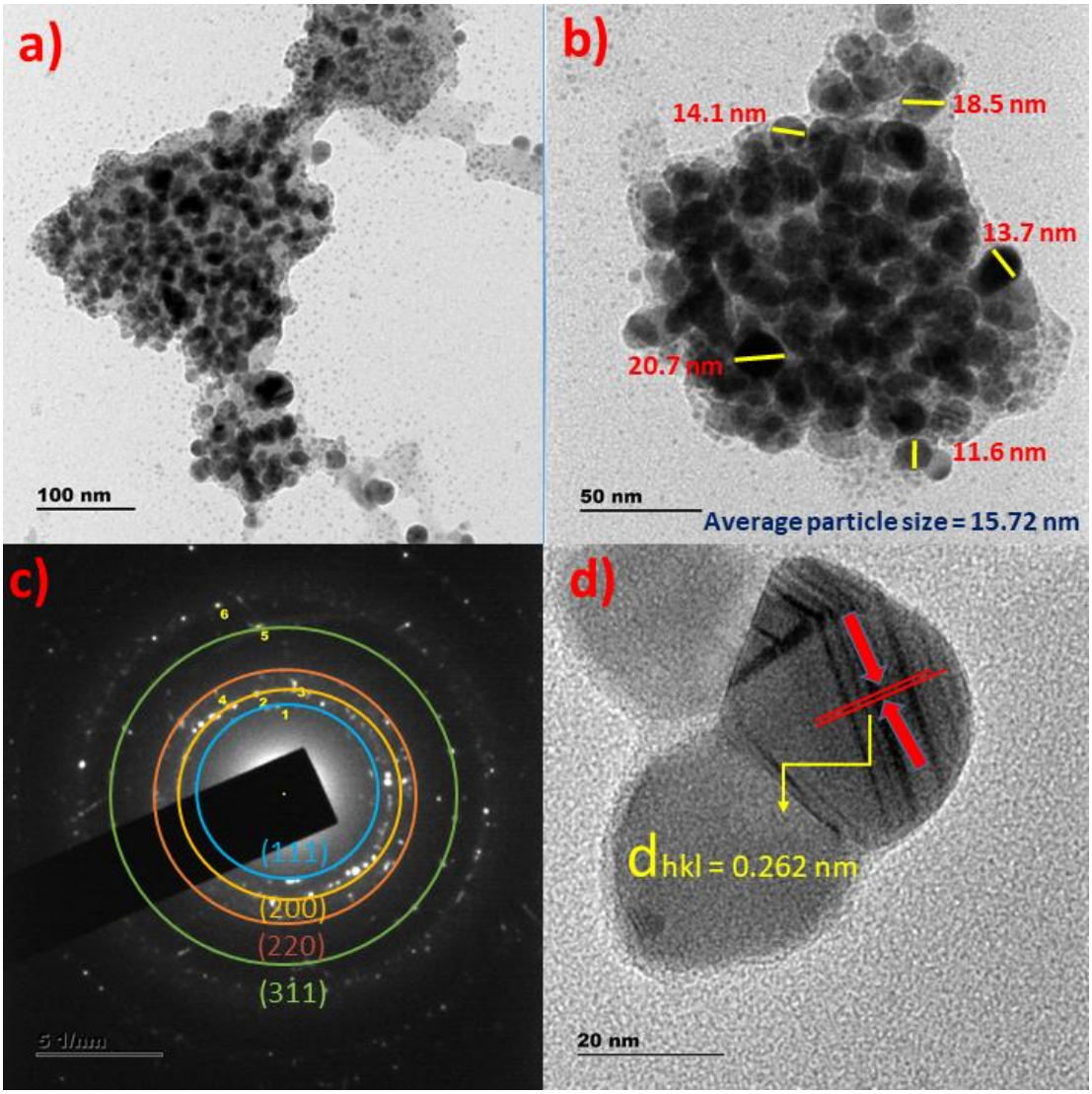

Figure 57. TEM micrographs of S-CuO NPs (C6) at (a) weak magnification (100 nm) and (b) strong magnification (50 nm) (c) SAED pattern (6 spots) and (d) HRTEM micrographs of lattice fringes of S-CuO NPs (C6) with IPS value of 0.262 nm.

The nearly spherical particles with varying sizes from 11.6 nm to 20.7 nm with an average particle size of 15.72 nm are as shown in Figure 57a and 57b.

The six spots corresponding to specific crystal planes were observed on SAED pattern of S-CuO NPs (Figure 57c). One of such planes is presented with d-spacing of 0.262 nm as shown in Figure 57d.

The Figure 58a, 58b and 58c presents the HRTEM micrographs with S-CuO NPs with magnified lattice fringes, IFFT patterns and profile of IFFT with d-spacing value for a specified plane (Figure 57d) respectively.

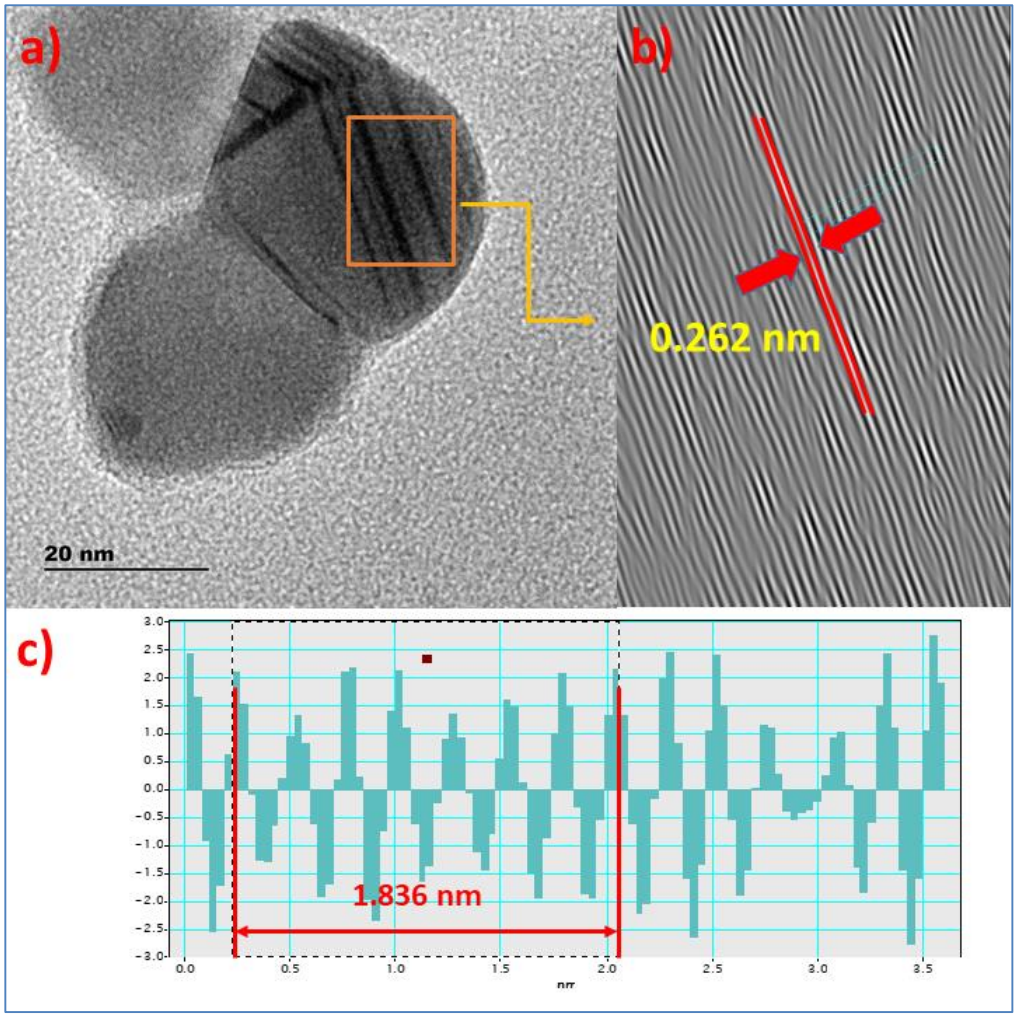

Figure 58. HRTEM morphology of S-CuO NPs (C6) (a) Enhanced lattice fringes (b) IFFT pattern (c) Profile of IFFT with IPS value.

The d_{hkl} value of 0.262 nm for a specific set of crystal planes at the surface of CuO NPs was deduced by using Gatan Digital Micrograph Software application.

The d-spacing values of the derived diffraction planes from spot 1 to spot 6 corresponds to major crystal planes of CuO. The absence of Cu and Cu_2O peaks in the XRD pattern can be possibly due to their presence in very small quantities. This SAED-HRTEM analysis is in good agreement with the previously arrived XRD results for the V-CuO NPs and S-CuO NPs.

4.6. Antibacterial activities of biogenic Ag NPs

The V-Ag NPs (A1) demonstrated superior antibacterial activities versus all the tested pathogens; *S. aureus, E. coli, P. aeruginosa,* and *E. aerogenes*. The present work evaluated synergistic influence of biomolecules with NPs against the four pathogens. The zone of

inhibitions for Chloramphenicol, DMSO and NPs with four concentrations (6.25, 12.5, 25 and 50 µg/µL) are as shown in Figure 59. V-Ag NPs were found to show better antimicrobial activity against *E. aerogenes* (Gram negative bacteria) than Gram positive bacteria which could be attributed to the structural differences in the cell walls of bacteria (Kaur et al. 2016).

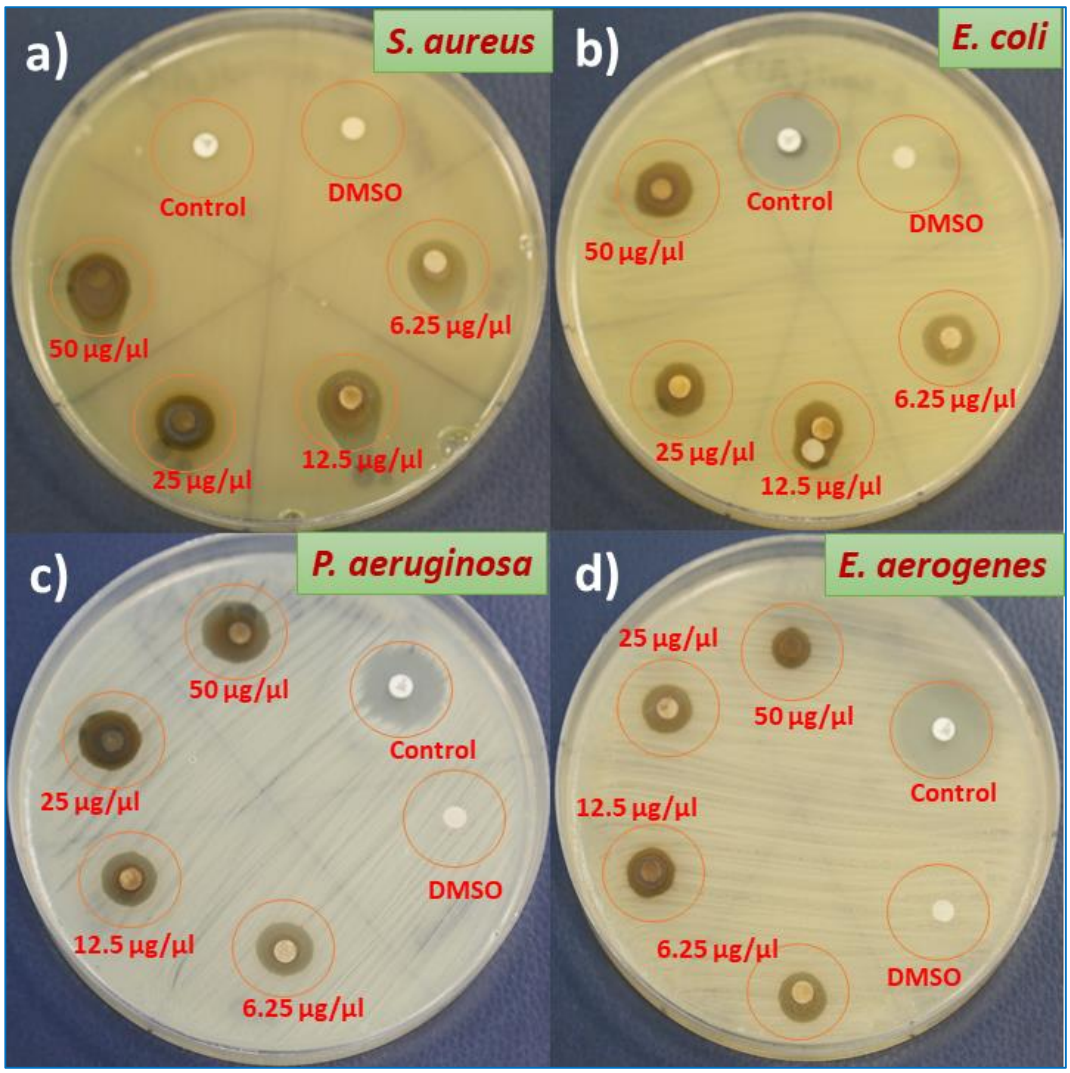

Figure 59. The antibacterial activity of V-Ag NPs (A1) versus bacterial strains,

(a) *S. aureus* (b) *E. coli* (c) *P. aeruginosa* (d) *E. aerogenes*

The antimicrobial activity of V-Ag NPs was highly appreciable against *E. aerogenes*. The maximum zone of inhibitions (mm) inscribed for 50 µg/µL of *V-SNS* against S. aureus, E. coli and E. aerogenes bacteria are 17 mm, 17 mm and 12 mm, respectively while the uppermost zone of inhibition (mm) noted against *P. aeruginosa bacteria* was 18 mm (Table 10). In addition, the lowest zone of inhibition exhibited by all the bacteria remained at 13 mm for the most diluted concentration of NPs.

Table 10. The zone of inhibitions for various bacteria by V-Ag NPs.

Concentration of NSs (µg/µL)	Bacterial strains and Zone of Inhibition in mm			
	S. aureus ATCC25923	*E. coli* ATCC25992	*P. aeruginosa* ATCC27853	*E. Aerogenes* ATCC13048
50	17	17	18	12
25	16	15	17	15
12.5	15	14	15	14
6.25	14	13	14	13
DMSO	6	6	6	6
Chloramphenicol	6	28	23	26

The antimicrobial resistance recorded for V-Ag NPs, was found to be superior when compared with few of the earlier results (Table 11) presented by many researchers even though few other workers reported higher inhibitions which could be due to the usage of higher concentrations of NS or presence of higher concentrations of bioactive compounds. The highest zone of inhibition (mm) recorded with Ag NPs against bacteria was 18 mm. Thus it can be concluded that the cumulative effect of Ag NPs coupled with phytochemicals (tannins, saponins and glycosides) of *leaf* extract proved to be detrimental for bacteria.

Even though many antimicrobial mechanisms were proposed by earlier researchers, the action of V-Ag NPs on the bacteria is unknown and yet to be exploited completely. Nanostructures were found to cause the death of bacteria adopting direct or indirect ways by attacking its cell wall, inhibiting RNA synthesis and preventing DNA replication (Figure 60). The direct mechanism of the interaction of nanostructures led to damage to the cell wall and generates ROS inside. Whereas, the indirect mechanism shows the interaction of NS with the bacterial environment outside the cell and generates reactive oxygen species (ROS) that further enters into the cell by damaging the cell wall. Both mechanisms finally led to cell death by affecting the DNA, ribosomes, and proteins of the bacteria (Abebe et al. 2020). It is assumed that the positive Ag^{+} in the NPs adsorb directly on to the cell wall of bacteria interacting with negatively charged species. This results in disruption of the cell wall and damage occurred by entering into the cell through the generation of ROS by the effect of visible/UV light radiation.

Table 11. Comparative statistics of antimicrobial activities of V-Ag NPs (A1) synthesised by using various plant extracts.

Sl. No.	Plant extract	Zone of Inhibition (mm)	Tested Pathogens	Reference
1	*Bergenia ciliata*	8.5	*S. aureus*	(Phull et al. 2016)
2	*Balloon flower plants*	12	*E. coli*	(Anbu et al. 2019)
3	*Aloe fleurentiniorum*	12, 14.5	*E. coli, S. aureus*	(Salmen and Alharbi 2020)
4	*Chenopodium murale*	12.7	*S. aureus*	(Abdel-Aziz et al. 2014)
5	*Ocimum Sanctum (Tulsi)*	14	*E.coli*	(Jain and Mehata 2017)
6	*Acanthospermum hispidum*	15, 16	*E. coli, P. aurognosa,*	(Ghotekar et al. 2019)
7	Banana peel extract	17, 16, 12	*E. coli, S. aureus, B. subtilis.*	(Ibrahim 2015)
8	*Vernonia amygdalina Del.*	17, 17, 18, 12	*S. aureus, E. coli, P. aurognosa, E. Aerogenes*	Present work
9	*Rosmarinus officinali*	17.2, 18.8, 31.2, 16.2	*E. coli, P. aurognosa, S. aureus, B. subtilis.*	(Khafri 2015)
10	*Citrus paradisi (grapefruit red)*	22	*E.coli*	(Ayinde et al. 2018)
11	*Coffea arabica*	23, 21	*E. coli, S. aureus*	(Dhand et al. 2016)

It is also assumed that the cumulative effect of V-Ag NPs and bioactive compounds of PE1 leaf extract displayed magnificent influence on bacteria as suggested by the recent researcher.

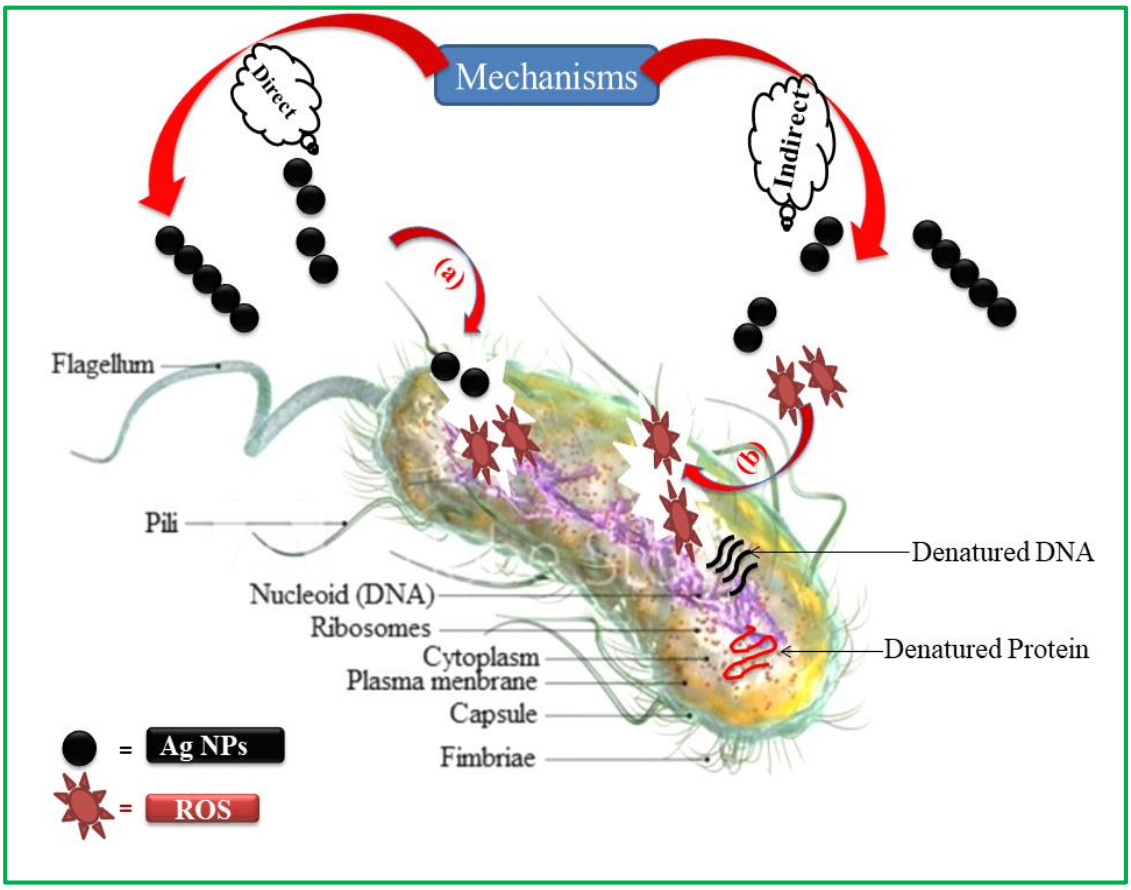

Figure 60. The mechanism of antibacterial activity of V-Ag NPs towards pathogens.

The mechanism of action of V-Ag NPs basically differs as there exist significant structural differences between Gram-negative and Gram-positive bacteria (Anbu et al. 2019). In addition, electrochemical charge variations across the cell membrane influences interaction with the released Ag^{+} ion by V-Ag NPs deteriorating the structural integrity of the membrane (Thangamani and Bhuvaneshwari 2019). The maximum antibacterial activity is recorded with Gram-negative bacteria than the Gram-positive bacteria due to their differences in their cell structure as well as the potentiality of nanostructures (Muthuvel et al. 2020).

On the similar lines, the antibacterial activities of the remaining silver nanoparticles were also determined and the zone of inhibition values are presented in the following Table 12, 13, 14 and 15 for A2, A3, A4 and A5 Ag NPs respectively.

Table 12. The zone of inhibitions for various bacteria by H-Ag NPs (A2).

Concentration of NSs (µg/µl)	Bacterial strains and Zone of Inhibition in mm			
	S. aureus ATCC25923	*E. coli* ATCC25992	*P. aeruginosa* ATCC27853	*E. Aerogenes* ATCC13048
50	19	14	12	8
25	18	10	11	8
12.5	17	15	11	6
6.25	15	13	11	6
Chloramphenicol	21	24	6	27
DMSO	6	6	6	6

Table 13. The zone of inhibitions for various bacteria by A-Ag NPs (A3).

Concentration of NSs (µg/µl)	Bacterial strains and Zone of Inhibition in mm			
	S. aureus ATCC25923	*E. coli* ATCC25992	*P. aeruginosa* ATCC27853	*E. Aerogenes* ATCC13048
50	16	14	16	9
25	15	14	15	13
12.5	16	12	14	14
6.25	15	12	14	15
Chloramphenicol	20	27	6	26
DMSO	6	6	6	6

Table 14. The zone of inhibitions for various bacteria by C-Ag NPs (A4).

Concentration of NSs (µg/µl)	Bacterial strains and Zone of Inhibition in mm			
	S. aureus ATCC25923	*E. coli* ATCC25992	*P. aeruginosa* ATCC27853	*E. Aerogenes* ATCC13048
50	14	11	10	12
25	12	11	15	12
12.5	16	12	12	14
6.25	15	11	15	15
Chloramphenicol	23	26	6	26
DMSO	6	6	6	6

Table 15. The zone of inhibitions for various bacteria by E-Ag NPs (A5).

Concentration of NSs (µg/µl)	Bacterial strains and Zone of Inhibition in mm			
	S. aureus ATCC25923	*E. coli* ATCC25992	*P. aeruginosa* ATCC27853	*E. Aerogenes* ATCC13048
50	18	9	16	11
25	18	13	15	12
12.5	16	14	16	13
6.25	14	11	15	15
Chloramphenicol	25	24	6	30
DMSO	6	6	6	6

The antibacterial activity of S-Ag NPs (A6) activity was pronounceable against *S. aureus*. The highest zone of inhibition (mm) recorded with 50 µg/µl of *S*-Ag NPs against *E. aerogenes* bacteria was 13 mm and the lowest zone of inhibition (mm) recorded against P. *aeruginosa* bacteria was 10 mm (Table 16). The wide zone of inhibitions of *S*-Ag NPs against pathogens confirm their great potentiality as a remedy for infectious diseases caused by the tested bacterial pathogens.

Table 16. The variation of zone of inhibitions for different bacteria by *S*-Ag NPs (A6).

Concentration of NPs (µg/µl)	Bacterial strains and Zone of Inhibition in mm			
	S. aureus ATCC25923	*E. coli* ATCC25992	*P. aeruginosa* ATCC27853	*E. Aerogenes* ATCC13048
50	11	12	10	13
25	11	10	8	10
12.5	6	8	6	8
6.25	6	6	6	6
Chloramphenicol	24	20	6	3
DMSO	6	6	6	6

Additionally, the standard disc chloramphenicol showed comparable zone of inhibition with the *S*-Ag NPs, which is small and it can be attributed to development of resistance by bacteria against chloramphenicol. These results in failed metabolism and thereby leading to interference and disruption of transcription in bacteria and hence causes antibacterial activity by *S*-Ag NPs. It is also believed that the synergistic effect of *S*-Ag NPs with bioactive compounds of extract would have played significance influence to inhibit the activity of pathogenic bacteria.

4.7. Antibacterial activities of biogenic Cu/CuO NPs

The V-CuO NPs (C1) demonstrated average antibacterial activities against all the tested pathogens; *S. aureus*, *E. coli*, *P. aeruginosa*, and *E. aerogenes* when compared with V-Ag NPs (A1). The present work evaluated synergistic influence of biomolecules with NPs against 4 pathogens. The zone of inhibitions for Chloramphenicol, DMSO and NPs with four concentrations (6.25, 12.5, 25 and 50 µg/µl) are as shown in Figure 61. V-CuO NPs were found to show better antimicrobial activity against *E. aerogenes* (Gram negative bacteria) than Gram positive bacteria which could be attributed to the structural differences in the cell walls of bacteria.

The antimicrobial activity of NPs was highly appreciable against *E. aerogenes*. The maximum zone of inhibition (mm) inscribed for 50 µg/µl of V-CuO NPs verses *S. aureus*,

E. coli and *P. aeruginosa* bacteria is 12 mm while the same inscribed against *E. aerogenes* bacteria is 15 mm (Table 17).

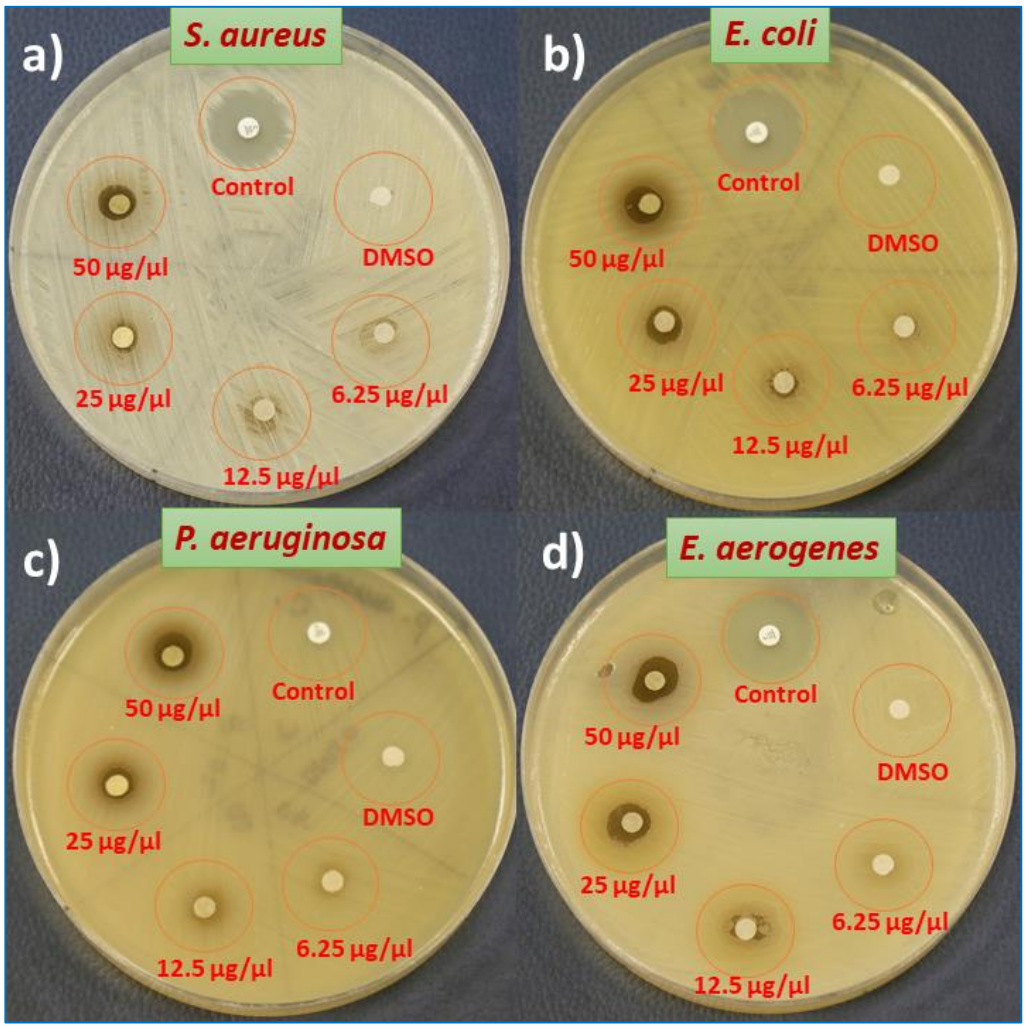

Figure 61. The antibacterial activity of VeA-CuO NPs versus bacteria,

(a) *S. aureus* (b) *E. coli* (c) *P. aeruginosa* (d) *E. aerogenes*

In addition, the lowest zone of inhibition exhibited by all the bacteria remained at 6 mm for the most diluted concentration of NPs. The pure copper oxide was proved to exhibit excellent antimicrobial activity. The varied zone of inhibitions as shown in Figure 61, exhibited by V-CuO NPs against pathogens confirm their superior potentiality to inhibit and cause death of pathogens. The bacterial resistance was found to enhance with increase in the concentration of the NPs for all the bacteria. The antimicrobial resistance recorded for V-CuO NPs, was found to be superior when compared with few of the earlier results (Table 18) presented by many researchers even though few other workers reported higher inhibitions which could be due to the usage of higher concentrations of NPs or presence of

higher concentrations of bioactive compounds. The uppermost zone of inhibition (mm) recorded with CuO NPs against bacteria was 15 mm.

Table 17. The zone of inhibitions for various bacteria by V-CuO NPs (C1)

Concentration of NSs (µg/µL)	Bacterial strains and Zone of Inhibition in mm			
	S. aureus ATCC25923	*E. coli* ATCC25992	*P. aeruginosa* ATCC27853	*E. Aerogenes* ATCC13048
50	12	12	12	15
25	8	11	10	13
12.5	6	8	6	12
6.25	6	6	6	6
DMSO	6	6	6	6
Chloramphenicol	25	29	6	27

The cumulative effect of CuO NPs coupled with phytochemicals (tannins, saponins and glycosides) of PE1 extract proved to be detrimental for bacteria. Even though many antimicrobial mechanisms were proposed by earlier researchers, the action of V-CuO NPs on the bacteria is unknown and yet to be exploited completely.

Table 18. Antimicrobial activities of Cu/CuO synthesised by using various plant and algal extracts.

Sl. No.	Plant extract	NPs	Zone of Inhibition (mm)	Tested Pathogens	Reference
1	*Syzygium aromaticum bud*	Cu	7	*E. coli*	(Rajesh et al. 2018)
2	*Brassica oleracea var. italic*	CuO	9	*C.albicans*	(Renuga et al. 2020)
3	*Leucaena leucocephala L. and*	CuO	11	*P. aeruginosa*	(Aher et al. 2017)
4	*S. lavandulifolia flower*	Cu/Cu_2O	12	*P. aeruginosa*	(Khatami et al. 2017)

5	*Ziziphus spina-christi (L.) Willd. fruit*	Cu	13	*E. coli* *S. aureus*	(Khani et al. 2018)
6	Green and black tea leaves	Cu	14	*S. aureus*	(Asghar et al. 2018)
7	*Achillea millefolium*	CuO	14	*S. aureus*	(Rabiee et al. 2020)
8	*Vernonia amygdalina Del leaves*	CuO	15	*E. aerogenes*	Present work
9	*Green Alga Botryococcus braunii*	Cu	17	*P. aeruginosa*	(Arya et al. 2018)
10	*Tabernaemontana divaricate leaves*	CuO	17	*E.coli*	(Sivaraj et al. 2014)
11	*Punica granatum peel*	CuO	18.6	*P. aeruginosa*	(Ghidan et al. 2016)
12	*Asparagus adscendens Roxb. Root and Leaves*	Cu	19	*E.coli*	(Thakur et al. 2018)
13	*Aloe vera Leaves*	CuO	21	*A. hydrophila*	(Kumar et al. 2015)

The maximum antibacterial activity is recorded with Gram-negative bacteria than the Gram-positive bacteria due to their differences in their cell structure as well as the potentiality of nanoparticles displayed magnificent influence on bacteria as revealed by the past study. The standard disc Chloramphenicol showed comparatively lesser zone of inhibition with the V-CuO NPs, which can be attributed to the development of resistance by bacteria against Chloramphenicol. The zone of inhibition values for CuO NPs was found to be moderately lower for *S. aureus*, *E. coli* and *E. aerogenes* except *P. aeruginosa* when compared with that of positive control Chloramphenicol. It is possibly due to the differences in the chemical structure of the bacterial cell walls and as a consequence different types of interactions occur between differently sized NPs and bacterial strains. The interaction between CuO NPs and microorganisms starts with adhesion of CuO NPs to the microbial cell wall and membrane, which is based on electrostatic attraction between the negatively charged microbial cell membrane and positively or less negatively charged CuO NPs. Zeta potential is another physico-chemical property influence antimicrobial activity since the interaction between

NPs and the cell membrane is based on electrostatic adhesion which is different for different bacterial strains. On the similar lines, the antibacterial activities of the copper nanoparticles were also determined and the zone of inhibition values are presented in the following table 19, 20, 21 and 22 for C2, C3, C4 and C5 Ag NPs respectively. Among these NPs, C2, C3 and C4 are crystalline Cu NPs but C5 exhibited partial amorphous nature.

Table 19. The zone of inhibitions for various bacteria by H-Cu NPs (C2)

Concentration of NSs (µg/µl)	Bacterial strains and Zone of Inhibition in mm			
	S. aureus ATCC25923	*E. coli* ATCC25992	*P. aeruginosa* ATCC27853	*E. Aerogenes* ATCC13048
50	6	9	6	10
25	6	6	6	8
12.5	6	6	6	8
6.25	6	6	6	6
Chloramphenicol	20	25	6	30
DMSO	20	25	6	30

Table 20. The zone of inhibitions for various bacteria by A-Cu NPs (C3)

Concentration of NSs (µg/µl)	Bacterial strains and Zone of Inhibition in mm			
	S. aureus ATCC25923	*E. coli* ATCC25992	*P. aeruginosa* ATCC27853	*E. Aerogenes* ATCC13048
50	11	12	10	13
25	11	10	8	10
12.5	6	8	6	8
6.25	6	6	6	6
Chloramphenicol	24	20	6	30
DMSO	6	6	6	6

Table 21. The zone of inhibitions for various bacteria by C-Cu NPs (C4)

Concentration of NSs (µg/µl)	Bacterial strains and Zone of Inhibition in mm			
	S. aureus ATCC25923	*E. coli* ATCC25992	*P. aeruginosa* ATCC27853	*E. Aerogenes* ATCC13048
50	8	8	6	6
25	6	12	6	6
12.5	6	14	6	6
6.25	6	14	6	6
Chloramphenicol	23	30	6	28
DMSO	6	6	6	6

Table 22. The zone of inhibitions for various bacteria by *EcS*-Cu NPs.

Concentration of NPs (µg/µl)	Bacterial strains and Zone of Inhibition in mm			
	S. aureus ATCC25923	*E. coli* ATCC25992	*P. aeruginosa* ATCC27853	*E. Aerogenes* ATCC13048
50	13	12	10	12
25	10	12	10	12
12.5	10	10	10	12
6.25	10	10	6	12
DMSO	20	22	6	28
Chloramphenicol	6	6	6	6

E-Cu NPs (C5) were found to show better antimicrobial activity against both Gram negative bacterial strains and Gram positive bacterial strains with slight lower zone of inhibition only for *P. aeruginosa* bacterial strains (Figure 62).

The antimicrobial activity of NPs was highly appreciable against *S. aureus* with ZoI of 13 mm. The maximum zone of inhibitions (mm) inscribed by *E*-Cu NPs against *E. coli, P. Aeruginosa* and *E. aerogenes* bacteria are 12 mm, 10 mm and 12 mm, respectively (Table 22). In addition, the lowest zone of inhibition was exhibited by *P. aeruginosa*

bacteria remained at 6 mm for the most diluted solution of NPs. In case of *E. coli*, and *S. aureus*, the ZoI increased from 10 mm to 13 mm and 10 mm to 12 mm on moving from 12.5 µg/µl to 50 µg/µl concentration, respectively. But *P. aeruginosa* and *E. aerogenes* bacterial strains exhibited almost constant ZoI for concentrations of NPs beyond 12.5 µg/µl. This behaviour is basically due to the structural differences between two types of bacteria as well as differences in the morphological features of Cu NPs (Rajivgandhi et al. 2019).

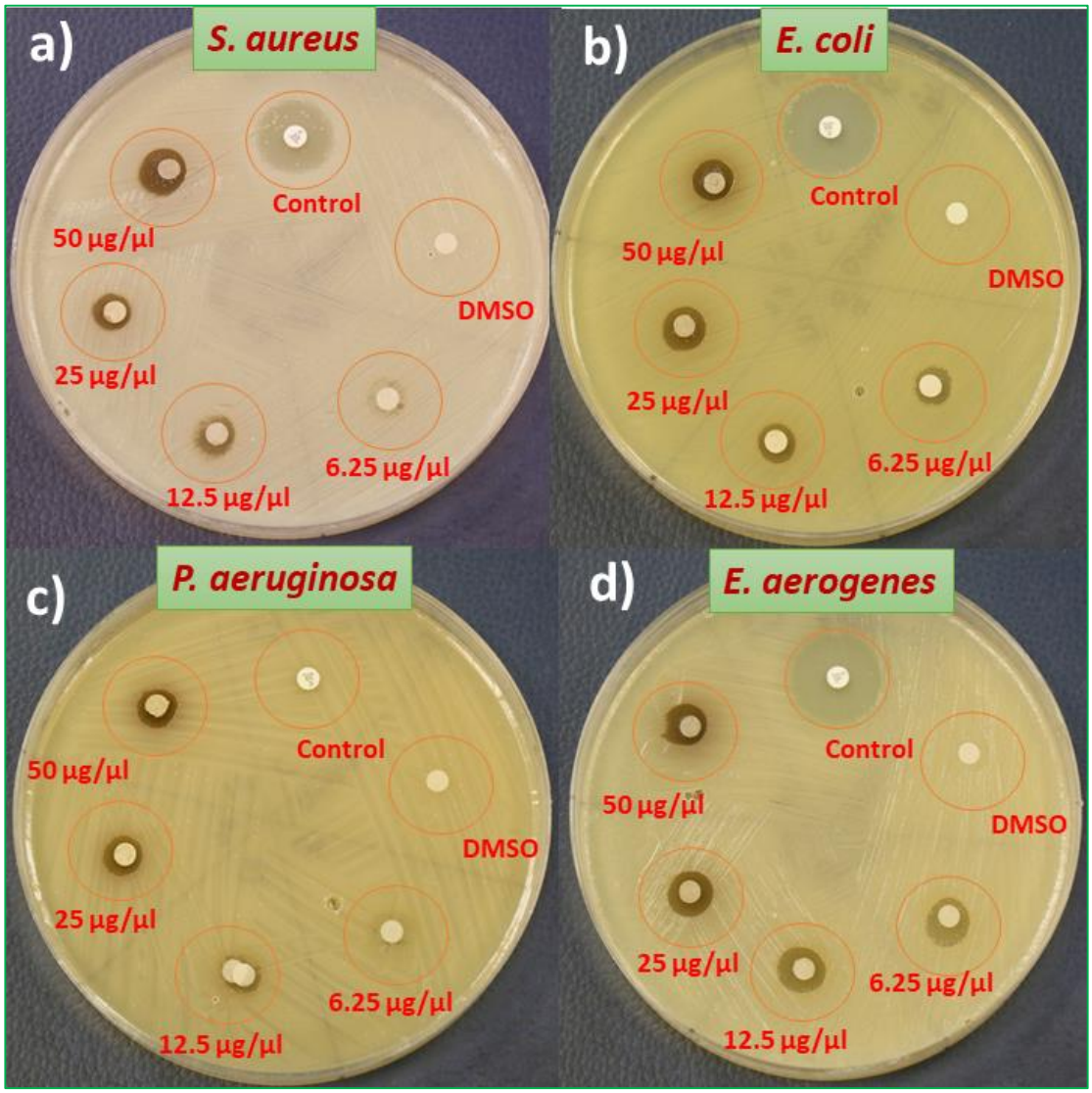

Figure 62. The antibacterial activity of *E*-Cu NPs (C5) verses bacteria,

(a) *S. aureus* (b) *E. coli* (c) *P. aeruginosa* (d) *E. aerogenes*

The extract of Syzygium guineense (Willd.) DC Plant leaves when applied to synthesize copper NPs yielded CuO NPs similar to what has happened with V-CuO NPs. The highest

zone of inhibition (mm) recorded with 50 µg/µl of *SyG*-CuO NSs against *S. aureus*, *E. coli and E. aerogenes* bacteria was 12 mm and the lowest zone of inhibition (mm) recorded against P. *aeruginosa* bacteria was 10 mm (Table 22).

Table 23. The zone of inhibitions for various bacteria by S-CuO NPs (C6)

Concentration of NSs (µg/µl)	Bacterial strains and Zone of Inhibition in mm			
	S. aureus ATCC25923	*E. coli* ATCC25992	*P. aeruginosa* ATCC27853	*E. Aerogenes* ATCC13048
50	12	12	10	12
25	10	12	10	12
12.5	10	10	10	12
6.25	10	10	6	12
Chloramphenicol	20	22	6	28
DMSO	6	6	6	6

Pure Cu and its oxides were proved to exhibit excellent antimicrobial activity. The wide zone of inhibitions of *S*-CuO NSs against pathogens confirm their superior potentiality to inhibit and cause death of pathogens. It was found that the bacterial resistance decreased with increase in the concentration of the nanoparticles for all the bacteria except *E. aerogenes*.

5. CONCLUSIONS AND RECOMMENDATIONS

5.1 Conclusions

The application of medicinal plants, *Vernonia amygdalina del., Hagenia abyssinica (Brace) JF. Gmel., Artemisia absinthium L., Carum copticum L., Echinops sp.* and Syzygium guineense (Willd.) DC plant extracts towards the green synthesis of silver and copper nanoparticles (Ag and Cu NPs) was successful. In addition, PE1 and PE6 plant extracts yielded CuO NPs. The UV-visible, UV-DRS, FT-IR, XRD, TGA-DTA, SEM, EDXA, TEM, HRTEM and SAED techniques were employed to characterize the NPs. The UV-visible spectra, XRD pattern and FTIR spectra substantiated the formation of crystalline Ag NPs in the presence of biomolecules (alkaloids, flavonoids, polyphenols, tannins, saponins, glycosides and proteins) of plant leaf, root and seed extracts. The absorbance maxima, λmax appeared in the wavelength ranges of 411 nm – 462 nm for Ag NPs and 403 nm – 454 nm for Cu/CuO NPs, confirmed the formation of silver and copper NPs, having energy gap varying in the range from 1.95 eV to 2.23 eV and 1.95 eV to 2.17 eV. The face centred cubic structure of silver was confirmed by the presence of peaks with 2θ values of 38.14^{o}, 44.7^{o}, and 64.50^{o}, and 77.42^{o} for 111, 200, 220 and 311 crystal lattice planes during XRD analysis. The peaks observed in the pattern at 2θ values = 35.76^{o}, 44.68^{o} and 64.37^{o} corresponds to (111), (200) and (220) lattice planes of face centred cubic structure of Cu NPs. In addition, partially crystalline and amorphous Cu NPs were also obtained along with the formation of highly crystalline CuO NPs from PE1 extract. The SEM-EDAX analysis confirmed the superficial morphology and composition of biogenic Ag and Cu/CuO NPs. The TGA curve revealed the two-step decomposition of Ag NPs, and three step decomposition for CuO NPs respectively. FT-IR spectral peaks substantiated the effective surface capping of biomolecules around the Ag and Cu NPs. TEM-HRTEM-SAED analysis of Ag and Cu NPs corroborated the existence of silver and copper by the observation of (111), (200), (220) and (311) lattice fringes and (111), (200), (220) lattice fringes in biogenic Ag and Cu NPs respectively. The interplanar d-spacing values varied from 0.126 nm to 0.262 nm for various planes of Ag and Cu NPs. The synergistic influence of surface amalgamated bioactive compounds and biogenic Ag and Cu NPs proved to exhibit highly effective antibacterial mechanism against pathogens, *S. aureus, E. coli, P. aeruginosa,* and *E. aerogenes* with 18 mm as a highest zone of inhibition. The antibacterial activity of all the Ag NPs was found to be superior when compared with that of Cu NPs. In addition, it can also be concluded that the leaf extracts of plants assisted in the formation of crystalline Ag and Cu NPs compared to root and seed extracts. Finally, it can also be concluded that the all the Ag NPs synthesized

by plant leaf, root and seed extracts exhibited higher degrees of crystallinity whereas, root and seed extracts of medicinal plants produced partially crystalline Cu and CuO NPs.

5.2 Recommendations

Authors recommendations towards futuristic research perspectives:

- The present work focused on the application of crude aqueous extract of Ethiopian medicinal plants for the green synthesis of Ag and Cu NPs. Therefore, there is a great scope in future to explore the effect of non-aqueous, solvent selective extract towards the synthesis of metallic nanoparticles.
- It is also very essential to extract specific biomolecules separately from the plants and apply them to synthesize metallic NPs to check exactly which phytochemical basically supports capping and stabilizing processes during the formation of metallic NPs.
- The present synthesis involved almost natural laboratory conditions for the green synthesis Ag and Cu NPs without imposing many constraints and hence optimization with respect to pH, temperature and ratio of precursor to plant extract can also be focused in the future work.
- The same green methodology using medicinal plants can be applied to synthesize bimetallic and core-shell nanostructures to evaluate the combined effect of two metallic NPs over the bacterial cell wall and its disintegration.
- The morphological features of Ag and Cu NPs such as size and shape, are expected to influence their antibacterial properties and thus effort can be made in future to explore the factors that influences and controls particle size and shape.
- Application of microscopic technique to examine the interaction of metallic NPs and bacteria is highly needed to reveal the exact mechanism of bacterial death on interaction with NPs.

References

Abdel-Aziz MS, Shaheen MS, El-Nekeety AA, Abdel-Wahhab MA (2014) Antioxidant and antibacterial activity of silver nanoparticles biosynthesized using Chenopodium murale leaf extract. Journal of Saudi Chemical Society 18:356–363. https://doi.org/10.1016/j.jscs.2013.09.011

Abebe B, Zereffa EA, Tadesse A, Murthy HCA (2020) A Review on Enhancing the Antibacterial Activity of ZnO: Mechanisms and Microscopic Investigation. Nanoscale Research Letters 15:190

Abera B (2014) Medicinal plants used in traditional medicine by Oromo people, Ghimbi District, Southwest Ethiopia. Journal of Ethnobiology and Ethnomedicine 10:. https://doi.org/10.1186/1746-4269-10-40

Aher Y, Jain G, Patil G, et al (2017) Biosynthesis of copper oxide nanoparticles using leaves extract of Leucaena leucocephala L. and their promising upshot against diverse pathogens. International Journal of Molecular and Clinical Microbiology 7:776–786

Ahmed S, Ahmad M, Swami BL, Ikram S (2016a) A review on plants extract mediated synthesis of silver nanoparticles for antimicrobial applications: A green expertise. Journal of Advanced Research 7:17–28. https://doi.org/10.1016/j.jare.2015.02.007

Ahmed S, Saifullah, Ahmad M, et al (2016b) Green synthesis of silver nanoparticles using Azadirachta indica aqueous leaf extract . Journal of Radiation Research and Applied Sciences 9:1–7. https://doi.org/10.1016/j.jrras.2015.06.006

Aminuzzaman M, Kei LM, Liang WH (2017) Green synthesis of copper oxide (CuO) nanoparticles using banana peel extract and their photocatalytic activities. AIP Conference Proceedings 1828:. https://doi.org/10.1063/1.4979387

Anbu P, Gopinath SCB, Yun HS, Lee CG (2019) Temperature-dependent green biosynthesis and characterization of silver nanoparticles using balloon flower plants and their antibacterial potential. Journal of Molecular Structure 1177:302–309. https://doi.org/10.1016/j.molstruc.2018.09.075

Annu, Ali A, Ahmed S (2018) Green Synthesis of Metal, Metal Oxide Nanoparticles, and Their Various Applications. Handbook of Ecomaterials 1–45. https://doi.org/10.1007/978-3-319-48281-1_115-1

Arya A, Gupta K, Chundawat TS, Vaya D (2018) Biogenic Synthesis of Copper and Silver Nanoparticles Using Green Alga Botryococcus braunii and Its Antimicrobial Activity. Bioinorganic Chemistry and Applications 2018:. https://doi.org/10.1155/2018/7879403

Asghar MA, Zahir E, Shahid SM, et al (2018) Iron, copper and silver nanoparticles: Green synthesis using green and black tea leaves extracts and evaluation of antibacterial, antifungal and aflatoxin B 1 adsorption activity. LWT - Food Science and Technology 90:98–107. https://doi.org/10.1016/j.lwt.2017.12.009

Ayinde WB, Gitari MW, Muchindu M, Samie A (2018) Biosynthesis of Ultrasonically Modified Ag-MgO Nanocomposite and Its Potential for Antimicrobial Activity. Journal of Nanotechnology 2018:1–10. https://doi.org/10.1155/2018/9537454

Azarbani F, Shiravand S (2020) Green synthesis of silver nanoparticles by Ferulago macrocarpa flowers extract and their antibacterial, antifungal and toxic effects. Green Chemistry Letters and Reviews 13:41–49. https://doi.org/10.1080/17518253.2020.1726504

Bar H, Bhui DK, Sahoo GP, et al (2009) Green synthesis of silver nanoparticles using latex of Jatropha curcas.

Colloids and Surfaces A: Physicochemical and Engineering Aspects 339:134–139. https://doi.org/10.1016/j.colsurfa.2009.02.008

Bhagwat TR, Joshi KA, Parihar VS, et al (2018) Biogenic copper nanoparticles from medicinal plants as novel antidiabetic nanomedicine. World Journal of Pharmaceutical Research 7:183–196. https://doi.org/10.20959/wjpr20184-10773

Bordbar M, Sharifi-Zarchi Z, Khodadadi B (2017) Green synthesis of copper oxide nanoparticles/clinoptilolite using Rheum palmatum L. root extract: high catalytic activity for reduction of 4-nitro phenol, rhodamine B, and methylene blue. Journal of Sol-Gel Science and Technology 81:724–733. https://doi.org/10.1007/s10971-016-4239-1

Cheirmadurai K, Biswas S, Murali R, Thanikaivelan P (2014) Green synthesis of copper nanoparticles and conducting nanobiocomposites using plant and animal sources. RSC Advances 4:19507–19511. https://doi.org/10.1039/c4ra01414f

Chung I, Rahuman AA, Marimuthu S, et al (2017) Green synthesis of copper nanoparticles using eclipta prostrata leaves extract and their antioxidant and cytotoxic activities. Experimental and Therapeutic Medicine 14:18–24. https://doi.org/10.3892/etm.2017.4466

Chung IM, Park I, Seung-Hyun K, et al (2016) Plant-Mediated Synthesis of Silver Nanoparticles: Their Characteristic Properties and Therapeutic Applications. Nanoscale Research Letters 11:1–14. https://doi.org/10.1186/s11671-016-1257-4

Day Z, Wandsnider L, Douglass MJ, University of Nebraska--Lincoln (2016) Preliminary studies in using X-ray diffraction for analyzing the atomic structure of Central Plains tradition constituents. 1 online resource (114 pages)

Delma MT, Jaya Rajan M (2016) Green Synthesis of Copper and Lead Nanoparticles using ZingiberOfficinale stemextract. International Journal of Scientific and Research Publications 6:134–137

Dessie Y, Tadesse S, Eswaramoorthy R (2020) Physicochemical parameter influences and their optimization on the biosynthesis of MnO2 nanoparticles using Vernonia amygdalina leaf extract. Arabian Journal of Chemistry 13:6472–6492. https://doi.org/10.1016/j.arabjc.2020.06.006

Dhand V, Soumya L, Bharadwaj S, et al (2016) Green synthesis of silver nanoparticles using Coffea arabica seed extract and its antibacterial activity. Materials Science and Engineering C 58:36–43. https://doi.org/10.1016/j.msec.2015.08.018

Din MI, Arshad F, Hussain Z, Mukhtar M (2017) Green Adeptness in the Synthesis and Stabilization of Copper Nanoparticles: Catalytic, Antibacterial, Cytotoxicity, and Antioxidant Activities. Nanoscale Research Letters 12:. https://doi.org/10.1186/s11671-017-2399-8

Dubey S, Sharma YC (2017) Calotropis procera mediated one pot green synthesis of Cupric oxide nanoparticles (CuO-NPs) for adsorptive removal of Cr(VI) from aqueous solutions. Applied Organometallic Chemistry 31:1–15. https://doi.org/10.1002/aoc.3849

Dudhane AA, Waghmode SR, Dama LB, et al (2019) Synthesis and characterization of gold nanoparticles using plant extract of Terminalia arjuna with antibacterial activity. International Journal of Nanoscience and Nanotechnology 15:75–82

Fuku X, Modibedi M, Mathe M (2020) Green synthesis of Cu/Cu2O/CuO nanostructures and the analysis of their electrochemical properties. SN Applied Sciences 2:902. https://doi.org/10.1007/s42452-020-2704-

5

Galan CR, Silva MF, Mantovani D, et al (2018) Green synthesis of copper oxide nanoparticles impregnated on activated carbon using Moringa oleifera leaves extract for the removal of nitrates from water. Canadian Journal of Chemical Engineering 96:2378–2386. https://doi.org/10.1002/cjce.23185

Ghidan AY, Al-Antary TM, Awwad AM (2016) Green synthesis of copper oxide nanoparticles using Punica granatum peels extract: Effect on green peach Aphid. Environmental Nanotechnology, Monitoring & Management 6:95–98. https://doi.org/10.1016/j.enmm.2016.08.002

Ghosh MK, Sahu S, Gupta I, Ghorai TK (2020) Green synthesis of copper nanoparticles from an extract of Jatropha curcas leaves: characterization, optical properties, CT-DNA binding and photocatalytic activity. RSC Advances 10:22027–22035. https://doi.org/10.1039/D0RA03186K

Ghosh S, Jagtap S, More P, et al (2015) Dioscorea bulbifera Mediated Synthesis of Novel Au core Ag shell Nanoparticles with Potent Antibiofilm and Antileishmanial Activity. Journal of Nanomaterials 2015:1–12. https://doi.org/10.1155/2015/562938

Ghotekar S, Pansambal S, Pawar SP, et al (2019) Biological activities of biogenically synthesized fluorescent silver nanoparticles using Acanthospermum hispidum leaves extract. SN Applied Sciences 1:1342. https://doi.org/10.1007/s42452-019-1389-0

Gul R, Jan SU, Faridullah S, et al (2017) Preliminary Phytochemical Screening, Quantitative Analysis of Alkaloids, and Antioxidant Activity of Crude Plant Extracts from Ephedra intermedia Indigenous to Balochistan. The Scientific World Journal 2017:1–7. https://doi.org/10.1155/2017/5873648

Gunalan S, Sivaraj R, Venckatesh R (2012) Aloe barbadensis Miller mediated green synthesis of mono-disperse copper oxide nanoparticles: Optical properties. Spectrochimica Acta - Part A: Molecular and Biomolecular Spectroscopy 97:1140–1144. https://doi.org/10.1016/j.saa.2012.07.096

Hemmati S, Mehrazin L, Hekmati M, et al (2018) Biosynthesis of CuO nanoparticles using Rosa canina fruit extract as a recyclable and heterogeneous nanocatalyst for C-N Ullmann coupling reactions. Materials Chemistry and Physics 214:527–532. https://doi.org/10.1016/j.matchemphys.2018.04.114

Huang W, Yan M, Duan H, et al (2020) Synergistic Antifungal Activity of Green Synthesized Silver Nanoparticles and Epoxiconazole against Setosphaeria turcica. Journal of Nanomaterials 2020:1–7. https://doi.org/10.1155/2020/9535432

Hussain RK, Aziz WJ, Ibrahim IA (2019) Antibacterial activity of CuO - cellulose nano rods depends on anew green synthesis (cotton). Journal of Nanostructures 9:761–767. https://doi.org/10.22052/JNS.2019.04.017

Ibrahim HMM (2015) Green synthesis and characterization of silver nanoparticles using banana peel extract and their antimicrobial activity against representative microorganisms. Journal of Radiation Research and Applied Sciences 8:265–275. https://doi.org/10.1016/j.jrras.2015.01.007

Ijaz F, Shahid S, Khan SA, et al (2017) Green synthesis of copper oxide nanoparticles using abutilon indicum leaf extract: Antimicrobial, antioxidant and photocatalytic dye degradation activities. Tropical Journal of Pharmaceutical Research 16:743–753. https://doi.org/10.4314/tjpr.v16i4.2

Issaabadi Z, Nasrollahzadeh M, Sajadi SM (2017) Green synthesis of the copper nanoparticles supported on bentonite and investigation of its catalytic activity. Journal of Cleaner Production 142:3584–3591. https://doi.org/10.1016/j.jclepro.2016.10.109

Jadhav MS, Kulkarni S, Raikar P, et al (2018) Green biosynthesis of CuO & Ag-CuO nanoparticles from Malus domestica leaf extract and evaluation of antibacterial, antioxidant and DNA cleavage activities. New Journal of Chemistry 42:204–213. https://doi.org/10.1039/c7nj02977b

Jain S, Mehata MS (2017) Medicinal Plant Leaf Extract and Pure Flavonoid Mediated Green Synthesis of Silver Nanoparticles and their Enhanced Antibacterial Property. Scientific Reports 7:1–13. https://doi.org/10.1038/s41598-017-15724-8

Javed B, Nadhman A, Mashwani Z-R (2020) Phytosynthesis of Ag nanoparticles from Mentha longifolia: their structural evaluation and therapeutic potential against HCT116 colon cancer, Leishmanial and bacterial cells. Applied Nanoscience. https://doi.org/10.1007/s13204-020-01428-5

Jawaad RS, Sultan KF, Al-Hamadani AH (2014) Synthesis of silver nanoparticles. Journal of Engineering and Applied Sciences 9:586–592. https://doi.org/10.5772/intechopen.75363

Judžentiene A (2016) Wormwood (Artemisia absinthium L.) oils. Essential Oils in Food Preservation, Flavor and Safety 849–856. https://doi.org/10.1016/B978-0-12-416641-7.00097-3

Kalińska A, Jaworski S, Wierzbicki M, Gołębiewski M (2019) Silver and Copper Nanoparticles—An Alternative in Future Mastitis Treatment and Prevention? International Journal of Molecular Sciences 20:1672. https://doi.org/10.3390/ijms20071672

Kambale EK, Nkanga CI, Mutonkole BPI, et al (2020) Green synthesis of antimicrobial silver nanoparticles using aqueous leaf extracts from three Congolese plant species (Brillantaisia patula, Crossopteryx febrifuga and Senna siamea). Heliyon 6:e04493. https://doi.org/10.1016/j.heliyon.2020.e04493

Kasithevar M, Saravanan M, Prakash P, et al (2017) Green synthesis of silver nanoparticles using Alysicarpus monilifer leaf extract and its antibacterial activity against MRSA and CoNS isolates in HIV patients . Journal of Interdisciplinary Nanomedicine 2:131–141. https://doi.org/10.1002/jin2.26

Kaur P, Thakur R, Chaudhury A (2016) Biogenesis of copper nanoparticles using peel extract of Punica granatum and their antimicrobial activity against opportunistic pathogens. Green Chemistry Letters and Reviews 9:33–38. https://doi.org/10.1080/17518253.2016.1141238

Khafri HZ (2015) Rosmarinus officinalis leaf extract mediated green synthesis of silver nanoparticles and investigation of its antimicrobial properties. Journal of Industrial and Engineering Chemistry 31:167–172. https://doi.org/10.1016/j.jiec.2015.06.020

Khaled JM, Alharbi NS, Kadaikunnan S, et al (2017) Green Synthesis of Ag Nanoparticles with Anti-bacterial Activity Using the Leaf Extract of an African Medicinal Plant, Ipomoea asarifolia (Convolvulaceae). Journal of Cluster Science 28:3009–3019. https://doi.org/10.1007/s10876-017-1271-4

Khani R, Roostaei B, Bagherzade G, Moudi M (2018) Green synthesis of copper nanoparticles by fruit extract of Ziziphus spina-christi (L.) Willd.: Application for adsorption of triphenylmethane dye and antibacterial assay. Journal of Molecular Liquids 255:541–549. https://doi.org/10.1016/j.molliq.2018.02.010

Khatami M, Heli H, Mohammadzadeh Jahani P, et al (2017) Copper/copper oxide nanoparticles synthesis using Stachys lavandulifolia and its antibacterial activity. IET Nanobiotechnology 11:709–713. https://doi.org/10.1049/iet-nbt.2016.0189

Kumar PPNV, Shameem U, Kollu P, et al (2015) Green Synthesis of Copper Oxide Nanoparticles Using Aloe vera Leaf Extract and Its Antibacterial Activity Against Fish Bacterial Pathogens. BioNanoScience

5:135–139. https://doi.org/10.1007/s12668-015-0171-z

Lediga ME, Malatjie TS, Olivier DK, et al (2018) Biosynthesis and characterisation of antimicrobial silver nanoparticles from a selection of fever-reducing medicinal plants of South Africa. South African Journal of Botany 119:172–180. https://doi.org/10.1016/j.sajb.2018.08.022

Lee SH, Jun B (2019) Silver Nanoparticles : Synthesis and Application for Nanomedicine. https://doi.org/10.3390/ijms20040865

Li R, Li Z, Dong Z, Khor KA (2016) A review of transmission electron microscopy of quasicrystals—How are atoms arranged? Crystals 6:1–16. https://doi.org/10.3390/cryst6090105

Li Z, Mi Y, Liu X, et al (2011) Flexible graphene/MnO2 composite papers for supercapacitor electrodes. Journal of Materials Chemistry 21:14706. https://doi.org/10.1039/c1jm11941a

Maham M, Sajadi SM, Kharimkhani MM, Nasrollahzadeh M (2017) Biosynthesis of the CuO nanoparticles using Euphorbia Chamaesyce leaf extract and investigation of their catalytic activity for the reduction of 4-nitrophenol. IET Nanobiotechnology 11:766–772. https://doi.org/10.1049/iet-nbt.2016.0254

Manandhar S, Luitel S, Dahal RK (2019) In Vitro Antimicrobial Activity of Some Medicinal Plants against Human Pathogenic Bacteria. Journal of Tropical Medicine 2019:1–5. https://doi.org/10.1155/2019/1895340

Manjari G, Saran S, Arun T, et al (2017) Catalytic and recyclability properties of phytogenic copper oxide nanoparticles derived from Aglaia elaeagnoidea flower extract. Journal of Saudi Chemical Society 21:610–618. https://doi.org/10.1016/j.jscs.2017.02.004

Marassi V, Di Cristo L, Smith SGJ, et al (2018) Silver nanoparticles as a medical device in healthcare settings: A five-step approach for candidate screening of coating agents. Royal Society Open Science 5:. https://doi.org/10.1098/rsos.171113

Mat Yusuf SNA, Che Mood CNA, Ahmad NH, et al (2020) Optimization of biogenic synthesis of silver nanoparticles from flavonoid-rich Clinacanthus nutans leaf and stem aqueous extracts . Royal Society Open Science 7:200065. https://doi.org/10.1098/rsos.200065

MEMON R, MEMON AA, SHERAZI STH, et al (2020) Application of synthesized copper nanoparticles using aqueous extract of Ziziphus mauritiana L. leaves as a colorimetric sensor for the detection of Ag+. TURKISH JOURNAL OF CHEMISTRY 44:1376–1385. https://doi.org/10.3906/kim-2001-51

Mittal AK, Chisti Y, Banerjee UC (2013) Synthesis of metallic nanoparticles using plant extracts. Biotechnology Advances 31:346–356. https://doi.org/10.1016/j.biotechadv.2013.01.003

Murthy HCA, Desalegn T, Kassa M, et al (2020) Synthesis of Green Copper Nanoparticles Using Medicinal Plant Hagenia abyssinica (Brace) JF. Gmel. Leaf Extract: Antimicrobial Properties. Journal of Nanomaterials 2020:1–12. https://doi.org/10.1155/2020/3924081

Muthulakshmi L, Rajini N, Nellaiah H, et al (2017) Preparation and properties of cellulose nanocomposite films with in situ generated copper nanoparticles using Terminalia catappa leaf extract. International Journal of Biological Macromolecules 95:1064–1071. https://doi.org/10.1016/j.ijbiomac.2016.09.114

Muthuvel A, Jothibas M, Manoharan C (2020) Synthesis of copper oxide nanoparticles by chemical and biogenic methods: photocatalytic degradation and in vitro antioxidant activity. Nanotechnology for Environmental Engineering 5:. https://doi.org/10.1007/s41204-020-00078-w

Nadagouda MN, Iyanna N, Lalley J, et al (2014) Synthesis of silver and gold nanoparticles using antioxidants

from blackberry, blueberry, pomegranate, and turmeric extracts. ACS Sustainable Chemistry and Engineering 2:1717–1723. https://doi.org/10.1021/sc500237k

Nagajyothi PC, Muthuraman P, Sreekanth TVM, et al (2017) Green synthesis: In-vitro anticancer activity of copper oxide nanoparticles against human cervical carcinoma cells. Arabian Journal of Chemistry 10:215–225. https://doi.org/10.1016/j.arabjc.2016.01.011

Nagar N, Devra V (2018) Green synthesis and characterization of copper nanoparticles using Azadirachta indica leaves. Materials Chemistry and Physics 213:44–51. https://doi.org/10.1016/j.matchemphys.2018.04.007

Naika HR, Lingaraju K, Manjunath K, et al (2015) Green synthesis of CuO nanoparticles using Gloriosa superba L. extract and their antibacterial activity . Journal of Taibah University for Science 9:7–12. https://doi.org/10.1016/j.jtusci.2014.04.006

Narasaiah P, Mandal BK, Sarada NC (2017) Biosynthesis of Copper Oxide nanoparticles from Drypetes sepiaria Leaf extract and their catalytic activity to dye degradation. IOP Conference Series: Materials Science and Engineering 263:. https://doi.org/10.1088/1757-899X/263/2/022012

Nasrollahzadeh M, Mohammad Sajadi S (2015) Green synthesis of copper nanoparticles using Ginkgo biloba L. leaf extract and their catalytic activity for the Huisgen [3+2] cycloaddition of azides and alkynes at room temperature. Journal of Colloid and Interface Science 457:141–147. https://doi.org/10.1016/j.jcis.2015.07.004

Nasrollahzadeh M, Mohammad Sajadi S, Rostami-Vartooni A (2015) Green synthesis of CuO nanoparticles by aqueous extract of Anthemis nobilis flowers and their catalytic activity for the A3 coupling reaction. Journal of Colloid and Interface Science 459:183–188. https://doi.org/10.1016/j.jcis.2015.08.020

Nasrollahzadeh M, Momeni SS, Sajadi SM (2017) Green synthesis of copper nanoparticles using Plantago asiatica leaf extract and their application for the cyanation of aldehydes using K 4 Fe(CN) 6. Journal of Colloid and Interface Science 506:471–477. https://doi.org/10.1016/j.jcis.2017.07.072

Nazar N, Bibi I, Kamal S, et al (2018) Cu nanoparticles synthesis using biological molecule of P. granatum seeds extract as reducing and capping agent: Growth mechanism and photo-catalytic activity. International Journal of Biological Macromolecules 106:1203–1210. https://doi.org/10.1016/j.ijbiomac.2017.08.126

Noor S, Shah Z, Javed A, et al (2020) A fungal based synthesis method for copper nanoparticles with the determination of anticancer, antidiabetic and antibacterial activities. Journal of Microbiological Methods 174:105966. https://doi.org/10.1016/j.mimet.2020.105966

Nzekekwu AK, Abosede OO (2019) Green synthesis and characterization of silver nanoparticles using leaves extracts of neem (*Azadirachta indica*) and bitter leaf (*Vernonia amygdalina*). Journal of Applied Sciences and Environmental Management 23:695. https://doi.org/10.4314/jasem.v23i4.19

Ortiz C, Torres R, Paredes D (2014) Synthesis, characterization, and evaluation of antibacterial effect of Ag nanoparticles against Escherichia coli O157:H7 and methicillin- resistant Staphylococcus aureus (MRSA). International Journal of Nanomedicine 1717. https://doi.org/10.2147/ijn.s57156

Phull A-R, Abbas Q, Ali A, et al (2016) Antioxidant, cytotoxic and antimicrobial activities of green synthesized silver nanoparticles from crude extract of Bergenia ciliata. Future Journal of Pharmaceutical Sciences 2:31–36. https://doi.org/10.1016/j.fjps.2016.03.001

Pirtarighat S, Ghannadnia M, Baghshahi S (2019) Green synthesis of silver nanoparticles using the plant extract of Salvia spinosa grown in vitro and their antibacterial activity assessment. Journal of Nanostructure in Chemistry 9:1–9. https://doi.org/10.1007/s40097-018-0291-4

Ponarulselvam S, Panneerselvam C, Murugan K, et al (2012) Synthesis of silver nanoparticles using leaves of Catharanthus roseus Linn. G. Don and their antiplasmodial activities. Asian Pacific Journal of Tropical Biomedicine 2:574–580. https://doi.org/10.1016/S2221-1691(12)60100-2

Prasad KS, Patra A, Shruthi G, Chandan S (2017) Aqueous extract of saraca indica leaves in the synthesis of copper oxide nanoparticles: Finding a way towards going green. Journal of Nanotechnology 2017:. https://doi.org/10.1155/2017/7502610

Priya, Banerjee., Mantosh, Satapathy., Aniruddha, Mukhopahayay., Papita, Das. (2014) Leaf extract mediated green synthesis of silver nanoparticles from widely available Indian plants: synthesis, characterization, antimicrobial property and toxicity analysis. Bioresources and Bioprocessing 1:3. https://doi.org/10.1186/s40643-014-0003-y

Rabiee N, Bagherzadeh M, Kiani M, et al (2020) Biosynthesis of Copper Oxide Nanoparticles with Potential Biomedical Applications. International Journal of Nanomedicine Volume 15:3983–3999. https://doi.org/10.2147/IJN.S255398

Rades S, Hodoroaba VD, Salge T, et al (2014) High-resolution imaging with SEM/T-SEM, EDX and SAM as a combined methodical approach for morphological and elemental analyses of single engineered nanoparticles. RSC Advances 4:49577–49587. https://doi.org/10.1039/c4ra05092d

Rajesh KM, Ajitha B, Reddy YAK, et al (2018) Assisted green synthesis of copper nanoparticles using Syzygium aromaticum bud extract: Physical, optical and antimicrobial properties. Optik 154:593–600. https://doi.org/10.1016/j.ijleo.2017.10.074

Rajivgandhi G, Maruthupandy M, Muneeswaran T, et al (2019) Biologically synthesized copper oxide nanoparticles enhanced intracellular damage in ciprofloxacin resistant ESBL producing bacteria. Microbial Pathogenesis 127:267–276. https://doi.org/10.1016/j.micpath.2018.12.017

Ramyajuliet M (2020) Biogenic synthesis of Copper nanoparticles using aquatic pteridophyte Marsilea quadrifolia Linn . rhizome and its antibacterial activity. Int J Nano Dimens, 11:337–345

Ravindra S, Murali Mohan Y, Narayana Reddy N, Mohana Raju K (2010) Fabrication of antibacterial cotton fibres loaded with silver nanoparticles via " Green Approach." Colloids and Surfaces A: Physicochemical and Engineering Aspects 367:31–40. https://doi.org/10.1016/j.colsurfa.2010.06.013

Reddy KR (2017) Green synthesis, morphological and optical studies of CuO nanoparticles. Journal of Molecular Structure 1150:553–557. https://doi.org/10.1016/j.molstruc.2017.09.005

Rehana D, Mahendiran D, Kumar RS, Rahiman AK (2017) Evaluation of antioxidant and anticancer activity of copper oxide nanoparticles synthesized using medicinally important plant extracts. Biomedicine and Pharmacotherapy 89:1067–1077. https://doi.org/10.1016/j.biopha.2017.02.101

Renuga D, Jeyasundari J, Shakthi Athithan AS, Brightson Arul Jacob Y (2020) Synthesis and characterization of copper oxide nanoparticles using Brassica oleracea var. italic extract for its antifungal application. Materials Research Express 7:045007. https://doi.org/10.1088/2053-1591/ab7b94

Rocha FS, Gomes AJ, Lunardi CN, et al (2018) Experimental methods in chemical engineering: Ultraviolet visible spectroscopy—UV-Vis. Canadian Journal of Chemical Engineering 96:2512–2517.

https://doi.org/10.1002/cjce.23344

Rosi F, Cartechini L, Sali D, Miliani C (2019) Recent trends in the application of fourier transform infrared (FT-IR) spectroscopy in Heritage Science: From micro: From non-invasive FT-IR. Physical Sciences Reviews 4:1–19. https://doi.org/10.1515/psr-2018-0006

Rostek E, Biernat K (2013) Thermogravimetry as a research method in the transformationprocesses of waste rubber and plastic products for energy carriers (WtE and WtL processes). Journal of Sustainable Development of Energy, Water and Environment Systems 1:163–171. https://doi.org/10.13044/j.sdewes.2013.01.0012

Roy A, Bulut O, Some S, et al (2019) Green synthesis of silver nanoparticles: Biomolecule-nanoparticle organizations targeting antimicrobial activity. RSC Advances 9:2673–2702. https://doi.org/10.1039/c8ra08982e

Sadeghi B, Gholamhoseinpoor F (2015) A study on the stability and green synthesis of silver nanoparticles using Ziziphora tenuior (Zt) extract at room temperature. Spectrochimica Acta - Part A: Molecular and Biomolecular Spectroscopy 134:310–315. https://doi.org/10.1016/j.saa.2014.06.046

Salmen SH, Alharbi SA (2020) Silver nanoparticles synthesized biogenically from Aloe fleurentiniorum extract: characterization and antibacterial activity. Green Chemistry Letters and Reviews 13:1–5. https://doi.org/10.1080/17518253.2019.1707883

Sánchez-Sanhueza G, Fuentes-Rodríguez D, Bello-Toledo H (2016) Copper Nanoparticles as Potential Antimicrobial Agent in Disinfecting Root Canals: A Systematic Review. International journal of odontostomatology 10:547–554. https://doi.org/10.4067/s0718-381x2016000300024

Sankar R, Manikandan P, Malarvizhi V, et al (2014) Green synthesis of colloidal copper oxide nanoparticles using Carica papaya and its application in photocatalytic dye degradation. Spectrochimica Acta - Part A: Molecular and Biomolecular Spectroscopy 121:746–750. https://doi.org/10.1016/j.saa.2013.12.020

Sharmila G, Sakthi Pradeep R, Sandiya K, et al (2018) Biogenic synthesis of CuO nanoparticles using Bauhinia tomentosa leaves extract: Characterization and its antibacterial application. Journal of Molecular Structure 1165:288–292. https://doi.org/10.1016/j.molstruc.2018.04.011

Shayegan Mehr E, Sorbiun M, Ramazani A, Taghavi Fardood S (2018) Plant-mediated synthesis of zinc oxide and copper oxide nanoparticles by using ferulago angulata (schlecht) boiss extract and comparison of their photocatalytic degradation of Rhodamine B (RhB) under visible light irradiation. Journal of Materials Science: Materials in Electronics 29:1333–1340. https://doi.org/10.1007/s10854-017-8039-3

Shende S, Ingle AP, Gade A, Rai M (2015) Green synthesis of copper nanoparticles by Citrus medica Linn. (Idilimbu) juice and its antimicrobial activity. World Journal of Microbiology and Biotechnology 31:865–873. https://doi.org/10.1007/s11274-015-1840-3

Shume WM, Murthy HCA, Zereffa EA (2020) A Review on Synthesis and Characterization of Ag 2 O Nanoparticles for Photocatalytic Applications. Journal of Chemistry 2020:1–15. https://doi.org/10.1155/2020/5039479

Siddiqi KS, Husen A (2020) Current status of plant metabolite-based fabrication of copper/copper oxide nanoparticles and their applications: a review. Biomaterials Research 24:11. https://doi.org/10.1186/s40824-020-00188-1

Singha R, Golam Rasul M, Ghosh P (2020) from the pet-benzene extract of Psidiumguajava and their biocidal

activity. Journal of Medicinal and chemical Sciences Journal homepage: www.jmchemsci.com Original Research Article Isolation of olean 3:15. https://doi.org/10.26655/jmchemsci.2020.2.4

Sivaraj R, Rahman PKSM, Rajiv P, et al (2014) Biogenic copper oxide nanoparticles synthesis using Tabernaemontana divaricate leaf extract and its antibacterial activity against urinary tract pathogen. Spectrochimica Acta - Part A: Molecular and Biomolecular Spectroscopy 133:178–181. https://doi.org/10.1016/j.saa.2014.05.048

Sorbiun M, Shayegan Mehr E, Ramazani A, Mashhadi Malekzadeh A (2018a) Biosynthesis of metallic nanoparticles using plant extracts and evaluation of their antibacterial properties ARTICLE INFO. Nanochem Res 3:1–16. https://doi.org/10.22036/ncr.2018.01.001

Sorbiun M, Shayegan Mehr E, Ramazani A, Taghavi Fardood S (2018b) Green Synthesis of Zinc Oxide and Copper Oxide Nanoparticles Using Aqueous Extract of Oak Fruit Hull (Jaft) and Comparing Their Photocatalytic Degradation of Basic Violet 3. International Journal of Environmental Research 12:29–37. https://doi.org/10.1007/s41742-018-0064-4

Sulaiman GM, Tawfeeq AT, Jaaffer MD Biogenic synthesis of copper oxide nanoparticles using Olea europaea leaf extract and evaluation of their toxicity activities : An in vivo and in vitro study Running Title : Copper oxide nanoparticles and evaluate their toxicity properties in vivo and in . https://doi.org/10.1002/btpr.

Taghavi Fardood S, Ramazani A (2016) Green Synthesis and Characterization of Copper Oxide Nanoparticles Using Coffee Powder Extract. Journal of Nanostructures 6:167–171. https://doi.org/10.7508/jns.2016.02.009

Tesfahuneygn G, Gebreegziabher G (2019) Medicinal Plants Used in Traditional Medicine by Ethiopians: A Review Article OPEN ACCESS. Journal of Genetics and Genetic Engineering 4:1–3

Thakur S, Sharma S, Thakur S, Rai R (2018) Green Synthesis of Copper Nano-Particles Using Asparagus adscendens Roxb. Root and Leaf Extract and Their Antimicrobial Activities. International Journal of Current Microbiology and Applied Sciences 7:683–694. https://doi.org/10.20546/ijcmas.2018.704.077

Thangamani N, Bhuvaneshwari N (2019) Green synthesis of gold nanoparticles using Simarouba glauca leaf extract and their biological activity of micro-organism. Chemical Physics Letters 732:136587. https://doi.org/10.1016/j.cplett.2019.07.015

Thiruvengadam M, Chung I-M, Gomathi T, et al (2019) Synthesis, characterization and pharmacological potential of green synthesized copper nanoparticles. Bioprocess and Biosystems Engineering 42:1769–1777. https://doi.org/10.1007/s00449-019-02173-y

Udayabhanu, Nethravathi PC, Pavan Kumar MA, et al (2015) Tinospora cordifolia mediated facile green synthesis of cupric oxide nanoparticles and their photocatalytic, antioxidant and antibacterial properties. Materials Science in Semiconductor Processing 33:81–88. https://doi.org/10.1016/j.mssp.2015.01.034

Uddin AKMR, Siddique MAB, Rahman F, et al (2020) Cocos nucifera Leaf Extract Mediated Green Synthesis of Silver Nanoparticles for Enhanced Antibacterial Activity. Journal of Inorganic and Organometallic Polymers and Materials 30:3305–3316. https://doi.org/10.1007/s10904-020-01506-9

Veisi H, Azizi S, Mohammadi P (2018) Green synthesis of the silver nanoparticles mediated by Thymbra spicata extract and its application as a heterogeneous and recyclable nanocatalyst for catalytic reduction of a variety of dyes in water. Journal of Cleaner Production 170:1536–1543.

https://doi.org/10.1016/j.jclepro.2017.09.265

Veisi H, Kavian M, Hekmati M, Hemmati S (2019) Biosynthesis of the silver nanoparticles on the graphene oxide's surface using Pistacia atlantica leaves extract and its antibacterial activity against some human pathogens. Polyhedron 161:338–345. https://doi.org/10.1016/j.poly.2019.01.034

Vishveshvar K, Aravind Krishnan M V., Haribabu K, Vishnuprasad S (2018) Green Synthesis of Copper Oxide Nanoparticles Using Ixiro coccinea Plant Leaves and its Characterization. BioNanoScience 8:554–558. https://doi.org/10.1007/s12668-018-0508-5

Wang Y, Wei S, Wang K, et al (2020) biological activities of silver nanoparticles synthesized by Cornus O ffi cinalis extract under 365 nm UV radiation †. 27173–27182. https://doi.org/10.1039/d0ra04482b

Widyaningtyas AL, Yulizar Y, Bagus Apriandanu DO (2019) Ag 2 O nanoparticles fabrication by Vernonia amygdalina Del . leaf extract: synthesis, characterization, and its photocatalytic activities. IOP Conference Series: Materials Science and Engineering 509:012022. https://doi.org/10.1088/1757-899X/509/1/012022

Williams DN, Ehrman SH, Holoman TRP (2006) Evaluation of the microbial growth response to inorganic nanoparticles. Journal of Nanobiotechnology 4:1–8. https://doi.org/10.1186/1477-3155-4-3

Wolde T, Bizuayehu B, Hailemariam T, Tiruha K (2016) Phytochemical Analysis and Antimicrobial Activity of Hagenia Abyssinica. International Journal of Advanced Research in Chemical Science 3:. https://doi.org/10.20431/2349-0403.0308003

Yaqub A, Malkani N, Shabbir A, et al (2020) Novel Biosynthesis of Copper Nanoparticles Using Zingiber and Allium sp. with Synergic Effect of Doxycycline for Anticancer and Bactericidal Activity. Current Microbiology. https://doi.org/10.1007/s00284-020-02058-4

Yoon KY, Hoon Byeon J, Park JH, Hwang J (2007) Susceptibility constants of Escherichia coli and Bacillus subtilis to silver and copper nanoparticles. Science of the Total Environment 373:572–575. https://doi.org/10.1016/j.scitotenv.2006.11.007

Yugandhar P, Vasavi T, Jayavardhana Rao Y, et al (2018) Cost Effective, Green Synthesis of Copper Oxide Nanoparticles Using Fruit Extract of Syzygium alternifolium (Wt.) Walp., Characterization and Evaluation of Antiviral Activity. Journal of Cluster Science 29:743–755. https://doi.org/10.1007/s10876-018-1395-1

Zainab J. Shanan (2018) Structural Analysis of Chemical and Green Synthesis of CuO Nanoparticles and their Effect on Biofilm Formation. Baghdad Science Journal 15:211–216. https://doi.org/10.21123/bsj.15.2.211-216

Zaman MB, Poolla R, Singh P, Gudipati T (2020) Biogenic synthesis of CuO nanoparticles using Tamarindus indica L. and a study of their photocatalytic and antibacterial activity. Environmental Nanotechnology, Monitoring & Management 14:100346. https://doi.org/10.1016/j.enmm.2020.100346

Zhang L, Yuan F, Zhang X, Yang L (2011) Facile synthesis of flower like copper oxide and their application to hydrogen peroxide and nitrite sensing. Chemistry Central Journal 5:1–9. https://doi.org/10.1186/1752-153X-5-75

Publications
Patents
Conference papers

7. Publications- 6/ Patent -1/ Conference presentation-1, from this work

Springer Link

Impact factor = 3.807
SCIE and Scopus Indexed Journal

Original Article | Published: 25 November 2020

Eco-friendly synthesis of silver nanostructures using medicinal plant *Vernonia amygdalina* Del. leaf extract for multifunctional applications

Tegene Desalegn, C. R. Ravikumar & H. C. Ananda Murthy

Applied Nanoscience (2020) | Cite this article

Metrics

Abstract

Ethiopian medicinal plant, *Vernonia amygdalina* Del. mediated green silver nanostructures (V-SNS) were successfully synthesized for the first time. The surface amalgamation of biomolecules of plant leaf extract around Ag nanostructures has also been approved by the most advanced techniques which were employed to characterize the NSs. The presence of absorbance maxima, λ_{max} at 454 nm confirms the formation of V-SNS. UV-DRS studies

Hindawi
Journal of Nanomaterials
Volume 2020, Article ID 3924081, 12 pages
https://doi.org/10.1155/2020/3924081

Hindawi

Impact factor = 2.223
SCI and Scopus Indexed Journal

Research Article

Synthesis of Green Copper Nanoparticles Using Medicinal Plant *Hagenia abyssinica (Brace) JF. Gmel.* Leaf Extract: Antimicrobial Properties

H. C. Ananda Murthy,[1] Tegene Desalegn,[1] Mebratu Kassa,[1] Buzuayehu Abebe,[1] and Temesgen Assefa[2]

[1]*Department of Applied Chemistry, School of Applied Natural Science, Adama Science and Technology University, P.O. Box, 1888 Adama, Ethiopia*
[2]*Department of Biotechnology, College of Natural and Computational Science, Debre Berhan University, Ethiopia*

Correspondence should be addressed to H. C. Ananda Murthy; anandkps350@gmail.com

Received 2 April 2020; Revised 6 May 2020; Accepted 13 May 2020; Published 1 June 2020

Academic Editor: Valeri P. Tolstoy

Indigenous medicinal plant of Ethiopia has been applied for the first time to investigate the synergistic influence of phytoconstituents in green copper nanoparticles (g-Cu NPs) towards the enhancement of antimicrobial properties of NPs. We report the green synthesis of Cu NPs using *Hagenia abyssinica (Brace) JF. Gmel.* leaf extract. The synthesized g-Cu NPs were characterized by UV-visible, UV-DRS, FT-IR, XRD, SEM, EDXA, TEM, HRTEM, and SAED techniques. The maximum

Ethiopian Journal of Science and Sustainable Development

e-ISSN 2663-3205 Volume 8 (1), 2021

Journal Home Page: www.ejssd.astu.edu.et

Research Paper

Medicinal Plant *Syzygium Guineense* (Willd.) DC Leaf Extract Mediated Green Synthesis of Ag Nanoparticles: Investigation of their Antibacterial Activity

Tegene Desalegn[1,*], H C Ananda Murthy[1,*], Yeshaneh Adimasu[2]

Published 2 November 2020

[1]*Department of Applied Chemistry, School of Applied Natural Science, Adama Science and Technology University, P O Box 1888, Adama, Ethiopia*

[2]*Department of Applied Biology, School of Applied Natural Sciences, Adama Science and Technology University, P O Box: 1888, Adama, Ethiopia*

Article Info

Article History:
Received 27 July 2020
Received in revised form 29 September 2020
Accepted 10 October 2020

Keywords:
Medicinal plants

Abstract

The medicinal plant, *Syzygium guineense* (Willd.) DC mediated green silver nanoparticles (*SyG*-Ag NPs) were successfully synthesized for the first time in Ethiopia. The synergistic influence of biomolecules of the plant leaf extract such as alkaloids, phenolic compounds, tannins, saponins and glycosides with Ag NPs towards the antibacterial activity has been investigated. The synthesized nanoparticles were characterized by UV-Vis, UV-DRS, FT-IR, XRD, SEM, EDXA, TEM, HRTEM and SAED techniques. The presence of absorbance maxima, λ_{max} at 452 nm confirms the formation of *SyG*-Ag NPs. The energy gap, E_g of NPs, was found to be 2.1 eV. FTIR spectra confirmed the presence of biomolecules in the extract and NPs. The presence of 4 sharp peaks in the XRD pattern of NPs confirmed highly crystalline nature of NPs. The purity of the NPs was confirmed by SEM-EDAX analysis. The average particle size of NPs was found

IOP Publishing *Mater. Res. Express* 7 (2020) 055016 https://doi.org/10.1088/2053-1591/ab9252

Materials Research Express

Impact factor = 1.449
SCI and Scopus Indexed Journal

CrossMark

PAPER

OPEN ACCESS

RECEIVED
14 April 2020

REVISED
30 April 2020

ACCEPTED FOR PUBLICATION
12 May 2020

PUBLISHED
20 May 2020

Electrochemical properties of biogenic silver nanoparticles synthesized using *Hagenia abyssinica (Brace) JF. Gmel.* medicinal plant leaf extract

H C Ananda Murthy[1], Tegene Desalegn Zeleke[1], C R Ravikumar[2], M R Anil Kumar[2] and H P Nagaswarupa[3]

[1] Department of Applied Chemistry, School of Applied Natural Science, Adama Science and Technology University, PO Box 1888, Adama, Ethiopia
[2] Research Centre, Department of Science, East West Institute of Technology, Bangalore, 560091, India
[3] PG Department of Chemistry, Davanagere University, Davanagere, 577001, India

E-mail: anandkps350@gmail.com

Keywords: green synthesis, *Hagenia abyssinica (Brace) JF. Gmel*, g-Ag NPs, EIS, charge transfer resistance

Int. J. Nano Dimens., 12 (2): 145-155, Spring 2021

ORIGINAL ARTICLE

Copper nanoparticles synthesized using Echinops sp. root extract for antimicrobial applications

Tegene Desalegn Zeleke

Department of Applied Chemistry, School of Applied Natural Science, Adama Science and Technology University, Adama, Ethiopia

Received 11 October 2020; revised 28 November 2020; accepted 01 December 2020; available online 29 December 2020

Abstract

Metallic nanoparticles synthesized using a green synthetic route has been found to be harmful to pathogens. An attempt was made to synthesize copper nanoparticles (*EcS*-Cu NPs) using the root extract of *Echinops sp.*, Ethiopian medicinal plant. The most advanced techniques were employed to characterize NPs. The presence of the highest absorbance at λ_{max} =454 nm confirms the formation of *EcS*-Cu NPs. The role of biomolecules as capping agents for EcS-Cu NPs was authenticated by FT-IR spectra. The presence of a single weak peak in the XRD pattern of NPs confirmed the amorphous nature of the NPs. The purity of the NPs was corroborated by the SEM-EDAX analysis. TEM-HRTEM-SAED analysis authenticated the presence of partially crystalline natured copper NPs with the appearance of weak concentric SAED rings. The *EcS*-Cu NPs showed significant synergistic antibacterial influence verses *S. aureus, E. coli, P. aeruginosa, and E. aerogenes.* The uppermost inhibition zone of 13 mm was inscribed against *S. aureus* bacteria. *EcS*-Cu NPs exhibited better antibacterial activities against gram positive and gram negative bacteria.

Keywords: *Amorphous; Biomolecules; Green Synthesis; Medicinal Plants: Pathogens.*

How to cite this article

Desalegn Zeleke T. Copper nanoparticles synthesized using Echinops sp. root extract for antimicrobial applications. Int. J. Nano Dimens., 2021; 12(2): 145-155.

Australian Government
IP Australia

CERTIFICATE OF GRANT

INNOVATION PATENT

Patent number: 2020102620

The Commissioner of Patents has granted the above patent on 11 November 2020, and certifies that the below particulars have been registered in the Register of Patents.

Name and address of patentee(s):

H C Ananda Murthy of Department of chemistry, School of Applied Science, Adama Science and Technology University Adama Oromia 2118 Ethiopia

Tegene Desalegn of Dean at School of Applied Science, Adama Science and Technology University Adama Oromia 2118 Ethiopia

Title of invention:

A PROCESS FOR SYNTHESIS OF COPPER AND COPPER OXIDE NANOSTRUCTURES

Name of inventor(s):

Murthy, H. C. Ananda and Desalegn, Tegene

Term of Patent:

Eight years from 7 October 2020

Priority details:

Number	*Date*	*Filed with*
202021043290	5 October 2020	IN

Dated this 11th day of November 2020

Commissioner of Patents

PATENTS ACT 1990

The Australian Patents Register is the official record and should be referred to for the full details pertaining to this IP Right.

DAYANANDA SAGAR COLLEGE OF ENGINEERING

(An autonomous institute affiliated to VTU, approved by AICTE & UGC,accredited by NAAC with 'A' Grade" & Accredited by NBA)

Shavige Malleshwara Hills, Kumaraswamy Layout, Bengaluru, Karnataka 560078

DSCE IQAC

VIRTUAL INTERNATIONAL CONFERENCE ON

"Recent Advances in Chemical and Biological Sciences"

(ViRACBS-2020)

Organized by

Department of Chemistry, Biotechnology and Chemical Engineering

Certificate of Oral Presentation

This is to certify that Dr./Mr./Ms. H C Ananda Murthy Of

Adama Science and Technology University, Adama, Ethiopia has presented a paper entitled

Silver Nanostructures Synthesized Using Medicinal Plant *Carum Copticum* Seed Extract For Antibacterial Application

in Virtual International Conference held on 7th to 9th, December, 2020 on "Recent Advances in Chemical and Biological Sciences" at Dayananda Sagar College of Engineering, Bengaluru, India.

Dr. K S Anantharaju, HOD, Chemistry

Dr. Ravishankar R, HOD, Chemical Engineering

Dr. S Kiran, HOD, Biotechnology

Dr. C P S Prakash, Principal

Article Acceptance Certificate

This certificate confirms that the following paper has been accepted for publication in Journal of Nanostructures

Title: Green Synthesis of CuO Nanostructures using Syzygium guineense (Willd.) DC Plant Leaf Extract and Their Applications
ID: JNS-2008-2106 (R1)

Authors: H C Ananda Murthy, Tegene Desalegn, CR Ravikumar, H P Nagaswarupa

Submit Date: 06 August 2020
Accept Date: 29 October 2020

Masoud Salavati-Niasari
Editor-in-Chief of Journal of Nanostructures

Approval of Investigators

We hereby declare that the research report entitled "**Green synthesis of copper and silver nanoparticles mediated by extracts of medicinal plant species of Ethiopia for potential antimicrobial applications**" is our original work; all sources are duly acknowledged and the report is compiled by incorporating the necessary comments and suggestions given by the reviewers.

Principal Investigators:

Name	Signature	Date
Tegene Desalegn Zeleke (PhD)	_____	_____
H C Ananda Murthy (PhD)	_____	_____

Approval of Reviewers

I hereby confirm that (PIs) Dr. Tegene Desalegn Zeleke and Dr. H C Ananda Murthy have accomplished their work as per the approved proposal and incorporated all the comments given by the reviewers in their terminal report of the project entitled ***Green synthesis of copper and silver nanoparticles mediated by extracts of medicinal plant species of Ethiopia for potential antimicrobial applications*** and hence the report qualifies for submission as standard research output.

Name	**Signature**	**Date**
Reviewer 1. Fedlu Kedir (PhD)	_____	_____
Reviewer 2. Enyew Amare (PhD)	_____	_____

Approval: **School Ethical Review Board (School Scientific Committee)**

Name	Signature	Date
1._____	_____	_____
2._____	_____	_____
3._____	_____	_____
4._____	_____	
5._____	_____	_____
6._____	_____	_____